An assessment of Grindalsmoen Aquifer, Elverum, Norway

Field observations and groundwater modelling

Ioannis Papadimitrakis

Master Thesis in Geosciences

Discipline: Environmental Geosciences
Department of Geosciences
Faculty of Mathematics and Natural Sciences

UNIVERSITY OF OSLO

August 2019

An assessment of Grindalsmoen Aquifer, Elverum, Norway – Field observations and groundwater modeling

2019

An assessment of Grindalsmoen Aquifer, Elverum, Norway – Field observations and groundwater modeling

Ioannis Papadimitrakis

http://www.duo.uio.no/

Print: Reprosentralen, Universitetet i Oslo

Abstract

The water supply of the city of Elverum depends on the waterworks of Grindalsmoen that is based on groundwater extraction. The background concentration of iron and manganese may in certain places be high. Thus, an in-situ treatment (Vyredox) is installed at the waterworks, producing good water supply quality. The municipality plans to expand the pumping rate due to the increasing population.

In this thesis the properties and the geometry of the Grindalsmoen phreatic aquifer were studied and a groundwater flow model in GMS was developed. Furthermore, chemical analysis for water samples from the area was conducted, to investigate the water quality. Near surface geophysical surveys and data from geotechnical drillings showed that the sediment thickness of the western part of the catchment ranges between 2-7 m while the thickness close to the Glomma river banks is up to 35 m. Therefore, the western part of the catchment was cut and only the eastern part was modeled. The cut was performed at the upper boundary of glaciofluvial deposits and where the sediment thickness starts to increase. The calculated flux from the cut area due to recharge associated with precipitation, was distributed to the western border. The flux was assigned with more strength at the northern part, because of the greater amount of water ending to it. Although the water table measurements were limited, the model was calibrated, using them. The model was run with and without the present pumping at the waterworks. Furthermore, different scenarios were tested on the model, including increased pumping rate and possible flux entering from the northern boundary of the catchment. The results showed that during the extraction of groundwater there is a significant amount of recharge from the river Glomma. This result needs further investigation. Furthermore, the results of the scenario with the flux from the north, showed similarities with the final calibrated model. Thus, it is concluded that there is flux from the northern boundary is rather small. Hence, more piezometric data are needed to quantify this potential flux.

The results from the water chemistry showed a problematic analysis with increased error in the electrical balance. Nevertheless, the ICP-MS analysis for iron and manganese showed that the groundwater after the treatment with the Vyredox method is safe for consumption.

Acknowledgements

First and foremost, I would like to thank my supervisor, Professor Per Aagaard, whose door was always open offering his guidance and advice with a smile in his face. As many other students in the past who worked with him, I was benefited from his experience and enormous stock of knowledge. Furthermore, his positive spirit, patience, motivation and encouragement during this project makes me say that I am honored working with such an intelligent scientist and kind person.

Besides my supervisor, I would like to thank my co-supervisor Clara Sena for her advices and guidance since the beginning of this thesis. Working with her helped me to develop a critical way of thinking and gain skills that I didn't have before. It was a pleasure working with such smart person and great hydrogeologist.

Moreover, a big "thank you" belongs to my co-supervisor Carlos Duque, who among other things, offered his help and hospitality at the University of Aarhus for a week. His way of teaching benefited me a lot to develop critical way of thinking as a groundwater modeler and initially inspired me to choose this project for my master thesis.

Even though we did not work a lot together with Helen French, I must admit that I enjoyed very much the talks that we had and appreciated her positive spirit and bright personality.

Furthermore, I would like to thank Mufak Naoroz and Magnus Kristoffersen for their help with the chemical analysis of the water samples. Special thanks to Anja Sundal and the master students from UiO and NMBU for their contribution to collect all the data during the field course in May used for this thesis.

It was also great, working together with Torill Oppistov during the field work during October 2018.

In addition, I must thank the friends who encouraged and supported me during this Norwegian adventure of mine.

Lastly and most importantly, I would like to thank my parents for all their support and faith they have showed to me.

Contents

List of figures

1 Introduction

The water supply of the city of Elverum depends on the waterworks of Grindalsmoen that is based on groundwater extraction. The background concentration of iron and manganese may in certain places be high. Thus, an in-situ treatment (Vyredox) is installed at the water works removing dissolved iron and manganese from the groundwater, producing good water supply quality. However, due to the population growth, the water demand is increasing gradually, so the municipality plans to expand their extraction rate. Therefore, the Grindalsmoen aquifer and its properties are essential for Elverum municipality and need to be thoroughly studied.

1.1 Objectives

The current master thesis investigates the hydrogeological conditions of the Grindalsmoen's aquifer in order to quantify the size and properties of the aquifer and its response to higher water demand.

The project aims at summarizing the geological-hydrogeological conditions of Grindalsmoen's aquifer, by developing a regional numerical groundwater flow model. The groundwater model can help Elverum municipality to increase the groundwater extraction in the future.

Furthermore, the water quality of both surface water and groundwater in the area is investigated and compared with the tap water after the Vyredox method.

2 Study area

2.1 Geographical location

Elverum municipality covering an area of 1 229 km^2 and with 21 123 inhabitants, is located at Hedmark, Norway's fourth biggest county. The city of Elverum is around 40 km west of the Swedish borders, laying at the banks of Glomma, the longest (600 km) (Weibull et al., 2019) and largest river of Norway. The Grindalsmoen area, where the aquifer is studied, and is located on the western side of the river Glomma across the city center of Elverum (figure 1).

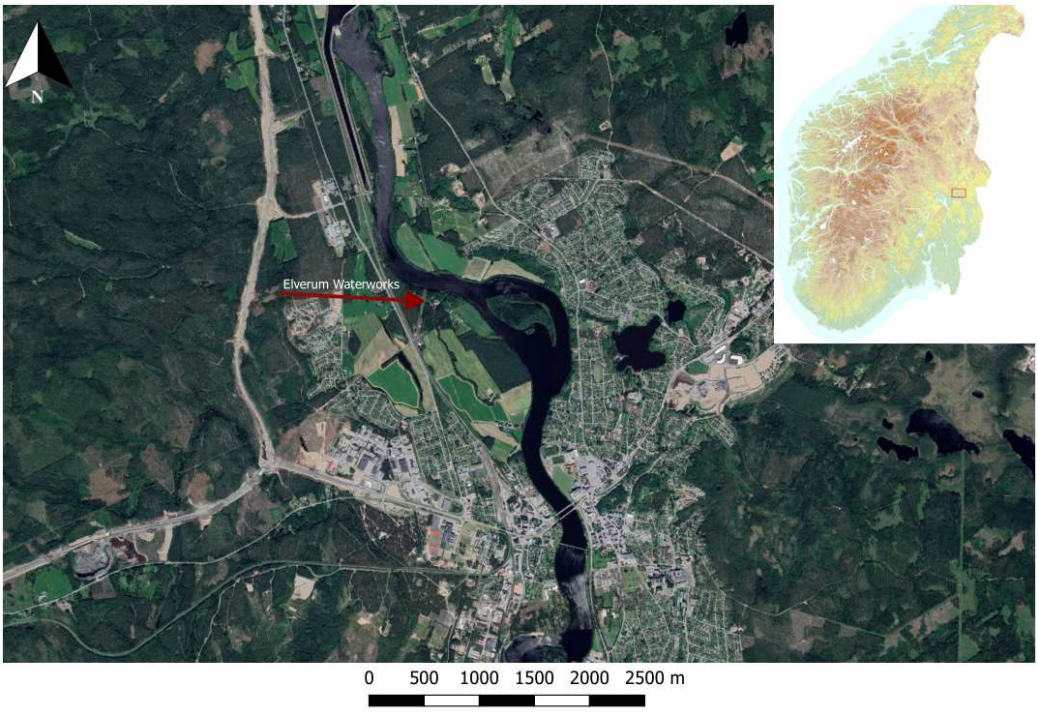

Figure 1 Geographical location of the study area.

2.2 Background information

2.2.1 Groundwater in Norway

In Norway, due to abundant surface fresh water, the groundwater as a source of drinking is limited to 15% of the water supply. This percentage is relatively low in

comparison with other European countries that use mostly groundwater (95 %) for their water supply. Every year up to 60 % of the wells drilled in Norway are used for other applications than for public water supply. Groundwater in Norway is mostly used for purposes of agriculture and renewable energy (heat pumps) (NGU, 2017).

2.2.2 Water Treatment plant

Elverum is one of the municipalities in Norway that uses groundwater as water supply. The Elverum waterworks is located at Lille Grindalsmoen (Figure 1) and provides drinking water to Elverum town and some parts of Hernes and Heradsbygd. The Kirkekretsen water works is located in Sørskogbyda and provides water to the settlement in Sørbygda (Elverum Kommune, 2018).

The aquifer supplying Elverum water works is the focus of the present thesis. As mentioned before, it is situated on the west banks of the Glomma river and started the water extraction in 1987. Since then it has been modernized over the years, it has now 4 production wells for daily supply to Elverum town and the wider area with almost 6 million liters of water.

More than 16 000 people not to mention the industry is supplied with water from the Grindalsmoen waterworks. Due to dissolved iron and manganese in the groundwater, a water treatment system purifying the groundwater in-situ was installed. The method called Vyredox, have had impressive success in removing iron and manganese from the groundwater over the years. Vyredox water treatment plant was installed at the Grindalsmoen waterworks after being designed by Vyrmetoder AB in cooperation with Elverum municipality (Ahmad, 2012).

Iron (Fe) is consisted in earth's crust at almost 5 w/w %, being the fourth in the series element in abundance. As an oxide, there is 3.7 w/w % of iron (II), (FeO) and 3.1 w/w % iron (III), (Fe2O3) in rocks of earth's crust. Manganese (Mn) abundance is about 0.10 w/w % in earth's crust while in groundwater although manganese is general more soluble than iron, iron content is almost 10 times more. There can be problems by various means by using water with high concentration in iron and manganese. Thus it is critical that the high content those metals to be decreased before the water is sent through the distribution systems (Braester and Martinell, 1988).

The behavior of both iron and manganese in aquifers depends on the redox conditions. They are dissolved in the water under reducing conditions as divalent Fe^{2+} and Mn^{2+}. The divalent form of iron (Fe^{2+}) may remain in solution in reduced groundwater, while it oxidizes to the trivalent form (Fe^{3+}), and will precipitate either as an oxide (Fe_2O_3) for example, or an oxyhydroxide (FeOOH) (Braester and Martinell, 1988).

The variation of the layers of soil and bedrock cause variation in the groundwater as well. Even though dissolved oxygen is contained in rain and snow the groundwater through its travel in the aquifer may consume the oxygen and turn reducing. Then, dissolved iron and manganese may increase. On the other hand, there can be places with a lower permeability layer above the aquifer, thus the surface water seep slower or even blocked to the groundwater. (Hallberg and Martinell, 1976).

A common reaction in the groundwater is the following:

$$Fe^{2+} + \frac{1}{4}O_2 + \frac{5}{2}H_2O \leftrightarrow Fe(OH)_3 + 2H^+ \qquad \text{eq. 2.1}$$

Redox potential (E_h) controls and defines the distribution of every redox equilibria equivalently with how pH determines the distribution of acid-base equilibria (Appelo and Postma, 2005). In other words, both the concentration of the electrons control and the hydrogen ions affect the equilibrium in the above equation. How Redox (E_h) potential and pH, affect the equilibria between the reduced and oxidized states of iron and manganese (Figure 2) (Hallberg and Martinell, 1976).

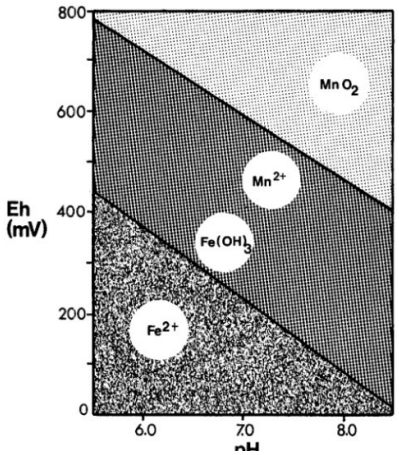

Figure 2 Eh – pH diagram showing the dissolved and precipitated iron and manganese phases (Hallberg and Martinell, 1976)

The lower of the two slopping lines, demonstrates the transition between Fe^{2+} / $Fe(OH)_3$ where, for the values of pH and E_h below the line the concentration of Fe^{2+} is higher than the Fe^{3+}. The above slopping line indicates the transition between Mn^{2+} and MnO_2 which is insoluble. While, Hallberg and Martinell (1976) state that the two slopping lines are not totally accurate, it is understandable that the redox potential and pH needs to be raised above the upper slopping line so all the iron and manganese to be oxidized and precipitated.

Iron and manganese can be oxidized by bacteria that utilizes the energy of reaction because they need to grow and reproduce. The ratio between iron and manganese that needs to be oxidized so to acquire equal amount of energy is 6/1. The amount of the bacteria increases as the process continues and some of the organic matter that it is contained in them, follow the water flow to the well where the Redox potential is higher. There it turns into a source of carbon for the bacteria, oxidizing favorably the manganese. Therefore it is understandable that with Vyredox method, iron is getting removed first and then manganese (Hallberg and Martinell, 1976).

To summarize, the principle of Vyredox process is to create a highly oxidized zone around the well by injecting aerated water periodically, treating this way the well by eliminating the dissolved iron and manganese before pumping occurs (Jaudon et al., 1989). Therefore, what actually happens is that iron and manganese precipitated and held in the strata (Hallberg and Martinell, 1976) (Figure 3). Due το "level" of the redox potential iron will be precipitated before manganese (Braester and Martinell, 1988) and eventually the supply well will have only water purified from iron and manganese.

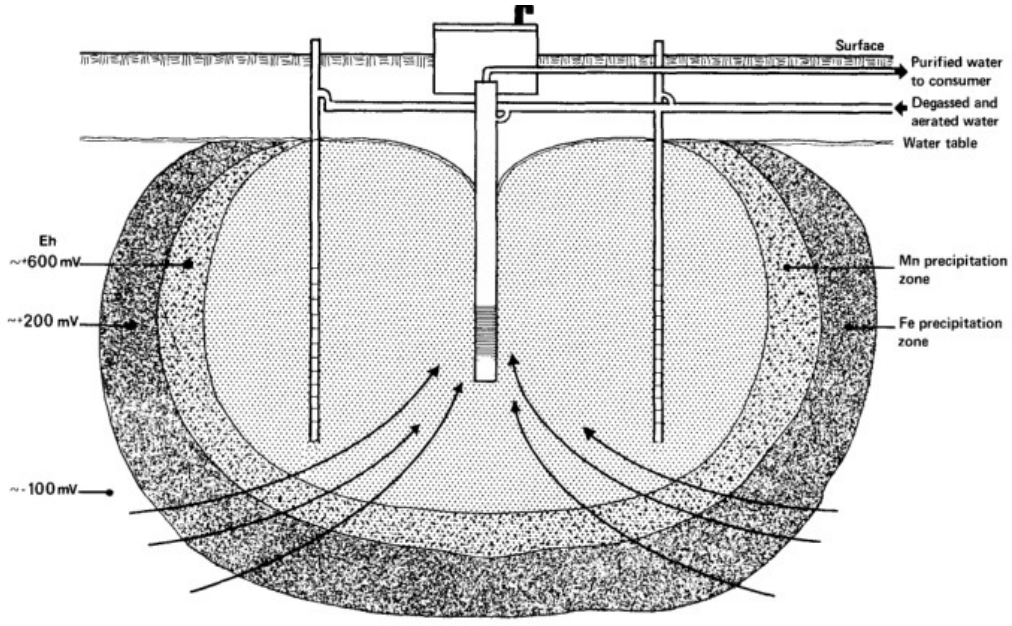

Figure 3 Vyredox method illustrated schematically, showing the iron and manganese precipitation zones with the groundwater to get filtered before the water is pumped (Hallberg and Martinell, 1976).

In Grindalsmoen waterworks a “ring” of 9 satellite wells are installed around the main pumping well which is well 4 (Figure 4). Those wells inject and pump water, to and from the aquifer materializing the Vyredox process from theory to praxis. The principle of the process is that firstly pumping needs to be stopped in the production well to be treated. Two of the satellite wells (for instance SB1 and SB3) pump water simultaneously for two hours with pumping rate of 6 L/s for two hours keeping it in the tank for 3 hours to be aerated by mixing it with atmospheric air, and to be degassed so that non-dissolved oxygen to be eliminated (Jaudon et al., 1989). The satellite well located between (SB2 in this case) the previous mentioned wells forces the oxygen-saturated water back to the aquifer. This process is repeated continuously perimetrically with all the remaining wells and lasts about 20 hours (Jaudon et al., 1989) . To establish a high redox zone in the aquifer the process needs to be stopped for 4 hours (Jaudon et al., 1989). As injecting aerated water, it is maintained a population of oxidizing bacteria, that contribute to the precipitation of the metals by their activity, maintaining that way a high pH and redox potential (Jaudon et al., 1989). Therefore, the step before the end is to use UV light to ensure that the water is clean and safe. Finally, the treated supply well can start pumping up out purified water supplying the municipality. The precipitation of iron and manganese is very effective in Vyredox method, but it is not known the exact mechanism of the precipitation.

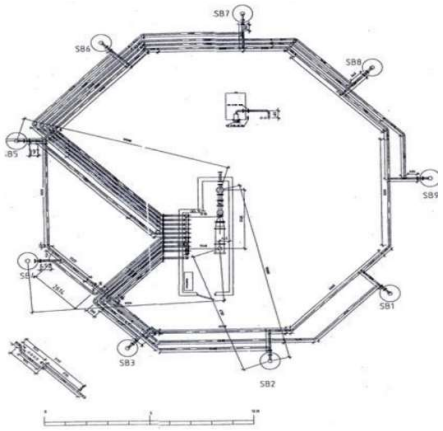

Figure 4. Birdseye schematic view of the production well and the 9 satellite wells around it.

2.2.3 Groundwater as a drinking source

Groundwater is theoretically better protected, by nature, to contamination than surface water. The distinct geological and topographical environment provides this protection and it is dependent on the geological structure, how close it is with surface water bodies, the thickness of the unsaturated zone as well as how fast the water flows (Gaut, 2011).

2.2.4 Previous Work

Grindalsmoen has been an area of interest for a long time for geological, hydrogeological and geochemical reasons. The need of the municipality to install a water works at the area as well as the earlier problem with the enriched water in iron and manganese, has led researchers and master students to study the area of Grindalsmoen.

Except the geological mapping of the area and the maps of quaternary and bedrock geology that can be found for the area in the Geological survey of Norway (NGU), the most relevant to this master thesis is the report from Gaut et al. (1981) about the Groundwater in loose sediments in Grindalsmoen area before the waterworks was installed. This report indicated the groundwater flow in the area with a piezometric map (Figure 5), as well as hydrogeological parameters and well log information.

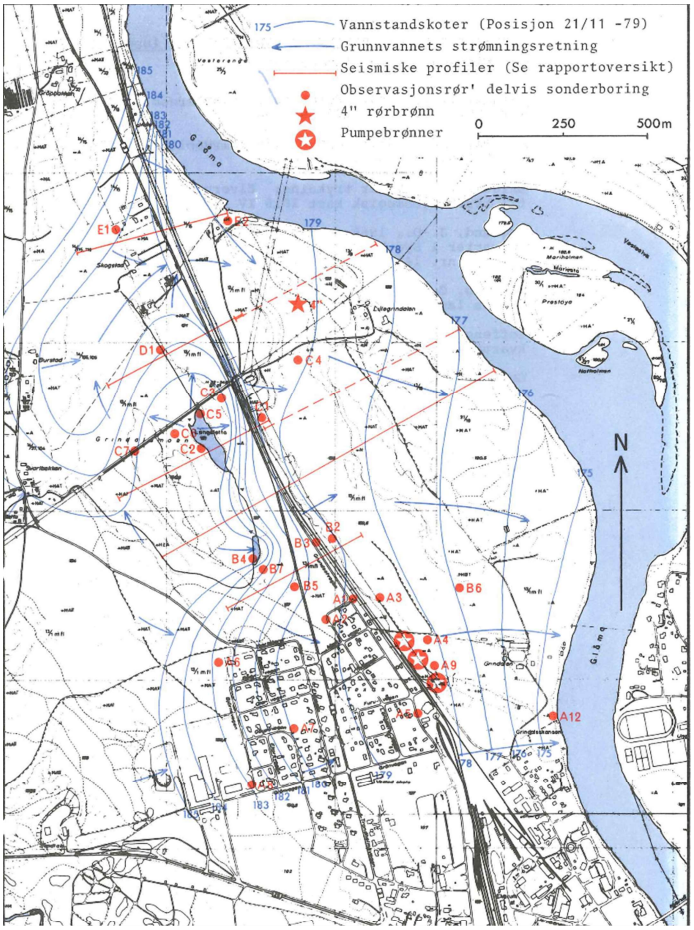

Figure 5 Piezometric map of hydraulic heads, as it was created in the area in 1981 (Gaut et al., 1981).

Furthermore, Knudsen (1983) studied the possible protection zones in the area of Grindalsmoen to install new pumping wells. Later in 1985, Knudsen again wrote a report about the long-term pumping tests at the wells installed.

In 1999 Randi Kalskin and Olav Hilmo from NGU published the report about the potential soils eligible for geothermal extraction, where they concluded that there is not interaction of the river Glomma and the groundwater pumped at the waterworks when pumping with the temperatures provided.

Finally, there are already written two master theses in the area from NMBU. Kharal (2017) wrote about the Hydrogeological conditions in Elverum water works and another one, been written at the same time with this thesis. The thesis written by Torill Oppistov from NMBU studies the flow of the groundwater locally at the waterworks investigating the protection zones.

2.3 Geological Setting

The study area consists of mainly glaciofluvial, fluvial and moraine sediments, with some organic material (bogs). The hard rock basement is for the most metamorphic granitic gneisses.

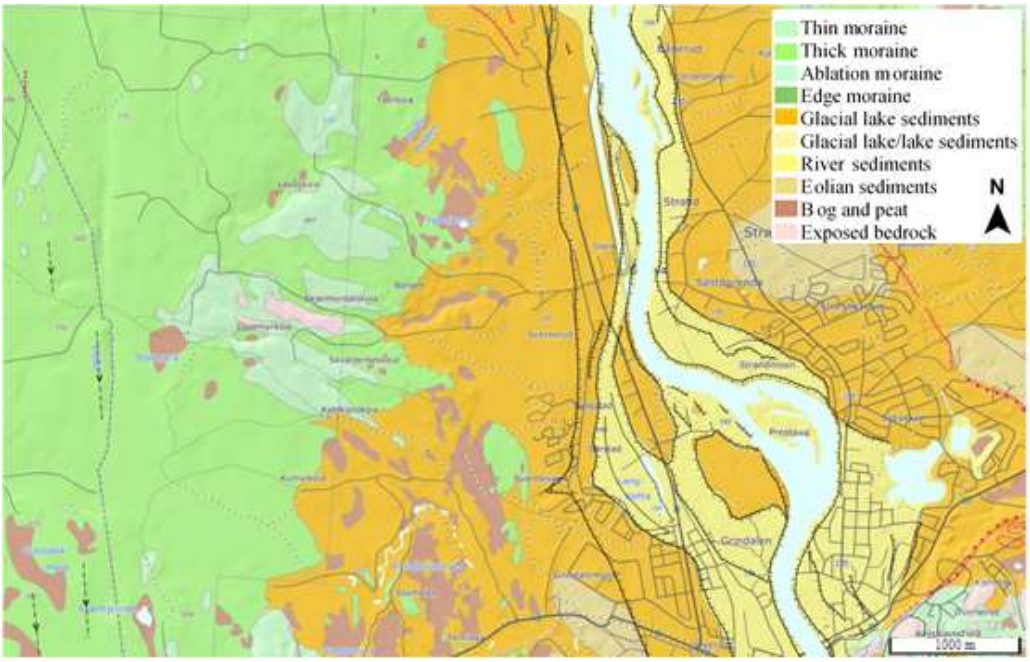

Figure 6 Sediment deposition in the study area.

The Till deposit as shown on the map (Figure 6) with the green and light green color, are partly basal till and partly ablation till that was transported and deposited by the ice margin of the last ice age (Hansen et al., 2005; Høgaas and Longva, 2016). The till is compressed, poorly sorted and can be either very thin less than 0.5 m (light green color), or thicker (darker green color) ranging between 0.5 to more than 10m.

The glaciofluvial deposits, are mainly composed of sands and gravel which were transported and deposited by glacier rivers around 9200 years ago (Hansen et al., 2005). These deposits have clearly defined formations and their thickness is often in the order of tens of meters (NGU, 2019).

Later up to present day, rivers exceeded the glaciofluvial sand and gravel and redeposited both sand and gravel. The fluvial sediments are better sorted and rounded. The thickness of those sediments ranges between 0.5 m to more than 10 m (NGU, 2019).

Peat and bog were formed by dead organic material. The thickness of these sediments is greater than 0.5m. The till material was transported and deposited by glaciers and contain anything from clay to boulders. These deposits have a thickness that exceeds 0.5 m (NGU, 2019).

3 Methods and available data

3.1 Field work

Field work is a fundamental element of hydrogeology since groundwater field and theoretical studies rely on data. Therefore, it is crucial for the hydrogeologist to appreciate the data collected, the uncertainties while collecting them as well as the further interpretation. It is essential for the hydrogeologist to comprehend the data requirements of the project (Moore, 2012).

A field trip to Elverum (1-9 June 2018) was conducted, in the frame of the field course "GEO4360 Field Methods in Hydrogeology". There important data were collected from field experiments and observations. These data were critical for the first approach to build the conceptual model of the Grindalsmoen aquifer.

Furthermore, a two days field expedition was ensued to the study area in October 2018. There were conducted measurements of groundwater properties and obtained a more detailed overview of the sediment cover distribution, as well as the topography of the study area.

3.2 Aquifer properties

The lithology and structures are some of the geological properties controlling groundwater flow and affecting the direction of it besides the yield of the wells. The term, hydraulic properties usually refers to the features characterizing the groundwater flow and the storage. Such features can be assessed by considering the aquifer geology or can be measured either in the field or in laboratory (Brassington, 2007).

3.2.1 Porosity

Theory

The porosity of an aquifer is defined to be "the percentage of the geological formation hosting an aquifer not occupied by solids" (Davidson and Wilson, 2011). In other

words, it expresses how much of the rock or sedimentary material is pore space or interstices. Porosity (n) is designated as the ratio of the volume of voids (V_v) to the total volume of material (V_t) (Hiscock and Bense, 2014), given by the equation below.

$$n = \frac{V_v}{V_t} \qquad \text{eq 3.1}$$

Porosity is a dimensionless parameter and can be expressed as a percentage as well by multiplying (eq 3.1) with 100 (Fitts, 2013).

Porosity takes different forms depending the geologic material (Figure 7). In sediments composed of particles that are rounded and angular, as of instance gravels, sands, clays and silts, porosity takes higher values than in sandstone and limestone, that are consolidated sediments. (Domenico and Schwartz, 1997).

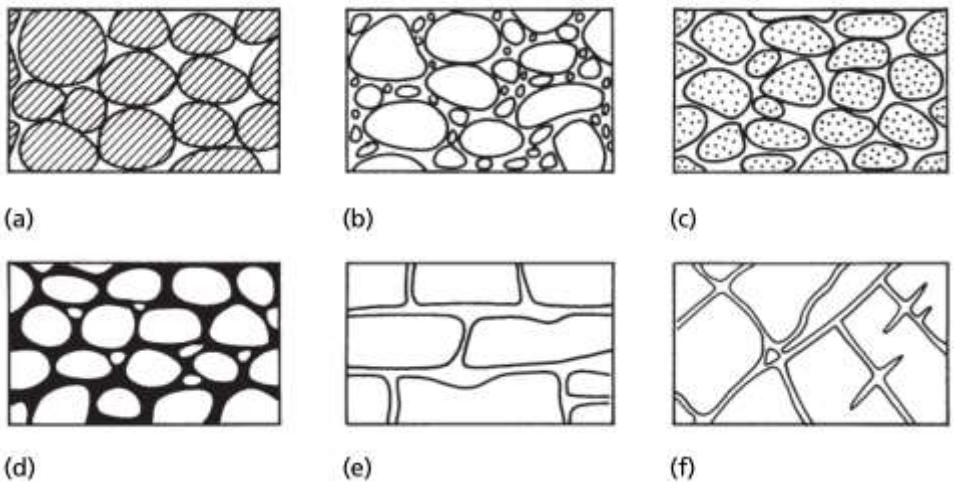

Figure 7. a-f: Illustration of different rock textures affecting the porosity (Hiscock and Bense, 2014).

Porosity is dependent on the composing grains. The shape and the arrangement of them as well as the degree of sorting, cementation and compaction has a crucial role on the values of the porosity. The value range of the porosity can be from 0 to 0.1 for unfractured and wheathered crystalline rocks respectively, to 0.4-0.7 for unconsolidated clay deposits (Hiscock and Bense, 2014). Nevertheless, more representative values for the sediments in the study area are listed in Table 1.

Table 1 Range of porosity for different geological materials (Hiscock and Bense, 2014)

Geological material	porosity, n
Fluvial deposits	0.05 -0.35
Glacial deposits	
-basal till	0.30-0.35
-lacustrine silt and clay	0.35-0.70
-outwash sand and gravel	0.25-0.50
-Loess	0.35-0.5

Data acquisition

Based on the geology of the catchment of Grindalsmoen aquifer, as mentioned before, the area is mainly covered with glaciofluvial sediments (Figure 6). The value of the porosity estimated, was obtained from the available data from the Gardermoen Project (Alfnes et al., 2003). There, the glaciofluvial sediments were studied in great detail during the airport construction. The glaciofluvial sediments covering area are similar with the glaciofluvial sediments in the study area.

3.2.2 Hydraulic conductivity

Theory

Groundwater can flow through many different materials with the properties of the medium to be affecting the nature and the speed of the flow. Darcy's law (eq. 3.2) describes the groundwater flow through "most granular material" towards the lower gradient (Domenico and Schwartz, 1997).

$$\frac{Q}{A} = q = -K\frac{dh}{dL} \quad \text{eq. 3.2}$$

Where Q is the volumetric flow rate (L^3/T), A the area (L^2), q the specific discharge (L/T), K the hydraulic conductivity (L/T) and dh/dL the hydraulic gradient.

The parameter that describes the properties and how easy the water flows through the porous media of an aquifer is the hydraulic conductivity (K) (Hiscock and Bense, 2014). Hydraulic conductivity can be measured in field or laboratory experiments It has dimensions of (L/T) and is given by the equation below:

$$K = \frac{-Q}{A(dh/dL)} \qquad \text{eq. 3.3}$$

Where Q is the discharge (L^3/T), A is the cross-sectional area in L^2 and dh/dL hydraulic gradient in L/L, while the negative sign indicates that the direction of the flow is towards the decreasing hydraulic head (Fetter, 2001).

In older publications hydraulic conductivity used to be mentioned as coefficient of permeability (Domenico and Schwartz, 1997). In nature hydraulic conductivity has a wide range of values. Depending the properties of the geological material the hydraulic conductivity takes higher values for coarser and fractured material for example, while it takes lower values for fine-grained silts and clays (Hiscock and Bense, 2014). The higher hydraulic conductivity is, the easier the fluid flows through the porous media. Moreover, is dependent on the density and viscosity of the water, properties that can be affected by conditions such as the water temperature (Brassington, 2007).

Hydraulic conductivity is unlikely to take the same values in a porous media, either considering it in regional or microscopic scale. A geologic formation can be either homogenous or heterogenous, if hydraulic conductivity has the same values or varies from place to place respectively within it. Furthermore, if hydraulic conductivity at a location in a geological formation does not depend on the direction of measurement, then the geological formation is isotropic. On the other hand if the hydraulic conductivity at a location in the formation differs with the direction of the measurement the formation at that specific point is anisotropic. (Hiscock and Bense, 2014).

Hydraulic conductivity depending the geological material can be found in literature. Some examples of the range of the hydraulic conductivity is given in the Table 2.

Table 2 Representative values for the hydraulic conductivity (Hiscock and Bense, 2014).

Geological material	m/s		m/d	
Fluvial deposits	1.00E-05	1.00E-02	8.64E-01	8.64E+02
Glacial deposits				
- basal till	1.00E-11	1.00E-06	8.64E-07	8.64E-02
- lacustrine silt and clay	1.00E-13	1.00E-09	8.64E-09	8.64E-05
- outwash sand and gravel	1.00E-07	1.00E-03	8.64E-03	8.64E+01
- loess	1.00E-11	1.00E-05	8.64E-07	8.64E-01

Data acquisition

Hydraulic conductivity was calculated in the area from data given by the results of infiltration tests, pumping and slug tests, in June 2018 in the frames of the course "GEO4360 Field Methods in Hydrogeology". In addition, soil samples from the area were collected for grain size distribution analysis and by using Hazen's and Gustafson's methods, it was estimated the hydraulic conductivity.

Infiltration tests

The infiltration tests were conducted using the Mariotte cylinder technique. Mariotte cylinder works as a self-irrigation system by conducting measurements while it keeps the head constant in a pit.

Figure 8. Mariotte cylinder infiltration test conducted in Elverum.

To conduct the infiltration test were used an acrylic cylinder with two hoses attached on, hold by a tripod, a cubic shaped porous sponge, with a hole in the middle, with dimensions 25x25x30 cm. The sponge supports the side walls of the pit while it reduces the risk of mis-measurements. Furthermore, several containers of water and a stopwatch were used. The equipment and its setup are illustrated in Figure 8.

First, a shaft was dug into the ground so to fit the sponge and to have an extra 10 cm depth from the surface. After the sponge was inserted into the pit and its walls were covered with the previously dug out soil so the sponge was filing, tight enough the whole pit. The cylinder attached on the tripod was placed above the pit with both hoses being entered into the sponge. The hoses needed to be hanged as vertical as possible. The supply hose reached the bottom of the sponge and the "level" hose was held by a wooden plate 10 cm bellow the sponge. After the equipment was set up the tap of the infiltrometer was closed and filled with water. Afterwards the pit was filled with water until a stable water level was accomplished and then open the tap of the

cylinder to let the water run into the sponge. Finally, with a timer it was recorded the water level as dropping and infiltrating into the ground. The hydraulic conductivity was calculated by Darcy's law.

Estimates based on grain size analysis

Grain size distribution was conducted to all the samples and grain size parameters was used to determine the hydraulic conductivity. Furthermore, some geotechnical drillings of the new road project (COWI, 2016) provided grain size distribution data that were analyzed.

Hazen's method

An empirical expression for hydraulic conductivity was introduced by Hazen and is expressed in eq. 3.4:

$$K = 0.01157\ D_{10}^2\ (m/s) \qquad \text{eq 3.4}$$

Where D_{10} is the effective grain size in millimeters at 10 % percentile of the grain size distribution. Requirement to use Hazen's method is $D_{60}/D_{10} \leq 5$. The constant 0.01157 may vary according to type of material.

Gustafson's method

Another empirical method was introduced by Gustafson in 1984. The method is based on empirical data from analyzed soil samples compared with results from trial pumping. The method works with a probable hydraulic conductivity, K_{50}, for a grain size curve:

$$K_{50} = E(U)D_{10}^2 \qquad \text{eq. 3.5}$$

Where

$$U = \frac{D_{60}}{D_{10}} \qquad \text{eq. 3.6}$$

The E(U) formula is expressed:

$$E(U) = 10.2E^6 * \frac{e^3}{1+e} * \frac{1}{g^2(U)} \quad \text{eq. 3.7}$$

Where the parameter e is given by:

$$e = 0.8\left(\frac{1}{2lnU} - \frac{1}{U^2-1}\right) \quad \text{eq. 3.8}$$

And the g(U) function by:

$$g(U) = \frac{1.30}{\log(U)}\frac{U^2-1}{U^{1.8}} \quad \text{eq. 3.9}$$

Gustafson's formula is increasingly complex in comparison with Hazen's formula, although it has a wider range of applications. Because it also uses D_{60} percentile in addition to the D_{10} percentile it is more applicable for unsorted soils. Due to its relation to the D_{60} percentile the Gustafson's formula results are somewhat higher to hydraulic conductivity compared to Hazen's. However, it has been shown to give quite reasonable values for quaternary deposits in Scandinavia.

3.3 Water Balance

Theory

The water budget of an aquifer, a catchment also named as water balance is a method of estimating the extend of future water resources (Allaby, 2013). It includes an assessment of every water supply source or recharge compared with the discharge or abstraction of water. The values of these resources are estimated by measuring the components of the hydrological circle, assuming that the water entering the aquifer is equivalent to the water going out from the system. Furthermore, it can be estimated by adding or subtracting changes in the aquifer storage (Brassington, 2007).

The general water balance equation may be expressed in eq 3.10 and 3.11 and illustrated schematically in Figure 9.

$$R + G_1 - G_0 - G_s - ET_d - Q_w = \frac{dV}{dt} \qquad \text{eq. 3.10}$$

in steady state:

$$R + G_1 - G_0 - G_s - ET_d - Q_w = 0 \qquad \text{eq. 3.11}$$

Where R is the recharge, G_1 and G_0 the groundwater inflow and outflow respectively through the bottom and the side boundaries of the aquifer. G_s is the discharge of the groundwater to the streams, ET_d the saturated zone's evapotranspiration, Q_w extraction of the wells and dV/dt is the volume of water stored in the region over time (Fitts, 2013).

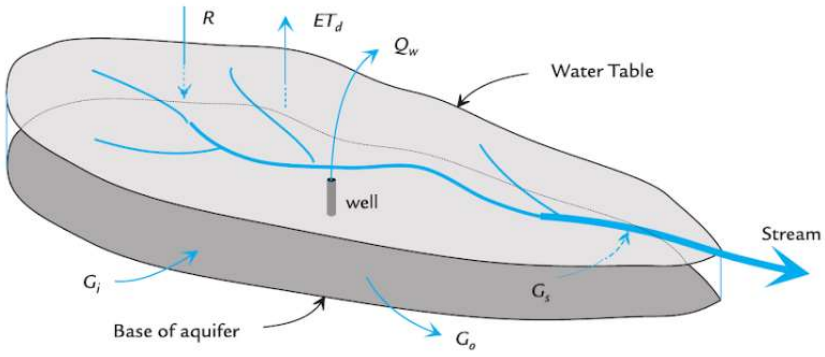

Figure 9. Illustration of the water balance of the saturated zone of an aquifer. (Fitts, 2013)

3.3.1 Catchment area

Theory

The water balance equation is commonly applied to a geographical region to establish the basic hydrologic characteristics. Ordinarily, this region is a catchment area (also called watershed or drainage basin). (Dingman, 2015)

The land and water surface that contribute to a river cross-section or at a specific stream is meant as catchment area (Sharma et al., 2016). The characteristics of the catchment control the paths and the movement of the water on and below the surface. Furthermore, most of the water at the catchment comes from precipitation, passes through the cross-section of the stream at the catchment outlet. Therefore it is understandable that the catchment concept is very essential (Dingman, 2015).

To delineate a catchment area, one first needs to select the position of the cross-section of the streams that outlines the catchment. This location is called catchment

outlet and it is chosen based on the analysis. The catchment outlet can vary between a position where a stream enters a lake or an ocean.

Although in the last years there have been developed open accessible and in relatively reliable digital tools for catchment delineation based on digital elevation models (DEM), a manual delineation provides a better overview of the catchment concept. A digital delineation method could contain errors due to "false readings from vegetation", regions of radar that have shadows etc. (Dingman, 2015). Therefore, a manual delimitation method can provide more accurate results about the boundary of the catchment, because it is based on a topographic map and hydrogeologist's critical judgement.

Data acquisition

The catchment area of the surface water of Grindalsmoen's, was delineated by a manual delineation method. A topographic map of 1:20000 scale of the area as well as, a digital elevation map (DEM) were used. A more detailed contour elevation lines were generated in geographical information system for accurate results.

3.3.2 Precipitation

Theory

The main "input vector" of the hydrological cycle is the precipitation. Precipitation includes rain, snow fall, hail, sleet or fog (Dingman, 2015). Atmospheric water derives the precipitation, so climatic factors such as temperature, wind and atmospheric pressure govern the quantity and the form of it (Viessman and Lewis, 1996). To measure the precipitation each country has set up a network of gauges, operated by local or national meteorological agencies.

Data acquisition

Precipitation data for the Grindalsmoen area were obtained from Norwegian water resources and energy directorate (NVE) map service NEVINA, that uses values from the Norwegian meteorological institute and their meteorological stations.

Furthermore, there were used data for comparison from the meteorological station of Fagertun in Elverum city, that was closest to the Grindalsmoen area. It operated from 1978-2013, but since the station has been shut down, data from the meteorological station in Stavsberg in Hamar, were used for comparison.

3.3.3 Evapotranspiration

Theory

The term evapotranspiration consists of evaporation from open water (lakes and rivers), interception loss (bare soil and surfaces that are vegetative), transpiration (evaporation from the plants) and snow surface and ice sublimation. Therefore, evapotranspiration combines all those processes that water, in soil or liquid phase on earth's surface converts to atmospheric vapor (Dingman, 2015). The rate of evapotranspiration depends on several factors such as water temperature, the humidity and the temperature of the air layer being above the water surface and wind speed (Hiscock and Bense, 2014).

There are daily and seasonal fluctuations in evapotranspiration. Thus, the rate of evapotranspiration is usually higher in the summer than in the winter as more water evaporates into warm air than in cooler air in areas that have strong variations in climate seasonally. The most important part is vegetation and transpiration. In areas with snow and ice during winters, there is not that much evapotranspiration in the winter. Therefore, it is difficult to measure directly the evapotranspiration rate (Fitts, 2013). In Norway transpiration by the vegetation is the important part, it can be seen by the growing season evapotranspiration is high while during the winter is negligible.

Data acquisition

For the estimation of evapotranspiration data, the report from NEVINA for the catchment area of Grindalsmoen was used. NEVINA uses precipitation data as well as temperature and vegetation cover data to estimate evapotranspiration.

3.3.4 Recharge

Theory

Groundwater is commonly moving, however the origin and the destinations of it, is sometimes uncertain. In upland regions most of the groundwater comes from recharge, i.e. infiltrated water originating from precipitation on earth's surface minus the evapotranspiration. In dry climates, usually the water from the bottom of open waters partially leaks and enters the subsurface. Since groundwater always moves from the highest to the lowest head, the discharge occurs from the saturated zone to lower elevation areas as for instance springs or the bottom of open waters that are in lower elevation than the water table, allowing the groundwater to go into the system as recharge (Fitts, 2013). Summarizing recharge of the groundwater is the quantity of the surface water reaching the water table by infiltration through the unsaturated zone or through the riparian zone directly (Hiscock and Bense, 2014).

Data acquisition

Based on the calculations of NVE's NEVINA report for the catchment area of Grindalsmoen the recharge value was obtained. The obtained value for the recharge was calculated automatically from NEVINA after subtracting the total evapotranspiration for the area from the total precipitation.

3.4 Wells

In Grindalsmoen besides the waterworks there are installed several wells (Figure 10). The types of these wells are pumping or energy wells and geotechnical drillings (some of the geotechnical wells could have removed). The location of the wells was obtained by GRANADA (National groundwater database) provided by the Geological Survey of Norway (NGU, Norges Geologiske Undersøkelse). In addition, two observation wells were drilled in the area by the students during the course "GEO4360 Field Methods in Hydrogeology" in June 2018, which were monitored, and tested with slug tests.

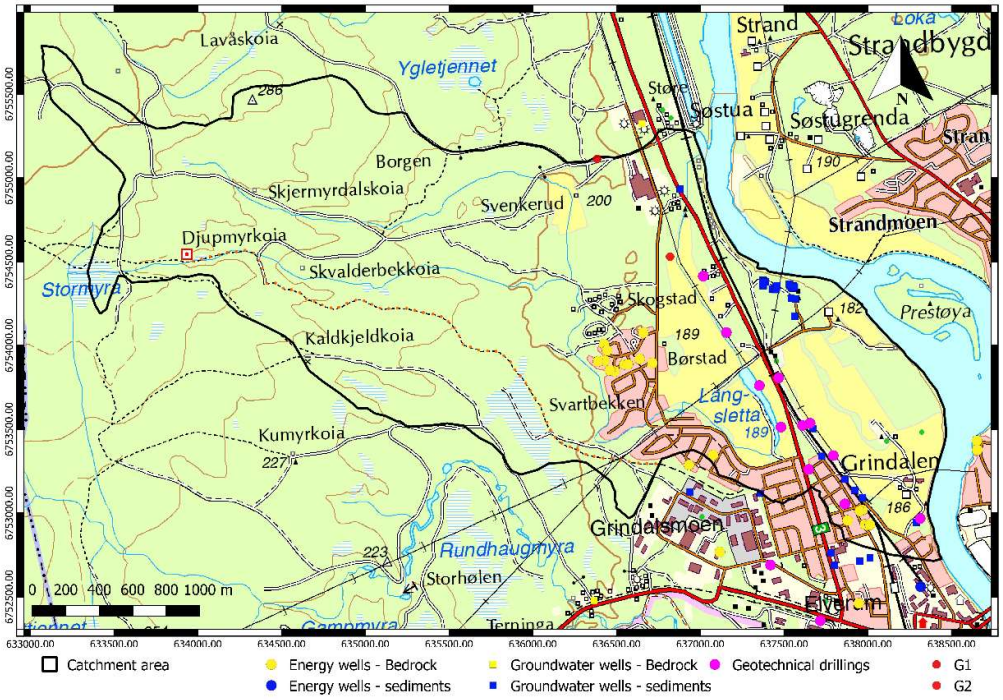

Figure 10 Map with the location of the wells in the area.

3.4.1 Pumping Tests

Theory

A pumping test is a method that can provide information about groundwater flow, aquifer properties and the yield of the well conducted the test. Such a test comprises controlled pumping at a previously determined rate and measurements of the groundwater level not only at the pumping well but at nearby observation wells as well (Brassington, 2007).

Compared to piezometer tests, pumping tests are more expensive since they are relatively “of larger scale” and more time consuming. Nevertheless, they are useful providing information about the aquifer like storativity and transmissivity. Moreover, besides the aquifer properties information, measurements about how the well performance variates with the pumping rate can be obtained. Finally, another advantage of the pumping tests is the information about the quality of the water that is pumped and how it variates through time (Hiscock and Bense, 2014).

A pumping test needs to be, carefully and wisely planned due to the cost of it. A cost that is dependent on the duration of the test as well as the number of the observation wells that are going to be used. The geological and hydrogeological setting of the site needs to be known. Already installed wells in the area are of big importance since they can provide information about the subsurface. The well log information can help to estimate preliminarily the transmissivity of the aquifer, through the aquifer thickness and the lithology (Singhal and Gupta, 2010).

The most common pumping tests are step drawdown test and the constant discharge test. The step drawdown test measures the performance and the efficiency of the well, while the constant discharge test measures the performance of the well and the aquifer properties.(Hiscock and Bense, 2014).

In step drawdown tests, while the pumping rate, Q, of the pumped well is increased in steps, the drawdown of the groundwater level, s, is measured. In this kind of tests, no observation wells are required and the variation of specific capacity (Q/s) is used to choose the size of the pump and the setting in long term scale for the production well. In the second case, where the constant discharge test takes place, there is a constant pumping rate from the pumped well with the potentiometric surface change to be monitored in three steps in one or in several observation wells nearby the pumped well. This test consists of three stages, including the measurements carried out before the pumping test, the pumping test in between, and eventually potentiometric recovery observations after the pumping test has finished (Hiscock and Bense, 2014).

Data acquisition

Pumping tests were conducted to the wells drilled, during the previous mentioned field course in early June 2018. Prior to the pumping test each well was flushed thus the well screens to be cleaned.

For the pumping test conducted in the area were used pressure loggers (divers), measuring automatically the pressure during the test. The divers were prior programmed using a computer.

Due to pumping during the pumping test conducted in 2018 in the waterworks the data could not be used. Nevertheless, in Ydalir that is on the other side of the river

banks and the sediments are similar, there have been conducted pumping tests. Sondre Gjengedal (in prep), who has conducted pumping tests in the area, was contacted and provided information about the test.

Furthermore, there were used and interpreted the data from the long-term pumping test in the area of Grindalsmoen (Knudsen, 1985). Although there were uncertainties for the thickness of the unsaturated zone and the geometry, the results are presented to give an approximation of the hydraulic conductivity.

3.4.2 Slug Test

Theory

The Hvorslev (1951) slug test method was used on the drilled wells to estimate the hydraulic conductivity of the region close to the boreholes (Rushton, 2003).

A slug test is performed with a sudden change in the water level of the borehole. This is caused, either by importing rapidly a specific volume of water, or by importing a solid cylinder again with specific volume in the borehole suddenly to create the same effect. While the water level recovers, it is measured with time, with the results to be interpreted (Hiscock and Bense, 2014).

Hvorslev slug test interpretation method is commonly used for piezometers open at their base only for a short interval. In 1951 Hvorslev, a geotechnical engineer presented a mathematical model for interpreting slug tests in piezometers or partially penetrating wells (Aqtesolv, 2015). This model was based on the finding that water level returns to the initial static level exponentially. The time needed to recover depends on the hydraulic conductivity of the porous medium and the piezometer design. h_0 is the height of the water level rising

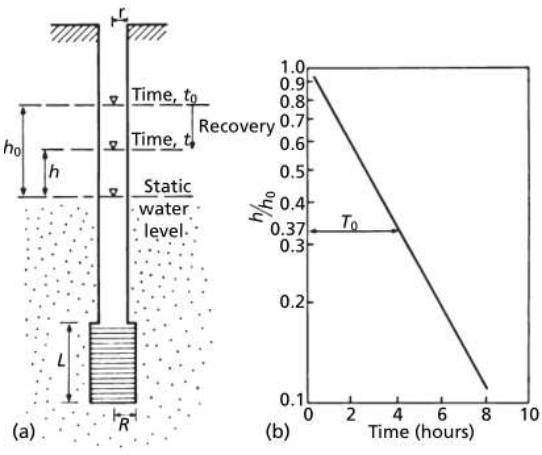

Figure 11. Hvorslev test showing (a) geometry of the piezometer and (b) the semi-logarithmic plot of analysis (Hiscock and Bense, 2014).

above the static water at the beginning of the slug test and h is the level of the water level after time t. Then the ratio h/h_0 with time, is plotted as a straight line in a semi-logarithmic plot, as shown in figure 11b (Hiscock and Bense, 2014).

Hvorslev's piezometer test geometry is illustrated at Figure 11a with the hydraulic conductivity (K) to be calculated by the following equation:

$$K = \frac{r^2 \log_e\left(\frac{L}{R}\right)}{2LT_0} \qquad \text{eq. 3.12}$$

Where r is the radius of the well, L is the length of piezometer, R the radius of the well screen and T_0 is the time that water rises or fall to 37 % of the change (Figure 11b) (Hiscock and Bense, 2014) .

Data acquisition

During the slug test in Grindalsmoen, first the well was flashed so the groundwater to clear the filter from fine particles. Then after the groundwater level was reached again to the initial level, the piezometer was entered the well and was sank approximately 10 cm below the water table. Afterwards the well was filled with water with the piezometer recording time while the water level was dropping at its initial level. Finally, the raw data was exported from the piezometer and interpreted, obtaining results for hydraulic conductivity.

3.4.3 Groundwater table

Theory

The best way to understand a groundwater system, as stated by Brassington (2007), is to have reliable groundwater level measurements or hydraulic head measurements. Such data sets can be obtained either by direct observations in piezometers, wells, surface water or by geophysical investigations, that will be described more thoroughly in chapter 3.5.

Groundwater level data are essential in hydrogeology as they can be used for numerous reasons, as for instance to define the groundwater flow through a

potentiometric map surface or to plot a hydrograph. Furthermore, the more values available for hydraulic head across the study area, the better it is for the numerical model of the groundwater flow, since it can be designed and tested to predict the future behavior of the aquifer in upcoming conditions (Hiscock and Bense, 2014).

Data acquisition

The data acquisition of the groundwater table was obtained by using water level dippers. A water level dipper is an instrument consisting by a measuring tape coiled on a drum with an electrode attached to the end of the tape. The electrode attached on the measuring tape was lowered down to the borehole until it reached the water. By the time the electrode hit the water a red light and a buzzer were activated on the drum, indicating that way the groundwater level. The depth to the water was noted down from the fixed datum point, that was the top of the casing and eventually the length of the casing was subtracted from the total length to give the depth to the water level from the surface. Later the depth to the water table was subtracted from the elevation above the sea level given by GPS measurements or by the digital elevation model if no GPS measurements wasn't provided, to give the elevation of the water table in meters above sea level (masl).

On the map (Figure 12) the measurement points of the water table measured by dippers can be shown with the wells and field observation points.

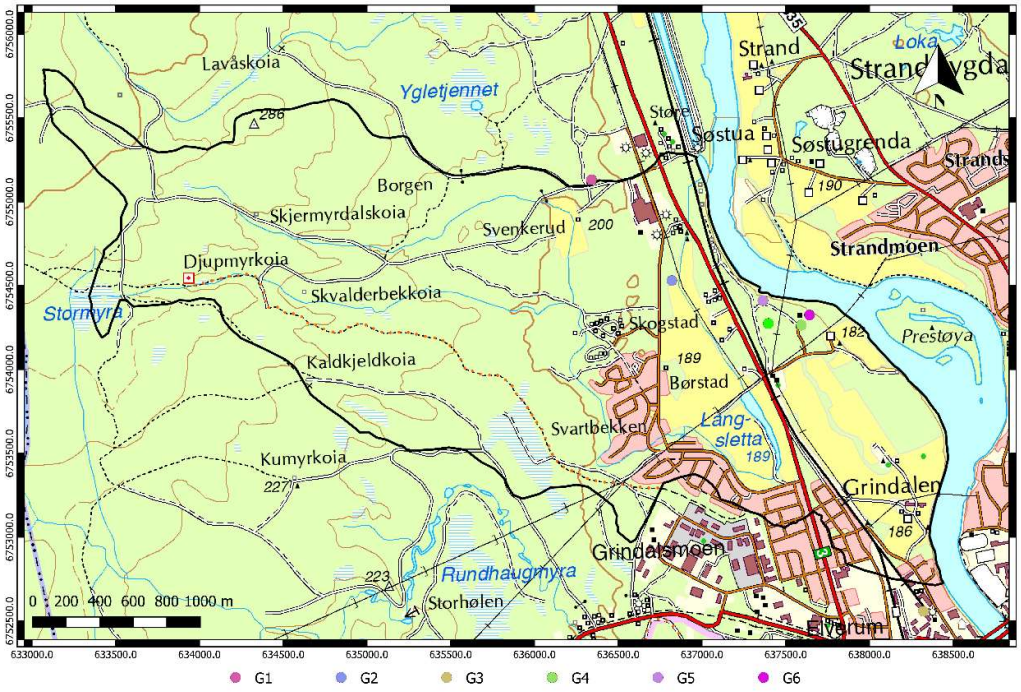

Figure 12 Map with the location of groundwater measurements obtained with water dippers in October 2018.

3.5 Near surface-geophysical surveys

To define the groundwater level as well as the depth to the bedrock, besides well logs, near surface geophysical investigations such as seismic refraction, ground penetration radar (GPR) and Electrical resistivity tomography (ERT) were used. These investigations were conducted in some locations of the study area during the field course “GEO4360 Field Methods in Hydrogeology” on June 2018.

Near-surface geophysical survey is an essential tool in hydrogeological and groundwater exploration, that in connection with the knowledge of the geological setting of the area can be useful to define the properties of the aquifer. The location of the available data is shown in Figure 13.

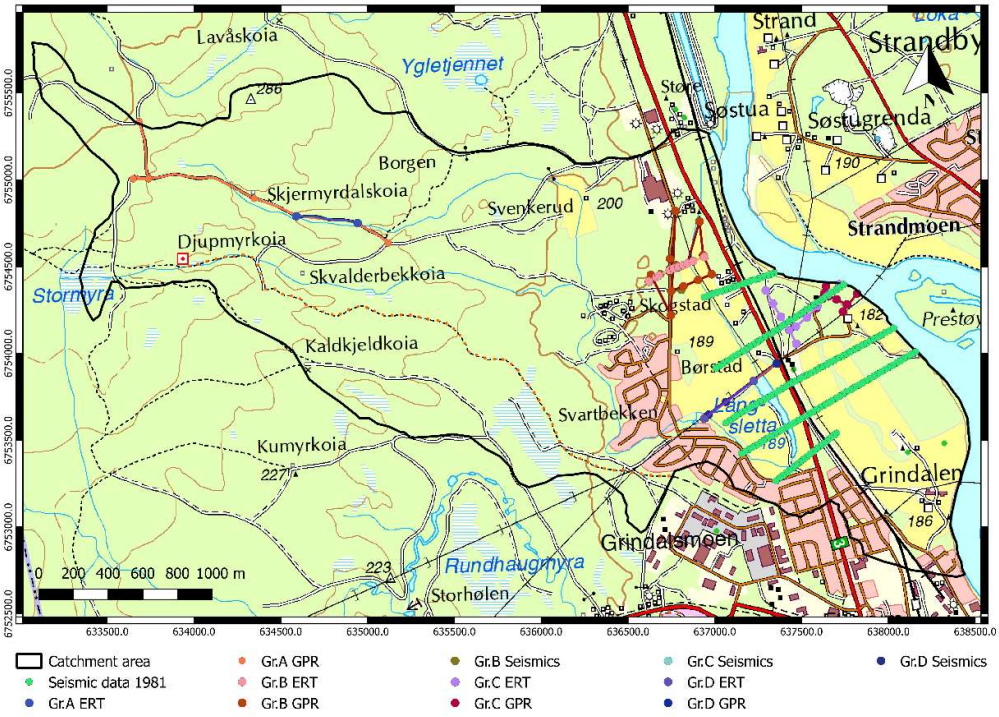

Figure 13 Location of the Near surface surveys conducted in the area.

3.5.1 Seismic refraction

Theory

Seismic refraction surveying is a relatively cheap and powerful geophysical survey method (Breivik et al., 2018). It has a primary strength to be able to analyze “lateral changes in the depth to the top of a refractor and the seismic velocity within it”. The Seismic velocity of the layers is usually obtained from seismic refraction method. From the seismic velocity one can derive information such as the geological type of the layer and the saturated aquifer thickness and water potential (Reynolds, 2011). Some examples of typical, seismic (P-wave) velocities of geological materials are presented at the Table 3.

Table 3 Range of P-wave velocities (Reynolds, 2011)

Material	V P (m/s)	Material	V P (m/s)
Air	330	Glacial moraine	1500–2700
Water	1450–1530	Sand and gravel (near surface)	400–2300
Soil	100–500	Sand and gravel (at 2 km depth)	3000–3500
Snow	350–3000	Clay	1000–2500
Solid glacier ice	3000–4000	Pemafrost	1500–4900
Sand (loose)	200–2000	Gypsum	2000–3500
Sand (dry, loose)	200–1000	Granites	4600–6200
Sand (water saturated, loose)	1500–2000	Gabbro	6400–7000

The principle based on the seismic refraction method is that, when a seismic wave hits on a boundary of a different velocity, the direction of the travel of the wave changes, when it enters the new medium. The seismic velocity across the boundary governs the amount of the change of the direction according to Snell's Law (Reynolds, 2011) (eq. 3.6).

$$\frac{sini}{sinr} = \frac{V_1}{V_2} \qquad \textit{For general refraction}$$

(eq 3.13)

$$sini_c = \frac{V_1}{V_2} \qquad \textit{For critical refraction}$$

Where V_1 is the velocity of the upper layer, V_2 the velocity of the lower layer, i and r are the angles of incidence and refraction and i_c is the critical angle (the angle that critical refraction occurs).

A seismic refraction survey is composed mainly from a source that is usually a sledge hammer on a metallic plate that generate P-waves. The produced waves are either direct, traveling along the top of the ground surface, by critical refraction travelling along the interface but in the lower layer or by reflection (Breivik, 2018). A set of geophones record on a seismograph the waves that are detected along them. The whole process is shown schematically in Figure 14. Each geophone's output is displayed as a single trace and the associated travel time is assessed and laid out on a time-distance graph (Reynolds, 2011).

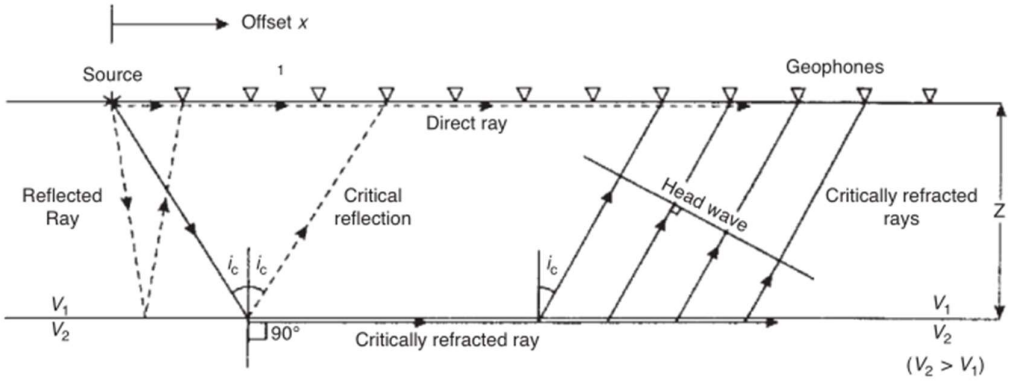

Figure 14 Diagram showing the paths for the direct, reflected and refracted rays (Reynolds, 2011).

Data acquisition

As mentioned before the seismic refraction seismic surveying was conducted during the field course "GEO4360 Field Methods in Hydrogeology" on June 2018, where they took place surveys along the area of Grindalsmoen (Figure13).

Figure 15. Seismic refraction survey in one of the locations in Grindalsmoen.

Several geophones were implanted in the ground, connected together with a cable, with the last spot of the cable to be a metallic plate. The metallic plate was stroked by a sledge hammer (Figure 15) creating the source of P-waves that were interpreted by a seismograph, connected at the start of the cable. The 50-200 Hz produced from the stroke, was enough energy to investigate targets at shallow depths. Geophone separation was 5 m and the energy source (metallic plate) to geophone offset 1 m.

After the seismic refraction survey, the seismic data were processed by the students of the course under the supervision of Asjbørn Breivik (UiO), who was responsible for the teaching of the seismic refraction survey during the field course.

3.5.2 Ground penetration radar

Theory

Ground penetration radar (GPR) is a geophysical survey was widely used for geologic applications since the 1970's but there has been an increase of its use in hydrogeological investigations in the recent years (Annan, 2005). GPR is an all-around and an inexpensive method that can be used to clarify a range of questions such as the geological structure and the material properties (Annan, 2005), or depths to bedrock and groundwater levels. It has a wide range of applications as for instance for environmental purposes, in engineering and construction and in archeology.

GPR is a geophysical investigation method that uses electromagnetic waves. A radar system consists of a signal generator, a transmitting and a receiving antenna as well as a console for controlling and managing the signal generation and recording. The transmitter antenna generates a wavetrain of radiowaves with frequency ranging from 50-550 Mhz for geological applications. Those radiowaves "propagate away in a board beam" traveling at high speeds (0.3 m/ns, in air). A receiver recording the reflected signals when they meet a "reflector" that is either a geologic structure or layer or just an object with different electromagnetic properties. The electromagnetic properties determine the wave propagation velocity along with the attenuation (Reynolds, 2011). A range of typical geological materials with relative radiowave velocities and dielectric constants is presented at the Table 4.

Table 4 Radiowave velocities and relative dielectric constants for manmade and geological materials (Reynolds, 2011)

Material	εr	V (mm/ns)	Material	εr	V (mm/ns)
Air	1	300	Sand and gravel (unsaturated)	3.5–6.5	118–160
Water (fresh)	81	33	Sand and gravel (saturated)	15.5–17.5	72–76
Water (sea)	81–88	33	Sand (wet)	10–32	53–95
Polar snow	1 1.4–3	194–252	Silt (unsaturated)	2.5–5	134–190
Polar ice	2 3–3.15	168–172	Silt (saturated)	22–30	55–64
Pure ice	3.2	167	Clay (dry)	2–5	134–212
Freshwater lake ice	4	150	Clay (wet)	8–40	47–106
Sea ice	2.5–8	78–157	Till (unsaturated)	7–21	65–113
Permafrost	2–8	106–212	Till (saturated)	24–34	51–61

Lower radar frequencies provide increased penetration depth but a loss at the profile resolution as well. For hydrogeological investigations higher frequencies are preferable with lower penetration depth and higher resolution.

As any geophysical survey, GPR has advantages and disadvantages. Some of the advantages of GPR are that is easy to handle. Furthermore, the collection of the data can be occurred fast and voids and trenches can be detected. Moreover, depths and lengths of targets can be determined. On the other hand, for GPR to work properly is required a flat and even terrain and the functionality in clay and salt pore water is not good. Last, the interpretation of the radargrams is a complex process in general (Breivik et al., 2018).

Data acquisition

Several GPR profiles (Figure 13) were taken in Grindalsmoen during the previously mentioned field course. Furthermore, a set of GPR profiles data was available from Kalskin and Hilmo (1999), and added manually in QGIS

A pulseEKKO PRO GPR on a SmartCart by Sensors & Software Inc. (Figure 16) was used to perform the survey. The GPR was adjusted on the SmartCart a special cart with four wheels, built for the GPR, making the survey easier to conduct. On the cart were applied two 50MHz antennas with two batteries and a DVL (digital video logger) with its battery, showing the preliminary results. Furthermore, there were adjusted on the cart a GNSS (Global Navigation Satellite System) receiver by Topcon Inc. (model HiPer II) that was tracking the position of the measurements and approximately the height above sea level as well as a odometer to record the profile length. With a button on the handle there were added marks in the datasets.

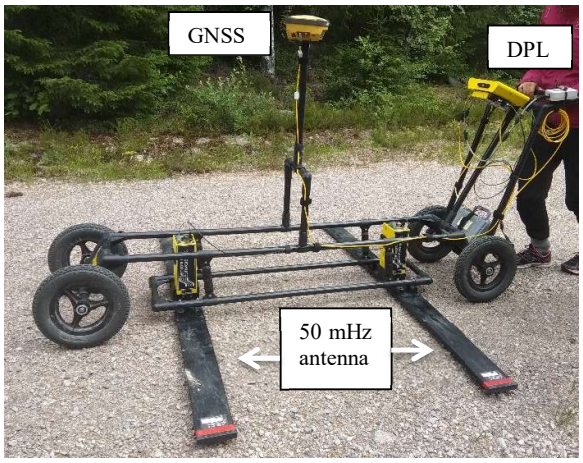

Figure 16.GPR PulseEKKO PRO on the SmartCart from Sensors & Software.

After taking the data, the profiles were interpolated with the processing software of PulseEKKO by the technical staff of the NMBU university, participating and helping at the course. The profiles were interpreted later gaining major information about the depth to the bedrock and the depth to the water table.

3.5.3 Electrical resistivity tomography

Theory

Commonly in the field are used four active electrodes, implanted in the ground each time (Breivik et al., 2018) . The placing of the potential electrodes is generally in line between the current electrodes (Figure 17) (Landviser LLC, 2002).

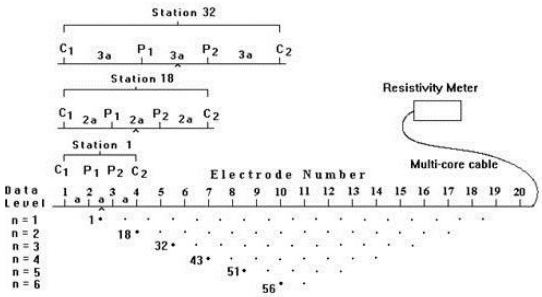

Figure 17. Dipole-dipole arrangement of the electrodes (Landviser LLC, 2002)

Either a direct current (DC) or a low frequency AC current of around 20 Hz, is adapted on outer two electrodes, so the voltage cab be measured at the two inner electrodes. As a result, a resistivity value occurs, converted by the measured voltage. In theory, that can be related with resistivities for materials already known (U.S. Environmental Protection Agency, 2016) Typical resistivity values as they were obtained from previous experiments are presented in the Figure 18.

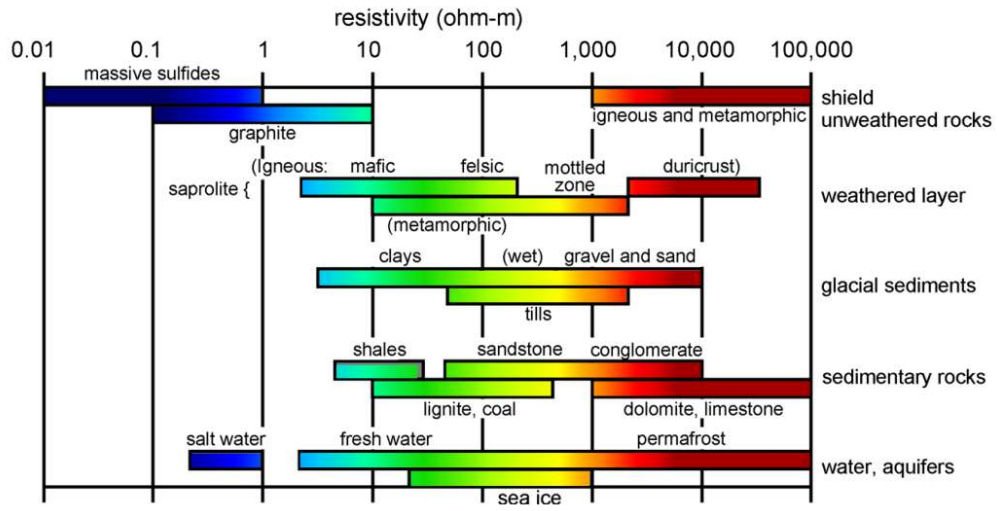

Figure 18 Range of resistivity on different types of material (Palacky, 1987) (modified)

Electrical Resistivity Tomography (ERT) or Subsurface Imaging (SSI) is an electrical resistivity method. It produces both a lateral and vertical variation in resistivity by using usually 50 electrodes divided in two strings of 25. They are connected by a multi-core cable where in the middle there is a switching box and resistance meter. The whole acquisition of the data sets is controlled by a laptop computer (Reynolds, 2011).

In electrical resistivity tomography is measured the “apparent resistivity of the ground to direct current flow”. It is the most used electrical resistivity method, because of

modern equipment and efficient electronics. The only thing required from the user is to implant many electrodes in the surface and the computer takes care of the rest.

Data acquisition

Depending on the location, the number of electrodes used, varied between 50 and 72 always with 5 m distance in between with dipole-dipole configuration as shown in the Figure18.

The data from the resistivity profiles were interpolated using 2D geophysical inversion software RES2DINV and interpreted manually in order to check the interfaces for the bedrock and groundwater table.

3.6 Conceptual aquifer model

According to Bredehoeft, (2005) a conceptual model gives the basic idea or constructed understanding of how systems and processes operate. Therefore, a conceptual model is the "cornerstone" of groundwater flow modelling. The data obtained from hydrogeological explorations, as well as information for geological background from literature, can be demonstrated in the conceptual model of groundwater flow. Hence, a conceptual model summarizes the gathered data and simplifies the topic, in order to investigate the system and the processes involved better (Betancur et al., 2012).

Boundary conditions, estimates of hydrogeological parameters, general directions of groundwater flow, sources and sinks of water and a field-based groundwater budget, essentially compose the conceptualization of the groundwater model (Anderson et al., 2015). Depending on the complexity of the hydrogeological systems some of the above aspects may not be applicable to the subsequent numerical model (Wagener et al., 2007).

As Anderson et al., (2015) states, "the model is always designed to answer a specific question or a set of questions ", and as reported by Kresic and Mikszewski, (2013), these major questions are among others the origin and the destination of the groundwater and the type of porous media through which it flows. Furthermore, the velocity and stored quantity of the groundwater, the previous behavior of the

groundwater system and the possibilities of natural or anthropogenic factors that will change it in the future, are questions that need to be answered. Thus, it is understandable that, if the conceptual model fits well the actual field data, the resulting numerical model will be more reliable to solve the problem under assessment.

The definition of the physical framework is the first step towards the conceptualization of the study area. According to Alley et al. (1999) several types of maps are potentially used for a conceptual model as for instance topographical maps helping to define the drainage network surface water bodies and water related activities. Furthermore, geological and hydrogeological maps that can inform the modeler about the deposits and bedrock and the boundary conditions of the aquifers respectively.

Moreover, critical for the construction of the conceptual model are the hydrological data. Such data are gathered mainly from precipitation and evaporation measurements, which are often managed and made available by environmental agencies of each country. Furthermore, according to Alley et al. (1999), maps of drainage network, estimates of discharge of the total groundwater to streams and measurements of spring discharge, surface water diversions and stream flows can be potentially used. Moreover, the history and spatial distribution of the pumping rates in aquifers among with the amount of groundwater consumption for different uses and how the return flows are distributed, are crucial data for the completion of the conceptual model. Crucial data is also the location of the recharge areas and maps presenting the hydraulic head (i.e. groundwater-level) of the aquifers.

3.6.1 Geographical Information System

Kresic and Mikszewski, (2013), state that living in the computer age has "revolutionized the fields of hydrogeology and environmental engineering". Hydrogeologist nowadays have not to be encumbered anymore with hand mapping, hand calculations and the most important hard-copy data storage by using geographical information system (GIS). GIS is the main tool to organize and analyze the gathered geological and hydrogeological data spatial in the nature. In addition, a GIS approach theoretically can build an environment of hydrogeological data

presented in 3D simulation of the actual world, having longitude, latitude and elevation (Kresic and Mikszewski, 2013).

Data acquisition

For the construction of the conceptual model of the Grindalsmoen aquifer a wide set of data was processed in the geographical information software QGIS (QGIS Development team, 2016). These data were obtained either from online sources or field observations and field work conducted in the area.

Topographical maps and digital elevation models were downloaded from Norwegian Mapping Authority and used to describe the topography of the area. Furthermore, as mentioned before based on the DEM file the catchment of Grindalsmoen aquifer was delineated. Finally, the DEM file was later used as top elevation in the numerical model of the groundwater flow.

In addition, well log data were imported after they were obtained, as mentioned before from Granada. This helped along with the geophysical data available, at the interpolation of the bedrock elevation. The interpolation method used for the bedrock elevation surface was a combination of inverse distance weighing (IDW), and nearest neighbor interpolation. IDW uses the existing values, to predict values around them, but due to the lack in the quantity of the existing values, a method like nearest neighbor interpolation was used, by adding manually values around the existing points with the knowledge of the topography and the thickness of the sediments.to obtain a bedrock elevation layer as smooth and accurate as possible. The interpolated layer was used as well in the numerical model as bottom elevation layer.

3.7 Groundwater Geochemistry

Groundwater geochemistry studies the geochemistry of groundwater and describe how it obtained its composition. The groundwater quality thus reflects the processes that controls groundwater's chemical composition. Contaminants may mobilize in groundwater and cause health problems. However, groundwater is generally of good quality, and well suited for human consumption. The groundwater quality can be

changed during long-term use or human activities, even if distinct results are not immediately, can affect it (Appelo and Postma, 2005).

A groundwater chemical analysis typically includes measurements for temperature, electrical conductivity, pH, alkalinity and the major cations (Ca^{+}, K^{+}, Mg^{+}, Na^{+}), as well as the major anions (Cl^{-}, NO^{-}_{3}, SO^{2-}_{4}, HCO^{-}_{3}) (Appelo and Postma, 2005). To certify its quality also other constitutes need to be analyzed according to the EC water Directive.

Typically, water analyses are used in maps showing how the water compositions are distributed regionally. Maps like these can be used to evaluate the aquifer mineralogy and how it can be related with the composition of the groundwater as well as to identify good groundwater quality aquifers (Appelo and Postma, 2005).

Besides groundwater water samples from Grindalsmoen aquifer there were taken surface water samples from streams as well as a drinking water sample from the station at the waterworks. The location of the groundwater and the surface water samples is shown at the map of Figure 19.

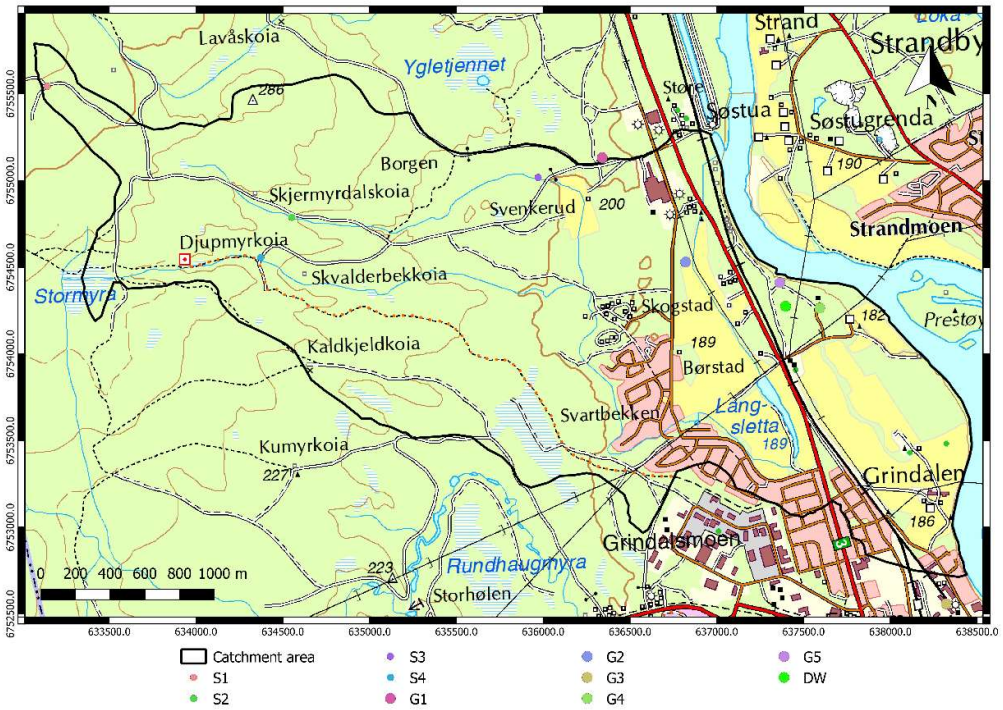

Figure 19 Map of the location of the water samples used for chemical analysis.

3.7.1 Groundwater Sampling

Groundwater sampling is of great importance in defining the hydrochemical conditions of an aquifer and the groundwater quality. To obtain a representative a water sample, the well or borehole needs to be flushed three or four times by removing the water in the well before sampling (Hiscock and Bense, 2014). This groundwater sampling protocol ensures that the sample pumped from the well is representative of the groundwater of the aquifer. The groundwater sampling can either be done by pumping or bailer. The pump may either be a submergible one, where water is lifted (as in most production wells) or by suction.

At Grindalsmoen, groundwater samples were collected from wells that were either already installed at the area or were drilled during the mentioned before course during June 2018.

The samples were mostly obtained with a peristatic pump while in some occasions the bailer sampling method was used.

Peristaltic Pump sampling

The principle of the operation of a peristaltic pump is to create a vacuum in an intake line to draw fluid (i.e. water) from a source. A mechanical peristaltic pump consists of a recharcheable electric motor. This motor powers a roller by squeezing a flexible tube to create that way a type of a displacement pump. During this alternating "compression and subsequent relaxation of the tube", fluid is being drawn in and pushed out of the other end of the tube (Grayline LLC, 2015).

While the pump rotates the fluid is pushed out and it keeps discharging (Grayline LLC, 2015). The operation can have pre-chosen pumping rate, or the pumping rate can be adjusted during the process and it continues until the fluid is discharged as long as the user needs.

For the groundwater samples obtained with a peristaltic pump in Grindalsmoen the tube of the discharge side of the pump was placed in a bucket. This created after a while steady state conditions to take the field measurements (i.e. pH, EC) as well as to take the sample.

Bailer sampling

According to Brassington (2007) the bailer sampler is the easiest device to get a groundwater sample from a borehole or a well. A bailer sampler is made of a plastic tube sealed at the bottom with weight, so it can sink. The process is quite simple as the tube is dropped down in the well attached with a string or a rope and it is filled with water.There was only one sample (sample G3) collected with the bailer method in Grindalsmoen, due to the limited size of the wells.

3.7.2 Field measurements

After obtained the water samples from either the peristaltic pump or the bailer sampler, it was followed a procedure to store the samples. This included first to be filtered so not to contain any particles, and stored in separate for inions and cations, to transfer to the lab later for further analysis. The sample for the cation analysis was acidified by adding 2-3 drops of HCl.

Electrical conductivity

Theory

Electrical conductivity (EC) measures the ability of a sample to conduct electric current through it, providing information about the amount of ions in the solution (Domenico and Schwartz, 1997). EC is measured in siemens per unit (i.e. µS/cm = µmho/cm) (Appelo and Postma, 2005).

Data acquisition

Figure 20 VWR PC 5000 L electrical conductivity meter

The measurements for the EC at Grindalsmoen were obtained by using a PC 5000 L electrical conductivity meter by VWR (Figure 20), which besides the EC measured the temperature of the water. Before the use of the EC meter it was calibrated with a standard solution to provide correct measurements. Furthermore, the probe of the measurement tool was rinsed, with distilled water, and dried with a wipe before and after every new sample measurement.

pH measurements

Theory

By measuring the pH basically, the acidity of the water is measured. The measurement is based on the concentration of the hydrogen ion present in the sample while mathematically is expressed as the negative logarithm of this concentration (pH= - log [H^+]). Higher pH means that the concentration of the hydrogen ion ([H^+]) is lower while lower pH means higher concentration of H^+. The pH of a sample is measured in pH units (0-14) with the pH for surface water to range from 6.5 to 8.5 and for groundwater 6 to 8.5 (Oram, 2014).

Data acquisition

pH was measured from several samples by using ORION model 250A pH meter. For this measuring instrument was applied almost the same protocol as the electrical conductivity measuring meter. Therefore, the instrument was calibrated with two standard solutions (pH 4. 7, and 10), before the use. Moreover, the probe was rinsed with distilled water and dried with wipes afterwards, before and after every sample measured.

3.7.3 Laboratory measurements

Alkalinity

Theory

As alkalinity of the water can be defined, the ability of an acid to neutralize to the solution. Titration is done on a filtered water sample. Alkalinity is measured either in meq/l , or in mg/l as a carbonate species (Rounds, 2012). Although, alkalinity is equal with the amount of all the dissociated weak acids, usually only the amount of the carbonate ions are important for measuring the alkalinity given by the eq. 3.14 (Appelo and Postma, 2005):

$$Alk \simeq m_{HC_3^-} + 2m_{CO_3^{2-}} \qquad \text{eq 3.14}$$

Data acquisition

The titration of the samples occurred with an auto-titrator, by constantly adding adjustable amount of HCl to the continuously stirring volume of the water sample. During the process the pH was measured constantly and as it was changing. This change was plotted corresponding to the volume of the added acid to create a curve. Afterwards, manually the point of the equivalence is found on the curve produced, with the alkalinity to be calculated in meq/l by the following eq:

$$A(meq/kgw) = 1000\frac{V_{Ep}N_{HCl}}{V_{smpl}} \quad \text{eq 3.15}$$

Where V is the volume of the water sample in ml, N is the molar strength, and subscripts Ep and smpl stand for end point and sample respectively.

Ion chromatography

Theory

With ion chromatography the ions are separated based on how they interact with a resin, so that their concentration is measured (Buckner, 2007). Therefore, the major ions and cations of the samples are determined.

The separation of the ionic species depends on their size and type. This occurs by the sample solutions passing through a chromatographic column, which is pressurized, with the ions to be absorbed there by the constituents of the column. Then the separation of the absorbed ions from the column begins while the eluent runs through it (Buckner, 2007). After the separation, through a conductivity detector the total ions are determined as electrical conductivity. Before the analysis of the sample a system calibration is required by having a standard solution as a reference. Thus, the data obtained from the sample can be compared with the initial solution and the ions are identified and evaluated within the sample. Eventually, a chromatogram is produced by a computer running showing the position of the peaks by converting each peak in it to a sample concentration (Naoroz, 2018).

Data acquisition

The water samples from Grindalsmoen were analyzed using Dionex ICS – 2000 Ion Chromatography system, for the major anions and cations. The machine uses chemical suppression of continuous eluent conductivity for the analysis to be conducted using 30 mM KOH as eluent.

Inductively coupled plasma mass spectrometry (ICP-MS)

Theory

Inductively coupled plasma mass spectrometry (ICP-MS) can identify and measure quantitatively a wide range of elements of the periodic table (Bazilio and Weinrich, 2012).

In ICP-MS first the sample is sprayed into a plasma where is dried out. “Singly-charged ions” are formed by the removal of an electron from the components, after the separation of the molecules. These ions are led to the mass spectrometer operating as a mass filtering device. There the ions are sorted by their mass-to-charge ratio. While exiting from the mass spectrometer and hit at the detector, it is released a “cascade of electrons” amplifying until they converted into a pulse that is measured. Then, the measured intensities of the pulses are compared with the references by a software. Finally, a calibration curve is produce to measure the concentration of the elements (PerkinElmer Inc., 2010).

Data acquisition

ICP-MS was used to determine the heavy metals in solutions in the water samples from Grindalsmoen.

The instrument used for the ICP-MS analysis is Aurora Elite M-90 by Bruker Daltonics, equipped with a Cetac ASX-250 autosampler and an ESI oneFAST sample introduction system. All the samples were first centrifuged to prevent existence of particles in the solution and afterwards diluted with 1% single distilled nitric acid (HNO_3). The samples from Grindalsmoen were analyzed for the following isotopes:

^{27}Al, ^{31}P, ^{55}Mn, ^{63}Cu, ^{66}Zn, ^{75}As, ^{111}Cd, ^{137}Ba, $^{206,207,208}Pb$, ^{57}Fe, ^{75}As, ^{121}Sb, by Magnus Kristoffersen at the ICP-MS laboratory of University of Oslo.

Although the samples were analyzed for the above isotopes, only the iron and manganese isotopes will be discussed in the current master thesis.

4 Numerical model of the groundwater flow

4.1 Mathematical background

The governing equation that is used in groundwater flow modelling embodies all the necessary simplifying assumptions for the mathematical representation of the hydrogeologic processes taken place. For representing the flow of water under Darcy's law in a continuous porous media, the governing equation is derived by considering a large enough cube of porous material. This cube represents the properties of the porous media and it is noted as representative elementary volume (REV) with volume ΔxΔyΔz (Figure 21) (Anderson et al., 2015).

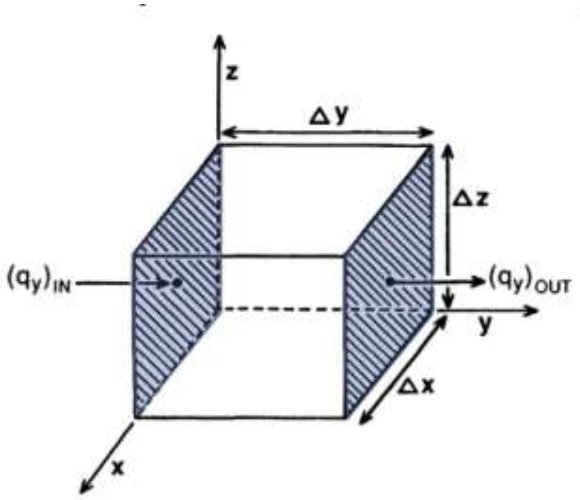

Figure 21 Components of the flow along y axis by representative elementary volume (REV) (ΔxΔyΔz) (Anderson et al., 2015).

After several mathematical operations and by combining Darcy's law and water mass balance equation, the governing equation for the groundwater flow was derived, representing in heterogeneous and anisotropic conditions a 3D transient groundwater flow is the following:

$$\frac{\delta}{\delta x}\left(K_x \frac{dh}{dx}\right) + \frac{d}{dy}\left(K_y \frac{dh}{dy}\right) + \frac{d}{dz}\left(K_z \frac{dh}{dz}\right) = S_s \frac{dh}{dt} - W^* \qquad \text{eq. 4.1.}$$

Where h is the hydraulic head that is the "variable of interest", x,y,z and t are the independent variables. K_x, K_z, K_y, are hydraulic conductivities with the subscripts

denoting anisotropic conditions, meaning that hydraulic conductivity can differentiate with directions. Furthermore, S_s is the specific storage and W^* is the volumetric inflow rate from sources and sinks (Anderson et al., 2015).

Although eq. 4.1, is the one used the most for numerical groundwater flow simulations, it is simplified when there are steady state conditions ($\delta h/\delta t = 0$) or/and there is a 2D model.

For a 2D model in an anisotropic, heterogenous, unconfined aquifer the differential equation is:

$$\frac{\delta}{\delta x}\left(K_x h \frac{dh}{dx}\right) + \frac{d}{dy}\left(K_y h \frac{dh}{dy}\right) = S_y \frac{dh}{dt} - R \qquad \text{eq. 4.2}$$

Where R is the recharge rate and S_y is the specific yield. In addition h is the head that is the flux expressed as volume of water per area of aquifer per time, (L/T), h the head (Anderson et al., 2015).

4.2 Modflow

There is a variety of software used for the computation of the above equations related with the groundwater flow modeling. The methods used by these software are the Finite difference method (FDM), the Finite element method (FEM) and the Analytic element method (AEM) (Fitts, 2013).

For the modeling of the groundwater flow of the Grindalsmoen aquifer MODFLOW-2005 (Harbaugh, 2005) was used with the graphical user interface (GUI) of Groundwater modeling system, GMS 10.3 (Aquaveo LLC, 2017). The method MODFLOW-2005 uses, is the finite difference method. The first version of MODFLOW was developed in 1984 by McDonald and Harbaugh and today the latest version is the most commonly used (Fitts, 2013).

Based on conservation of mass and Darcy's law, the series of the algebraic equations used by finite difference method, are computed within an orthogonal network of nodes for unknown heads individually for those nodes. The result is a grid of cells, that each cell's physical properties (K_x, K_y, K_z and S) are homogenous (Fitts, 2013).

In order to have a more accurate results at a location, the dimensions of the cells within the grid can vary (Figure 22).

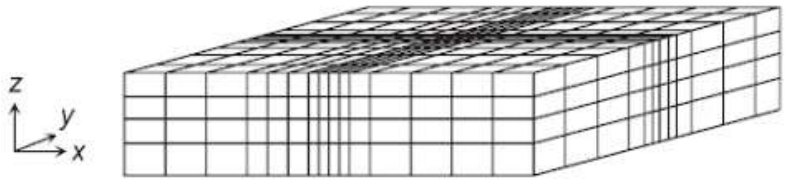

Figure 22. Grid with different dimensions of cells (Fitts, 2013)

4.3 Modeling strategy

After constructing the conceptual model of the aquifer in QGIS the polygons created were imported and used in GMS. The initial though was to develop a groundwater flow model in MODFLOW covering the whole catchment area. Nevertheless, due to the small thickness of the sediments in parts of the aquifer, the model had converging problems due to the dry cells.

The model was eventually cut and the recharge from the recharge corresponding to the cut part of the model was introduced by assigning constant flux along the boundary with injection wells. The injection rate of the wells representing the flux was assigned after delineating two smaller catchments in the cut area showing approximately how the flux would be distributed on the wells.

A sensitivity analysis was performed at the hydrogeological parameters to investigate the range of the values. These values are used later as limits in the calibration of the model. The calibration targets were chosen from water table measurements and the calibration was conducted by assigning the parameters to into zones with different values. Eventually, after performing a calibration on the model the scenarios were run. The modeling procedure can be shown in the flow chart below (Figure 23).

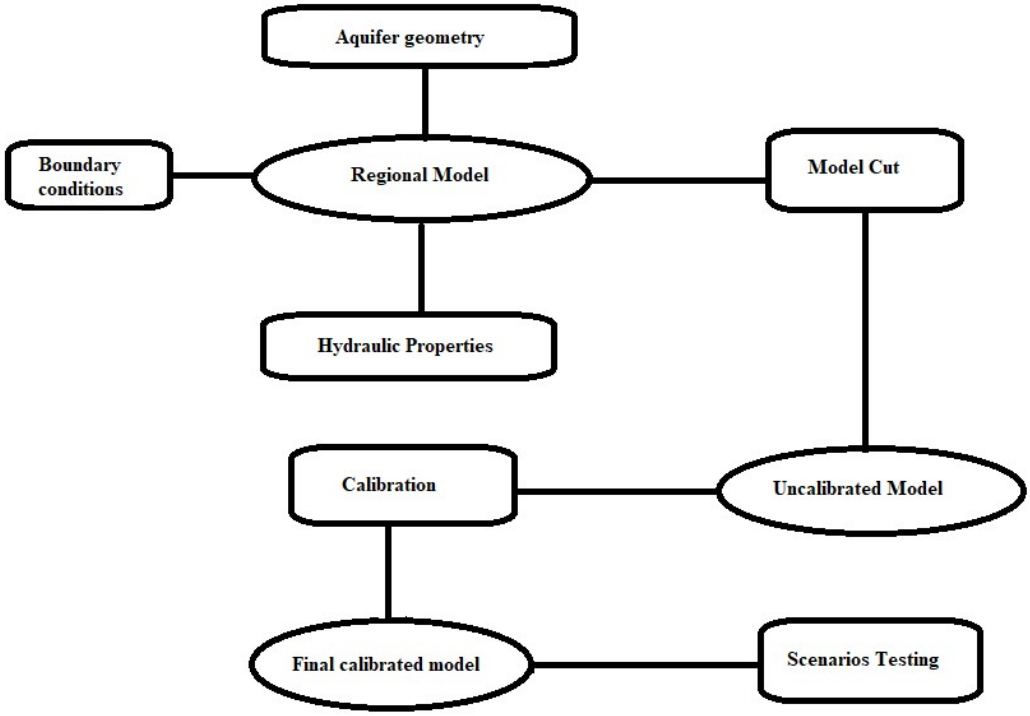

Figure 23 Description of the modeling procedure with a flow chart.

4.4 Model geometry and extent

The model geometry was decided after studying all the available data for the depth to the bedrock. The data included geophysical investigations, well logs available from NGU and reports from the authorities of the new road constructed in the area. Furthermore, the elevation of the model was taken from the DEM file of the area. Finally, a one-layer model was created with a 30 x 30 meters grid dimensions.

By trial and error, it was selected an area in the aquifer where the thickness of the aquifer was enough to avoid dry cell problems taking into consideration the groundwater provided by the area eliminated from the model.

The cut of the model was performed at the equipotential elevation line of 225 masl, the, at upper western boundary of glaciofluvial sediments. Furthermore, another reason except the geology, is that the groundwater flows from the higher area in map towards east to river Glomma. Therefore, equipotential lines of the hydraulic heads will be, more or less parallel to the elevation contour lines. This is a very common case, especially when modeling unconfined aquifers. Moreover, when a model cut

needs performed, at location other than the aquifer's physical boundary the cut occurs either at an elevation contour line or perpendicularly to it.

4.5 Boundary conditions

4.5.1 Theory

The locations that water flows into or out of the region of the model because of external factors are represented by boundary conditions (Winston, 2019). There are three types of boundary conditions in groundwater flow models as they are classified mathematically: Specified flow boundary, Specified head boundary and Head – dependent boundary (Anderson et al., 2015).

The specified head boundary (Dirichlet conditions), is the boundary that the head of the boundary cell is set beforehand as a known value. The flow across the boundary is computed as the head across a section of the boundary is specified (Barnett et al., 2012)

The specified flow boundary (Neumann conditions), is the boundary where the derived head is specified. In other words, the hydraulic head's gradient is specified at the boundary, indicating that across the boundary the flow rate is specified (Barnett et al., 2012).

The boundaries at which the flux is set to zero are characterized as no- flow boundaries, indicating impermeable boundaries with inactive cells. In MODFLOW it is considered as a no-flow boundary the grid's perimeter (Kresic, 2007).

The head - dependent boundary (Cauchy conditions), according to Darcy's law and by using a gradient that is computed by the difference of the specified head out of the boundary, the head is computed at the node near or on the boundary (Anderson et al., 2015).

In the numerical model of the groundwater flow developed for the Grindalsmoen aquifer, all the above boundaries were applied with the form of "packages" in MODFLOW.

4.5.2 Glomma Boundary

The eastern boundary of the regional model developed, is the river Glomma, where along the river banks a specified head boundary (CHD package) was assigned. The hydraulic heads along the river were generated from GMS with a linear interpolation of the values of the north and south limits of the river. The values for the north and south limits of the river were assigned from measurements of the water table of river Glomma during the field expedition on June 2018.

4.5.3 Streams

The streams were modeled as rivers. Initially it was intended to be modeled as drains using the Drain package (DRN) however the streams, seemed to feed water the into the aquifer and not only drain water from it. Therefore, the package used in MODFLOW was the RIV. The water level along the stream line was measured in some points during the field course on June 2018.

4.5.4 No flow boundary

The side boundaries that represent the topographic drainage area divides were defined as no-flow boundaries.

4.5.5 Lake

Lake Langsletta was modeled as general head boundary (GHB package). The starting head of the lake was measured during the field course on June 2018.

4.5.6 Western boundary

At the western boundary of the model there was assigned the calculated flux from the cut area due to recharge associated with precipitation by adding the amount of recharge along all the border defining the flux for each cell.

4.6 Assignment of hydrogeological properties

4.6.1 Recharge

The recharge value assigned to the model in GMS was the one that NEVINA report estimated.

4.6.2 Porosity

Porosity is not used by MODFLOW equation (eq 4.1). It is only needed when modeling the transport. Nevertheless, GMS allows the modeler to assign the value of porosity in case of modeling transport later. Therefore, porosity value was homogeneously assigned to the whole grid without affecting the flow, and in case it was decided to do transport. The chosen value was after taking under consideration Alfnes et al. (2003) at Gardermoen project where the sediments were similar with this case.

4.6.3 Hydraulic conductivity

Hydraulic conductivity was assigned in zones. The assignment and the differentiation were decided mainly based on the sediments and in the progress from the sensitivity analysis and the calibration of the model.

4.6.4 Anisotropy of the hydraulic conductivity

The anisotropy of the hydraulic conductivity was used as a parameter on the model since there was built a one-layer model. Initially before the calibration there were assigned two different values for the anisotropy (based on sediment type) of the hydraulic conductivity based on the case in Gardermoen (Alfnes et al., 2003). There the sediments have similarities with the sediments at Grindalsmoen. Nevertheless, while calibrating the model it was decided to use more zones of values depending on sediments, to be calibrated.

4.7 Calibration

For the calibration of the model there were used observed groundwater data obtained during the field work and from the results of the geophysical surveys. Furthermore, the areas with bogs are considered flooded by groundwater and therefore can be assumed as indicators of the groundwater table. Therefore, the elevation from the digital elevation model was obtained for the bogs and was used as groundwater table data. The location of the calibration targets is presented in the map of Figure 24. The calibration of the model was done without the pumping at the Grindalsmoen waterworks.

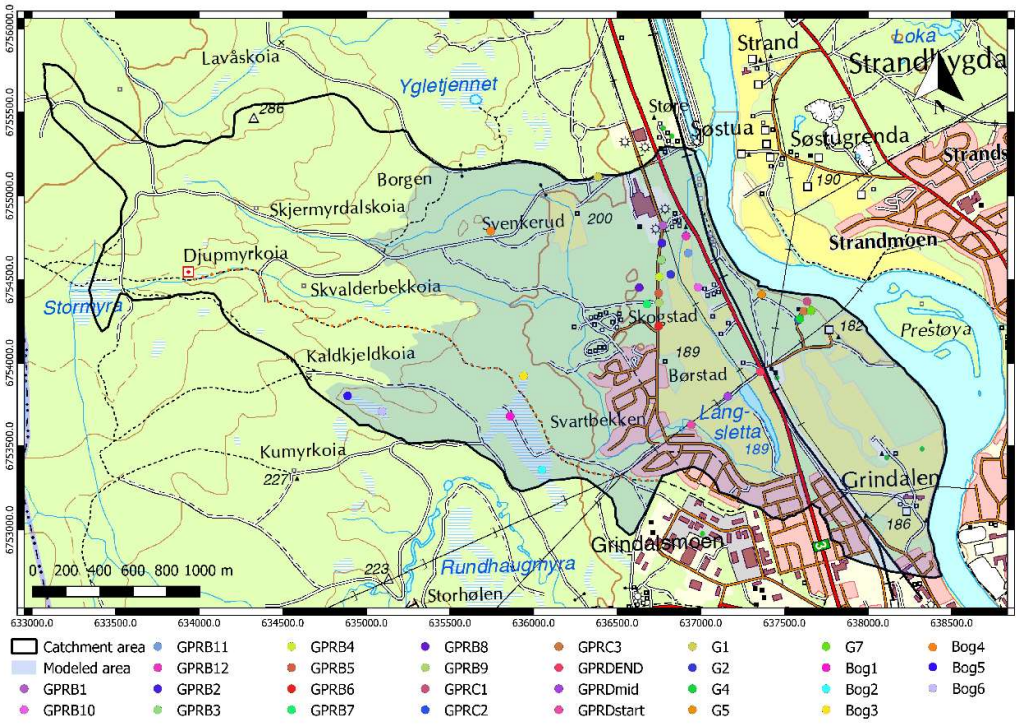

Figure 24 Map of the calibration targets used for the calibration of the model.

After importing the observation points at the model, there was used automated parameter estimation with PEST (parameter estimation) (Doherty, 2003), using a nonlinear parameter estimation algorithm to assist in the data interpretation and the model calibration (AQUAVEO, 2017).

The parameters used for the calibration of the model were the hydraulic conductivity values for the different zones (based on different sediment types) assigned as well as the anisotropy of the hydraulic conductivity values. The minimum and maximum

limits of the values calibrated were adjusted every time after each run, depending on the calibration results and the returned values, to obtain the best fitting value possible.

4.8 Modeling different scenarios

The calibrated model was used to explore the way the system would react to the increase of pumping rate due to increasing needs of water and to investigate the possibility of groundwater entering the system from the northern boundary, because the modeled area represents just the catchment of the surface water. Moreover, the old piezometric map from Gaut et al. (1981) (Figure 5) indicated that there is flux from the north outside of the catchment.

The scenarios modeled include:

- Increase of the pumping rate of the supplying wells in the water works. The total pumping rate was increased 50 % to investigate how the aquifer reacts to the increased pumping in case of future population growth.

- Investigation of the possibility for flux coming from the northern border. A set of injection wells was installed at the northern no-flow boundary of the model injecting water in the system representing the possible flux from the northern boundary.

- Investigation of how the model reacts with the inflow from the northern boundary, and after assigning the current pumping rate to the wells of the Grindalsmoen waterworks.

5 Results

5.1 Water balance

5.1.1 Catchment

The delineated catchment covers an area of approximately 7.7 km2 (Figure 25). The catchment gives an indication of the area that is modeled but it doesn't necessarily imply to the physical boundaries of the of the aquifer.

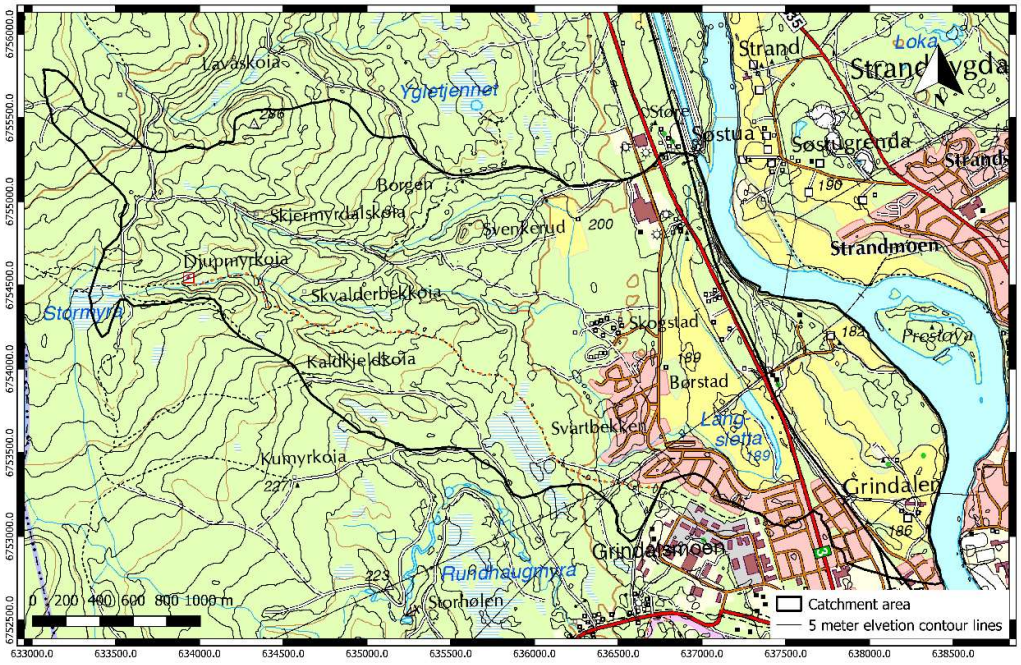

Figure 25 Map of the catchment area of the Grindalsmoen aquifer

5.1.2 Precipitation

Precipitation data were obtained from the meteorological station of Fagertun in Elverum, that was in operation from 1978 – 2013, from whom all the years were used. Furthermore, the data from the near meteorological station of Stavsberg in Hamar that is around 30 km west of the study area, have recovered for the last 10 years. The mean monthly precipitation from both stations was calculated and the results are presented for comparison (Figure 26).

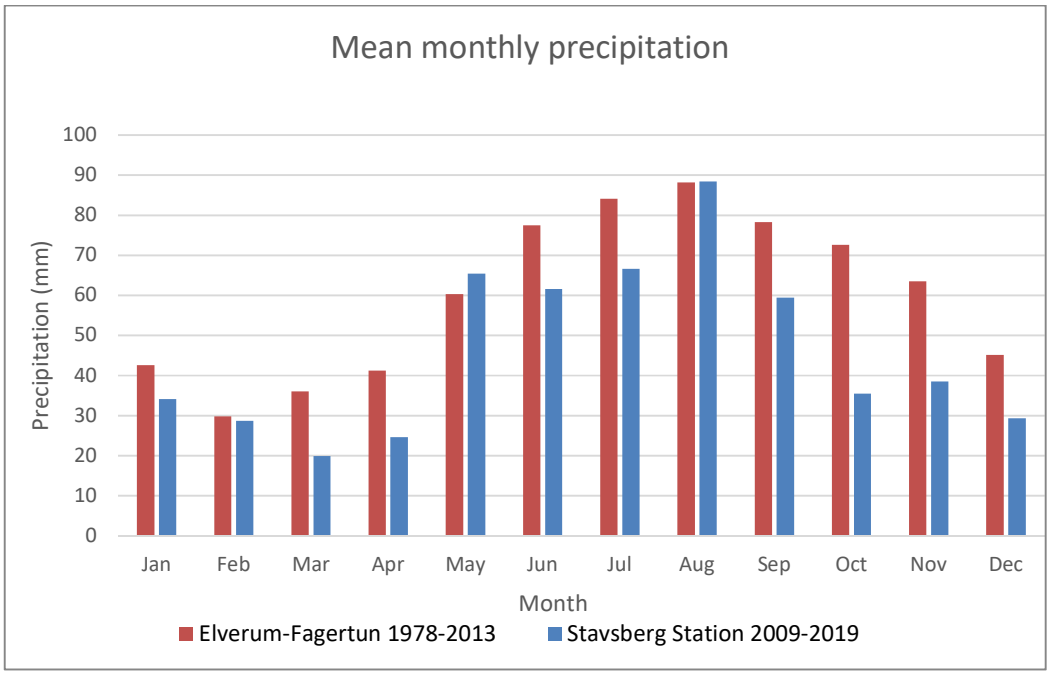

Figure 26 Graph showing the mean monthly precipitation data from Fagertun and Stavsberg stations.

The trend of the precipitation is similar for most of the years with the precipitation at the Stavsberg station to be less in most of the months. The annual average precipitation from the Stavsberg station was calculated to be 575 mm, while from the Elverum-Fagertun station 642mm.

Nevertheless, it was decided to use the results that were obtained and from NVE's NEVINA web tool for the chosen catchment area of Grindalsmoen, where the annual precipitation value was estimated to be 660 mm, with summer precipitation of 359 mm, and 302 mm during the winter.

5.1.3 Temperature and Evapotranspiration

Elverum Fagertun station is a precipitation station and does not have measurements for the temperature. However, to represent the Elverum area it was used the temperature record from the Norwegian forest museum situated at Elverum at the Glomma banks and only 5 km away the Fagertun station. The record from Stavsberg, Hamar, is complete.

The mean temperature data for the last 10 years for both the stations (Figure 27) show that the temperature in the area is below 0 from December until March. The average

annual temperature for the last 10 years in Stavsberg was calculated to be 5.13 ºC, while in Elverum 5.18 ºC.

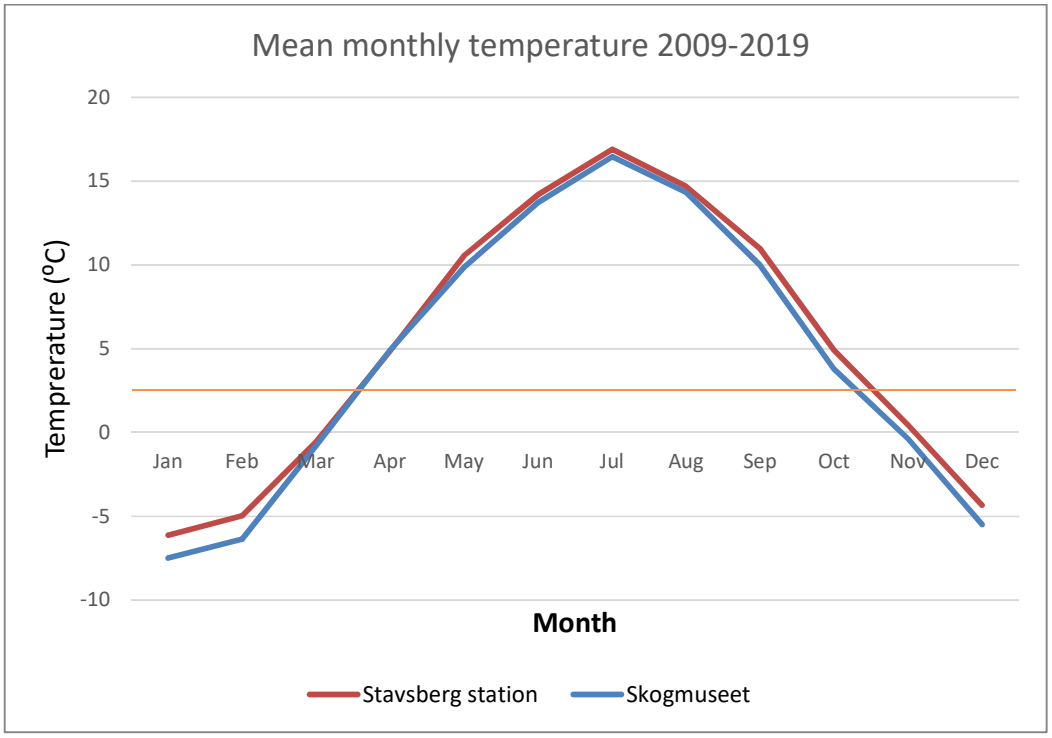

Figure 27 Mean monthly temperature data from the two stations with the orange line representing the mean annual temperature obtained from the NEVINA report.

From the NEVINA report the mean annual temperature is 2.6 ºC. During the winter months is -3.9 ºC, the summer is 11.7 ºC and in July and August 13.5 and 14.3 ºC respectively.

The annual evapotranspiration value according to NEVINA's report generated for the catchment area of Grindalsmoen was calculated to be 376 mm.

5.1.4 Recharge

The annual recharge was calculated from NEVINA to a total value for the area of Grindalsmoen to be 284 mm (Figures B6, B7 in Appendices).

5.1.5 Groundwater table

The groundwater level was obtained from piezometric measurements, GPR and ERT surveys as mentioned in the methods chapter. The location of the measurements is

shown at the map of the Figure 13. Ideally all groundwater level data, should be obtained for the same time period, however they are taken from two campaigns (June and October 2018).

The groundwater level measurements were used for the later calibration of the numerical model of the groundwater flow.

Groundwater table field measurements

Although there were several water table data from literature, due to the chronological difference only the groundwater table measurements conducted during the field work and the field course, were taken under consideration. The location of the measurements is presented in the map of the Figure 28, while the groundwater table measurements are presented at Table A1 in appendices.

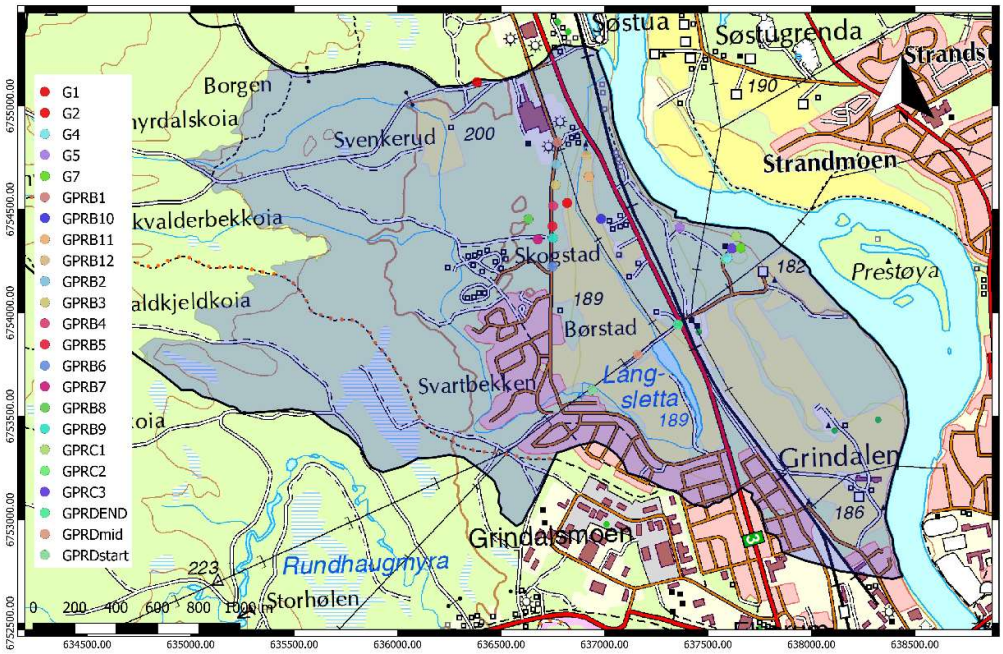

Figure 28 Map of the location of the groundwater table measurements.

Electrical Resistivity Tomography

ERT profiles were used mostly to compare the results with GPR. After interpreting the ERT profiles based on the relative resistivity values, the groundwater table was defined in most of the locations where the ERT surveys were conducted.

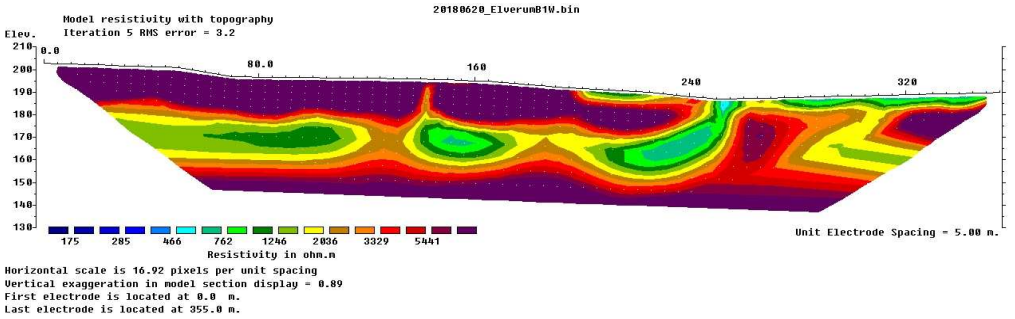

Figure 29 Interpreted data showing the relative resistivity from the area of Skogstad in Grindalsmoen.

The presented ERT profile (Figure 29) was taken at the area of Skogstad (Figure 13). According to the known resistivity ranges, it seems that the water table is around 170 m. At the 260m of the profile the anomaly occurring at the resistivity is due an artificial pipe.

Ground Penetration Radar

The GPR profiles obtained from the mentioned before field course in the area, showed the reflector of the groundwater table at the location conducted (Figure 13). At the presented GPR profile (Figure 30), the red line represents the saturated zone and as a result the groundwater table.

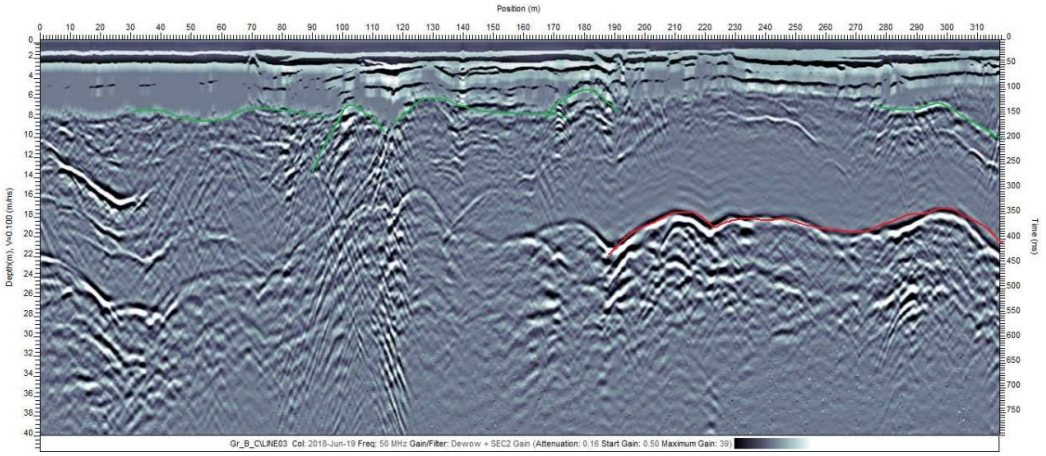

Figure 30 GPRB profile showing the depth to depth to the water table with the green and the bedrock with red color.

The above GPR profile was taken from the area near the lake Langsletta (Figure 13) showing the bedrock to be at 18 – 22 m depth.

5.2 Aquifer geometry

This section will present the results for the geometry of the Grindalsmoen aquifer as they were obtained after processed the available data.

5.2.1 Bedrock elevation

The bedrock elevation is one of the most important steps in hydrogeological investigations as it often represents the aquifer bottom boundary. The bedrock surface of Grindalsmoen, i.e. the lower boundary of the aquifer was defined after interpreting the data from the geophysical investigations available in the area, by field observation and well log data. The location of the available depths to the bedrock is presented in the map of the Figure 31.

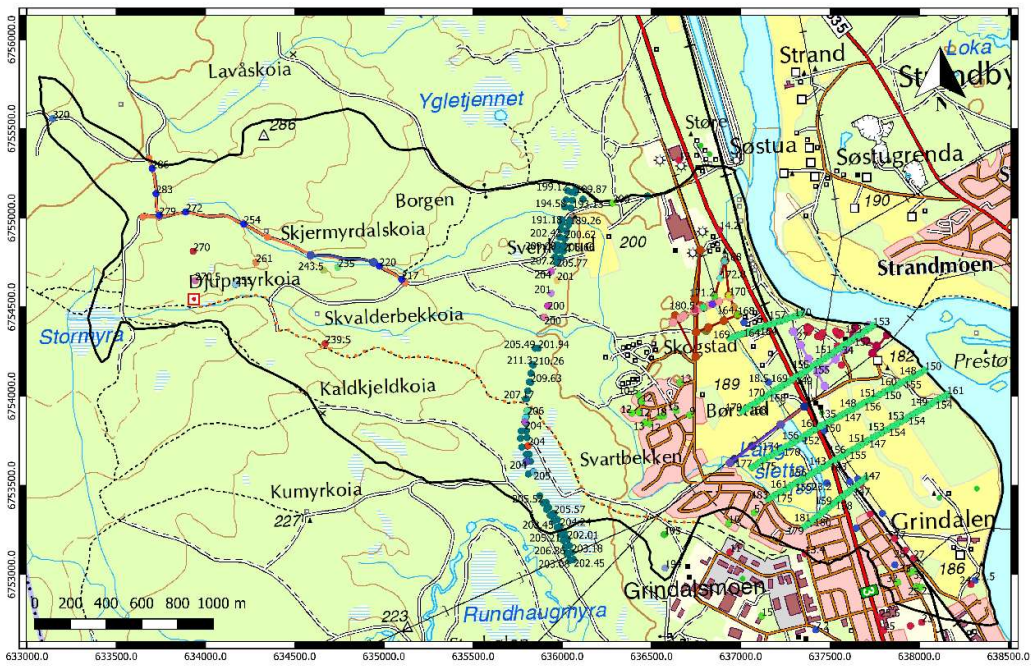

Figure 31 Map with the location and the elevation (masl) of the known bedrock elevation.

Geophysical investigations

Electrical Resistivity Tomography

The interpretation of the relative resistivity values was conducted, but it was used in most of the cases to compare with the GPR profiles because the surveys were

conducted almost in the same location. An example of an ERT profile is presented in the Figure 29. This ERT profile, shows that according to the known resistivity ranges, the elevation of bedrock to seems to be around 150-158 masl.

Ground Penetration Radar

The GPR profiles were critical for the definition of the bedrock elevation. From the GPR profile presented earlier (Figure 30), shows the shallow depth of the water table (~ 6m) with green color in this location. Furthermore, the results from the available processed data from Kalskin and Hilmo (1999) are presented in Figres A16-A21 in appendices

Seismic refraction

The data for the seismic refraction were mostly at the same location where the GPR were conducted. Therefore, there were not used a lot because there were not provided a lot of data. Nevertheless, from the seismic data at the area of the waterworks, interpreted by the students of the course the thickness of the first layer to was 8.90 m (Figure A22 in appendices).

Well logs and field observations

The information from the wells obtained from NGU (Granada database) was very useful as well for the definition of the bedrock elevation with the location and the depths to the bedrock of the wells to be shown on the map of the Figure 10.

Furthermore, field observations from bedrock outcrops and thin sediments, especially on the western part of the catchment area were useful to define the bedrock elevation.

5.2.2 Sediment thickness

With the digital elevation model (DEM) representing the top of the sediments, it was produced a sediment thickness layer (Figure 32) by using raster calculator in QGIS and subtracting the bedrock elevation from the DEM.

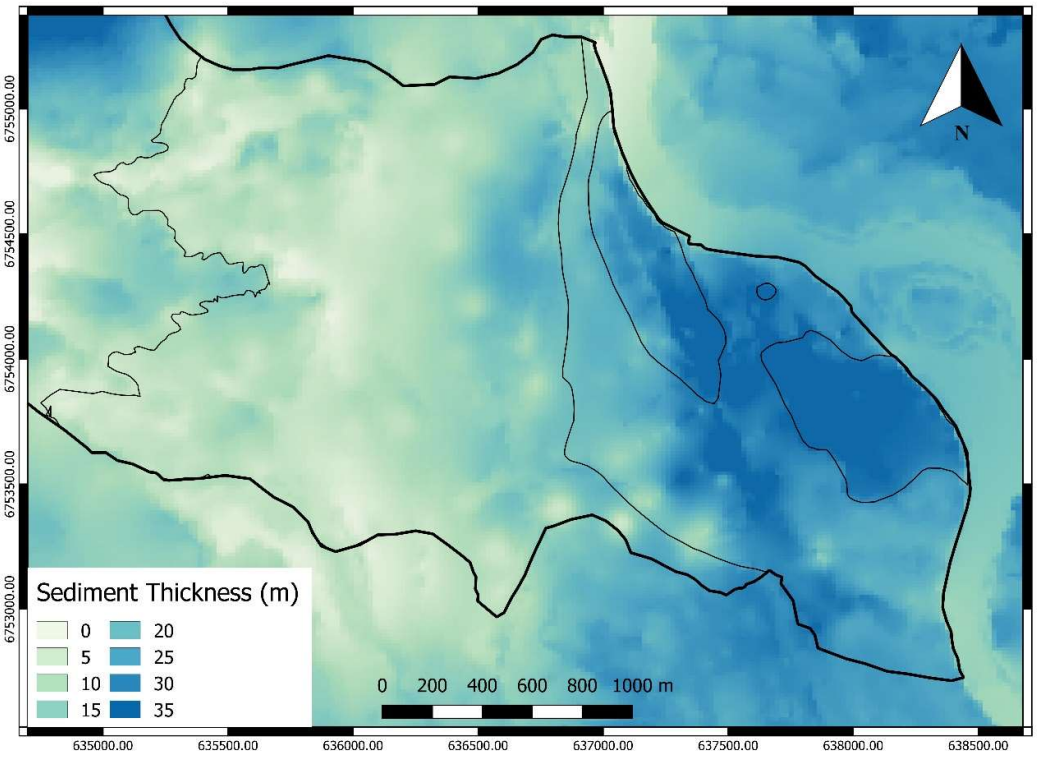

Figure 32 Thickness of the sediments of Grindalsmoen area. The areas outside the modeled area may have uncertainties due to the lack of bedrock elevation measurements.

The thickness in the western part is very small starting from 1m reaching barely the 7 meters thickness. Moving to the east towards the middle of the catchment and into the glaciofluvial sediments begin the thickness of the aquifer starts to increase gradually and eventually reaches a depth of around 35 meters at the area of the waterworks.

5.3 Aquifer properties or Hydrogeological parameters

5.3.1 Hydraulic conductivity

The results and the location of the obtained hydraulic conductivity values depending on the method applied, are presented in the following sections more extended in tables.

Infiltration tests

The hydraulic conductivity values obtained from the infiltration tests conducted in the area during the field course in June 2018 are presented on the Table 5.

Table 5 Results and locations of the infiltration tests conducted in the area of Grindalsmoen.

Infiltration Test	UTMX	UTMY	K(m/s)	K (m/d)
Inf.GRA1	634292.40	6754949.15	1.66E-04	1.44E+01
Inf.GRA2	635976.60	6754904.49	1.32E-05	1.14E+00
Inf.GRB1	636749.00	6754494.00	1.70E-04	1.47E+01
Inf.GRB2	636820.00	6754530.00	3.16E-06	2.73E-01
Inf.GRC1	637593.06	6754263.36	4.66E-05	4.02E+00
Inf.GRC2	637665.05	6754320.28	1.62E-04	1.40E+01
Inf.GRD1	637106.31	6753732.64	1.10E-04	9.50E+00
Inf.GRD2	637186.23	6753787.55	1.63E-03	1.41E+02

Slug test – Hvorslev's analysis method

The slug tests conducted in the area gave the hydraulic conductivity values. The values were obtained from slug tests from the years 2018 and 2019 and are presented on the Table 16, with the location of the slug tests.

Table 6 Results of hydraulic coductivity obtained from slug tests by location.

Slug test	UTMX	UTMY	K (m/s)	K (m/d)
Slug test GRA-2018	636340.13	6755132.04	3.36E-08	2.91E-03
Slug test GRB-2018	636820.00	6754530.00	2.91E-09	2.52E-04
Lerkeveien Well 2019	636139.10	6754418.10	1.26E-07	1.09E-02

The hydraulic conductivity values from the slug tests are very low. The slug tests were conducted by the students, so maybe due to the lack of experience there might be inherit problems.

Pumping Test

The pumping tests that took place in Ydalir that is located on the other side of the river. The transmissivity value from the data provided by Gjengedal in prep., was calculated to be 1.43E-03 m^2/s and the thickness of the saturated thickness 3m. Therefore, the hydraulic conductivity from the pumping test was calculated to be 4.7E-04 m/s (4.0E+01 m/d).

Furthermore, the data from the long-term pumping by Knudsen (1985) were interpreted and are presented, to have an approximation for the hydraulic conductivity at the area of Grindalsmoen waterworks.

The hydraulic conductivity values from the pumping test as well as the approximate values of the Grindalsmoen waterworks pumping test are in a range of 2.39E-05 m/s (2.07E+00 m/d) to 1.11E-03 m/s (9.59E+01 m/d).

Grain size analysis

The location of the soil samples is shown on the map of the Figure 33. For the samples of the field course there was used Hazen's method while for the samples from the new road there were used both Gustafson's and Hazen's methods.

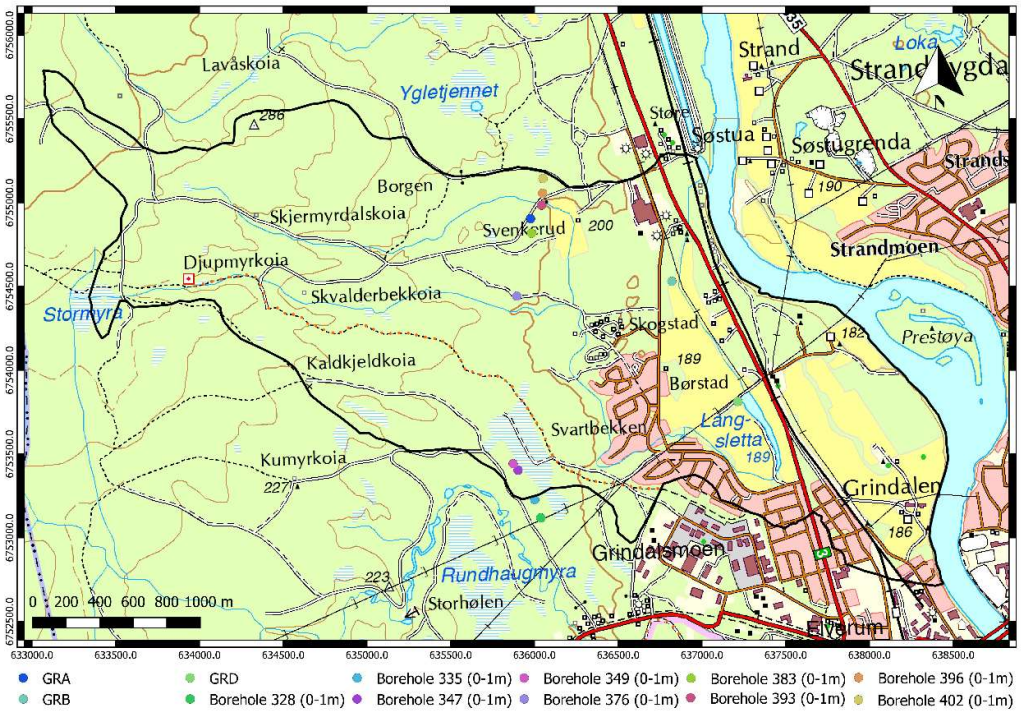

Figure 33 Map with the locations of the samples for the grain size analysis.

The obtained hydraulic conductivity values estimated from the Hazen and Gustafson methods are presented in the Table 7.

Table 7 Hydraulic conductivity values as they were obtained from Hazen and Gustafson methods.

	Hazen K		Gustafson K	
Sample	m/s	m/d	m/s	m/d
GRA	3.00E-05	2.59E+00	-	-
GRB	2.30E-04	1.99E+01	-	-
GRD	4.90E-05	4.23E+00	-	-
Borehole 328 (0-1m)	1.04E-05	8.99E-01	2.94E-05	2.54E+00
Borehole 335 (0-1m)	4.63E-06	4.00E-01	4.20E-03	3.63E+02
Borehole 347 (0-1m)	1.67E-06	1.44E-01	1.04E-03	8.99E+01
Borehole 349 (0-1m)	2.34E-05	2.02E+00	2.29E-05	1.98E+00
Borehole 376 (0-1m)	2.60E-06	2.25E-01	4.77E-05	4.12E+00
Borehole 383 (0-1m)	3.75E-06	3.24E-01	1.28E-05	1.11E+00
Borehole 393 (0-1m)	1.26E-05	1.09E+00	2.88E-05	2.49E+00
Borehole 396 (0-1m)	4.59E-05	3.97E+00	1.30E-04	1.12E+01
Borehole 402 (0-1m)	4.59E-05	3.97E+00	8.42E-04	7.27E+01

5.4 Numerical modeling

5.4.1 Regional model

The result of the initial simulation before the cut of the model is presented in the Figure 34 to show the extend of the problem while the new modeled area as it was explained in chapter 4.4 is presented in Figure 35.

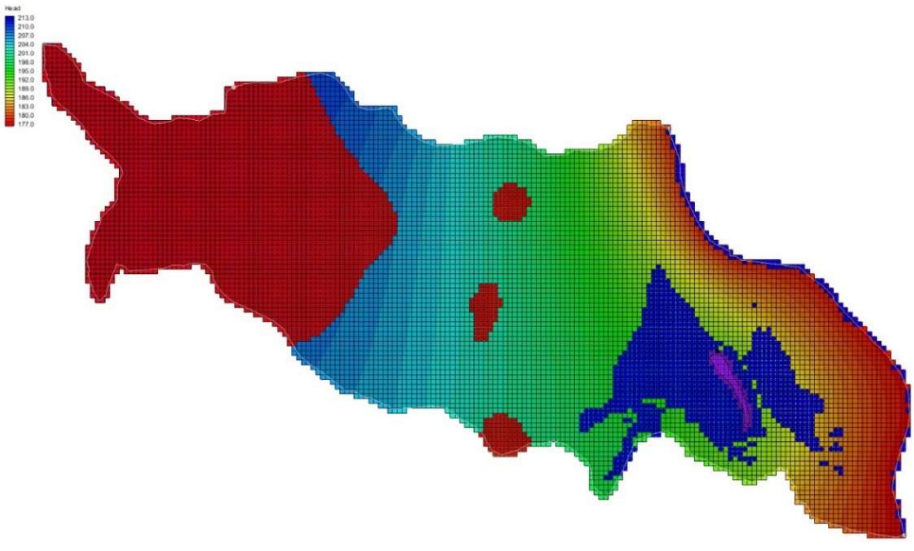

Figure 34 Groundwater flow simulation in GMS showing the many dry cells generated with red and the flooded areas with blue.

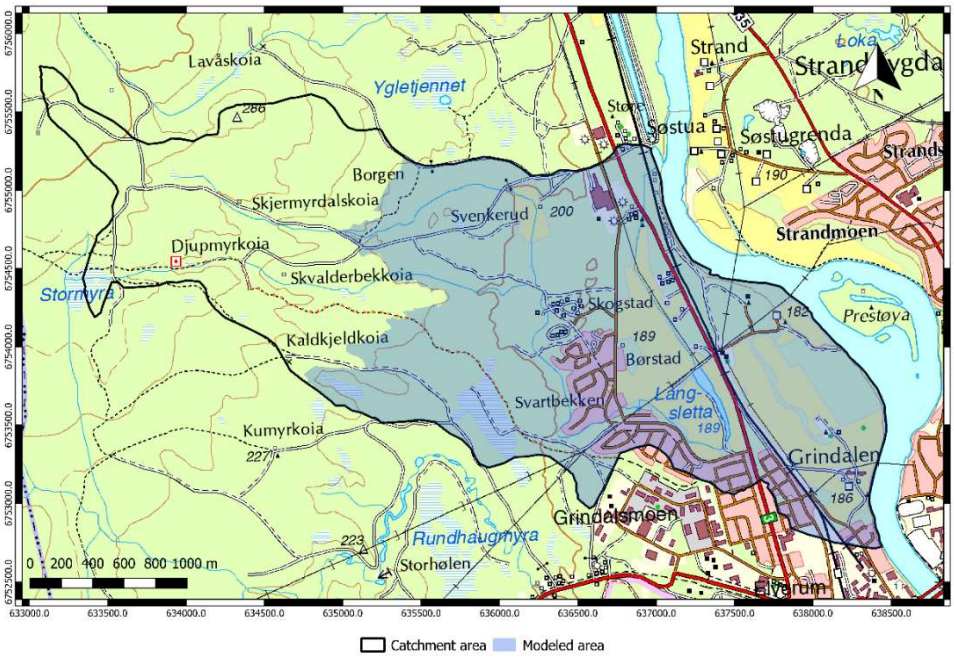

Figure 35 Map showing the new modeled area after the cut of the western part of the catchment.

5.4.2 Boundary conditions

The boundary conditions as they were assigned are presented in Figure 36. The physical boundaries surrounding the catchment area, except the river Glomma and the western boundary, were modeled as no flow boundaries.

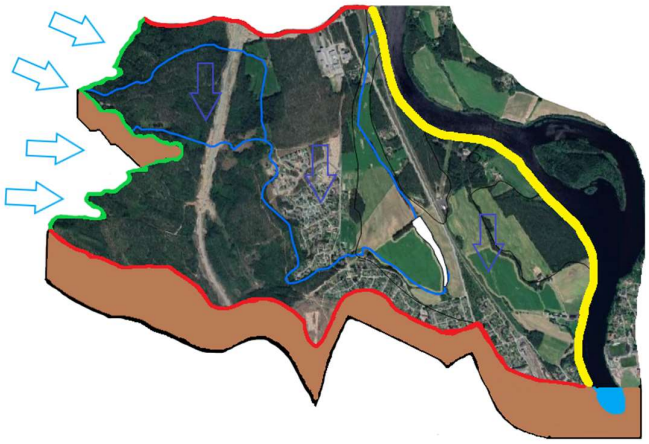

Figure 36 Conceptual model of the area showing with yellow the Specified head (river Glomma), The red color represents the no flow boundary. The western boundary is with green, the streams with blue modeled as rivers and the General head boundary (lake Langsletta) with white. The blue light blue arrows represent the flow from the western cut area while the darker blue the recharge.

Western boundary

Because the catchment area was cut, the recharge from the western cut area was assigned as a flux boundary by adding injection wells across the western boundary.

The recharge was calculated by multiplying the estimated value obtained from NEVINA with the number of the cells and the area of each cell. The obtained number from this calculation is 1963.494 m^3/d.

Initially the flux was distributed evenly to every cell but due to extremely high head values, giving flooding the south-western part of the boundary. Investigating further the sub-catchments of the area it was found that most of the water ends up on the upper part of the western boundary (Figure 37). Therefore, the flux was distributed to the wells with more weight to the wells corresponding to the northern part of the boundary.

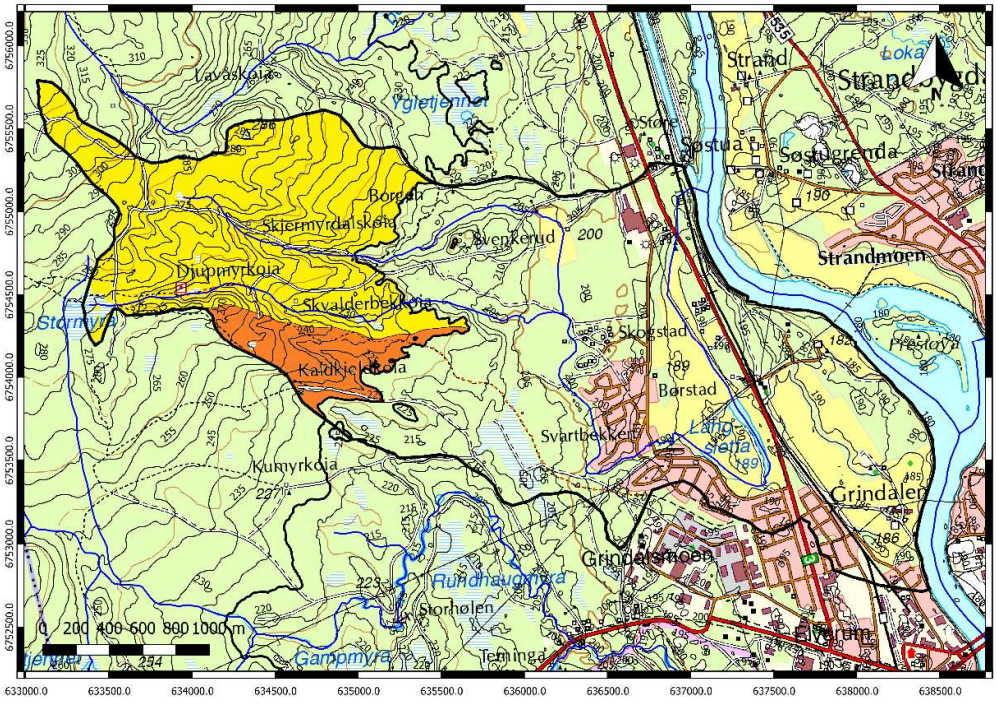

Figure 37. Map with the two smaller catchments ending up to the modeled catchment area.

The flux assigned to the wells corresponding to the smaller catchment was 25 % of the total recharge of the western cut part although the water ending to it seems to be

even less. This was decided after running several simulations with the model not to converge with lower values at those wells

For the upper part of the western boundary instead of the remaining 75 % of the total flux, there was assigned 70% of the total to the wells. Reason for this was that some of the groundwater was drained in the western part from the streams, transferring it to the modelled part. The percentage of the flux that decided to be assigned as flux to the injection wells was defined after a manual calibration with the observed values, since it was not applicable to calculate the exact amount of water.

River Glomma

River Glomma was modeled as a constant head boundary with the heads of the river to be simulated after assigning the field measurements of the heads at the at the southern and the northern nodes of the model arc. At the northern node, the head assigned was 179 masl and at the southern node of the arc the head value was 177 masl.

Lake

Lake Langlsetta was modeled as a general head boundary in GMS as mentioned before with the general head to be assigned to the whole boundary to be 186 masl, as it was measured during the field course in the area in June 2018.

Streams

Modelling the streams was one of the biggest challenges that came up at the current model. After modeling the streams as drains and with no success and trying the Stream (STR) package with no success either as mentioned at the methods chapter it was decided the streams to be modeled as rivers. The RIV package was used to model the streams.

Recharge

The recharge was equally assigned to the modeled with the estimated number from NEVINA to be 284 mm/y (0.00087 m/d), while the recharge from the cut area was assigned as flux through injection wells on the western boundary as mentioned before.

5.4.3 Hydraulic conductivity zones

The hydraulic conductivity zones were assigned based on the different sediments and after the model tested and calibrated. There were used 7 different hydraulic conductivity zones (Figure 38), Table8).

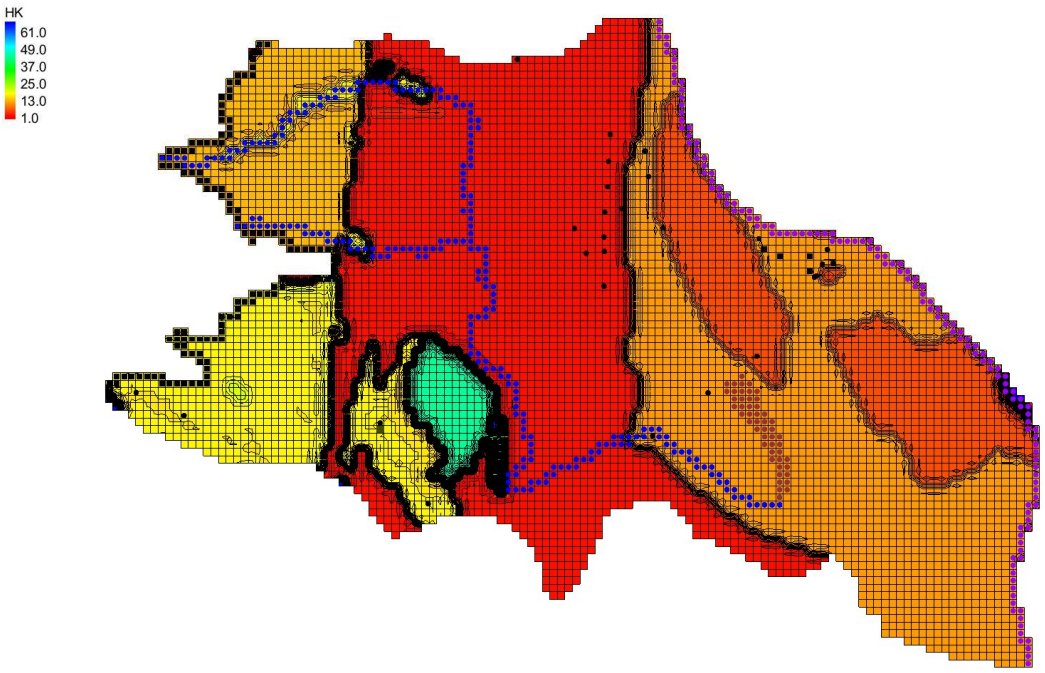

Figure 38. Map with the hydraulic conductivity zones as they were assigned in MODFLOW.

Furthermore, for the anisotropy of hydraulic conductivity there were used 4 different calibration zones for the area (Figure 39), (Table 9).

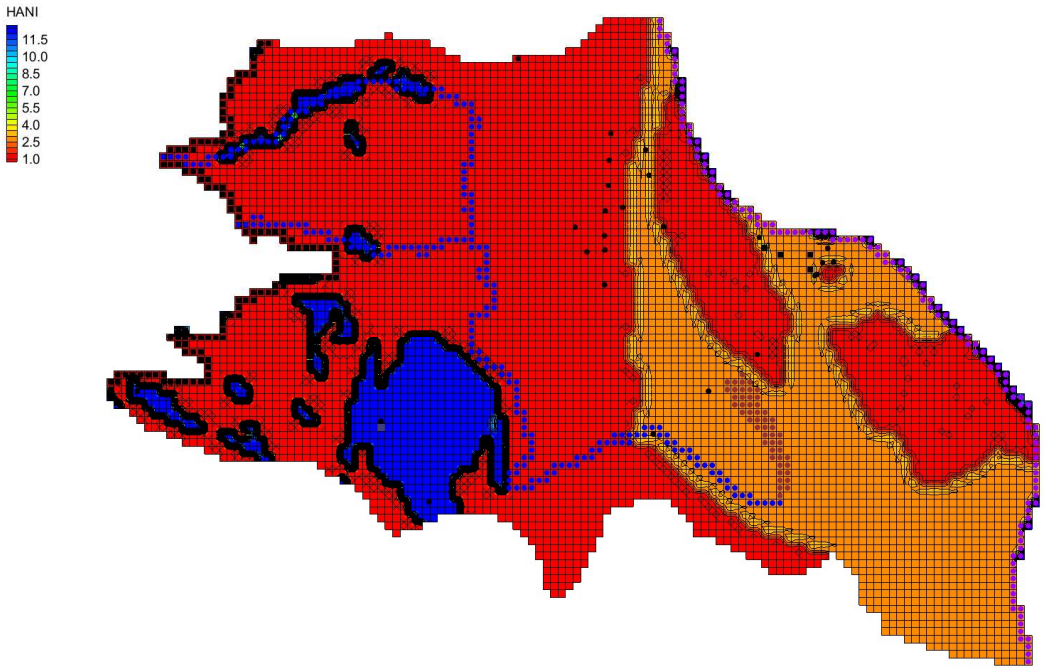

Figure 39. Map with the anisotropy zones as they were assigned in MODFLOW.

Hydraulic conductivity and anisotropy of hydraulic conductivity values for the chosen zones as they occurred after the calibration are presented in table and table respectively.

Table 8 Hydraulic condativity values in zones with description, as they were used after calibration.

Zone	K (m/s)	K(m/d)	Description
1	7.38E-05	6.38E+00	Glaciofluvial sediments near the river banks
2	1.34E-04	1.16E+01	Fluvial sediments
3	2.89E-05	2.50E+00	Glaciofluvial sediments in the middle
4	5.15E-04	4.45E+01	Till material
5	1.97E-04	1.70E+01	Peat and bog
6	1.52E-04	1.32E+01	Northern western part of the glaciofluvial
7	2.07E-04	1.79E+01	Southern western part of the glaciofluvial

Table 9 Anisotropy of the horizontal hydraulic conductivity values in zones with description, as they were used after calibration.

Zone	Anisotropy of Horiz. K	Description
1	1	Glaciofluvial sediments near the river banks
2	2.95	Fluvial sediments
3	1.035	Rest glaciofluvial sediments
4	12.261	Till material and bog

5.4.4 Calibration

In order to obtain a better match with the groundwater table, the parameters horizontal hydraulic conductivity for the different zones and the anisotropy of the hydraulic conductivity were calibrated.

The observation points used for the groundwater level are shown at Figure 24. The ranges of the values used were occurred from the sensitivity analysis applied on the model.

The calibration of the model was one of the biggest challenges of this master thesis. There were run different calibrations with more zones assigned to calibrate. Nevertheless, the decided hydraulic conductivity and anisotropy of the hydraulic conductivity zones used (Figure 38, Figure 39), provided the best match for the computed and observed heads (Figure 40).

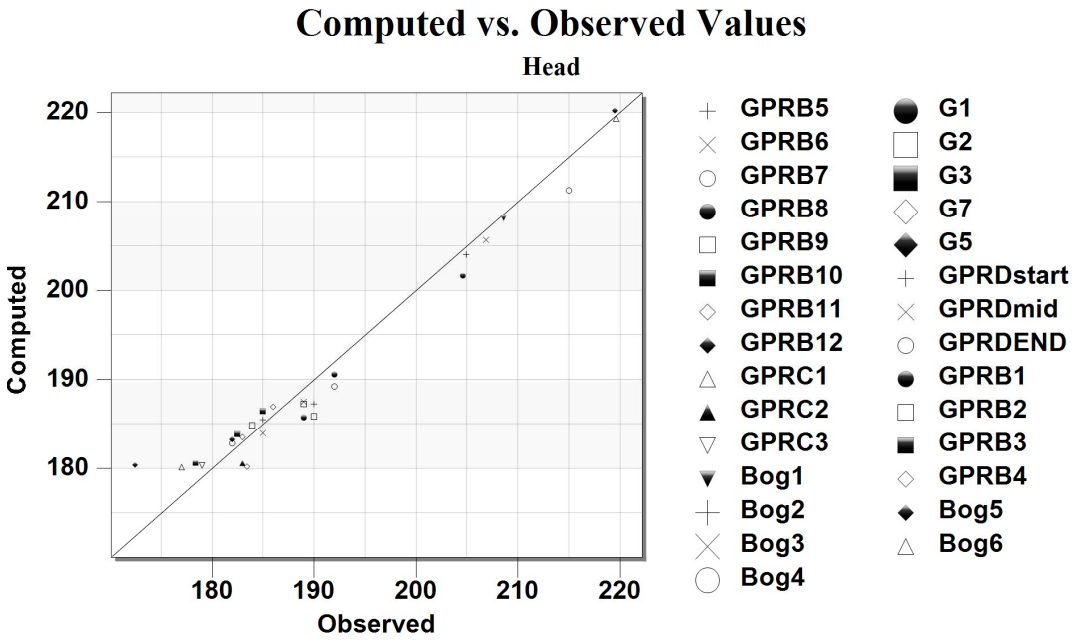

Figure 40 Graph of the fit of the computed heads with the observed values for the calibrated model.

5.4.5 Water budget and groundwater flow simulations

The water budget is an essential task in any groundwater flow modelling, as it describes the aquifer in an overall way. The simulations after the calibration of the

model, calculate the water budget of the modeled area differently with and without pumping at the Grindalsmoen waterworks.

Water budget without the pumping

The water budget of the groundwater system without the pumping is presented at the Table 10 as it was calculated in GMS.

Table 10 Water budget for the final calibrated model without the pumping with the water flow in and out of the aquifer .

Sources/Sinks	Flow in (m^3/d)	Flow out (m^3/d)
CONSTANT HEAD – River Glomma	0.00	-3796.98
WELLS - Western Bound / Pumping	1597.59	0.00
RIVER LEAKAGE – Streams	0.00	-2549.65
HEAD DEP BOUNDS - lake Langsletta	710.05	0.00
RECHARGE	4039.01	0.00
Total Source/Sink	6346.65	-6346.63

The water budget generated from modflow as shown on the table above, states that every day, 6346.65 m^3 of water get into the groundwater system with the most of it to be the surface recharge from both the modeled area (63.64%) as well as from the upper cut area added by injection wells (25.1 %). Moreover, the lake Langsletta feeds the system with 710.05 m^3 water in daily basis.

On the other hand, 6346.63 m^3 of water in total is taken out of the system. Around 60 % of the total water flows to the river Glomma and the 40 % is drained out from the streams that were modeled using the river boundary. The stream is draining most of the groundwater from the aquifer near the western boundary where the slope is steeper. The highest amount of the groundwater that flows towards the river Glomma is at the northwestern part of the river until the location of the waterworks.

There was not any flow from the river Glomma, when there was not any pumping from the waterworks, hence river Glomma can be characterized as a gaining river.

Simulation of the groundwater flow without the pumping

The simulation without the pumping as it was generated in GMS is shown in the Figure 41.

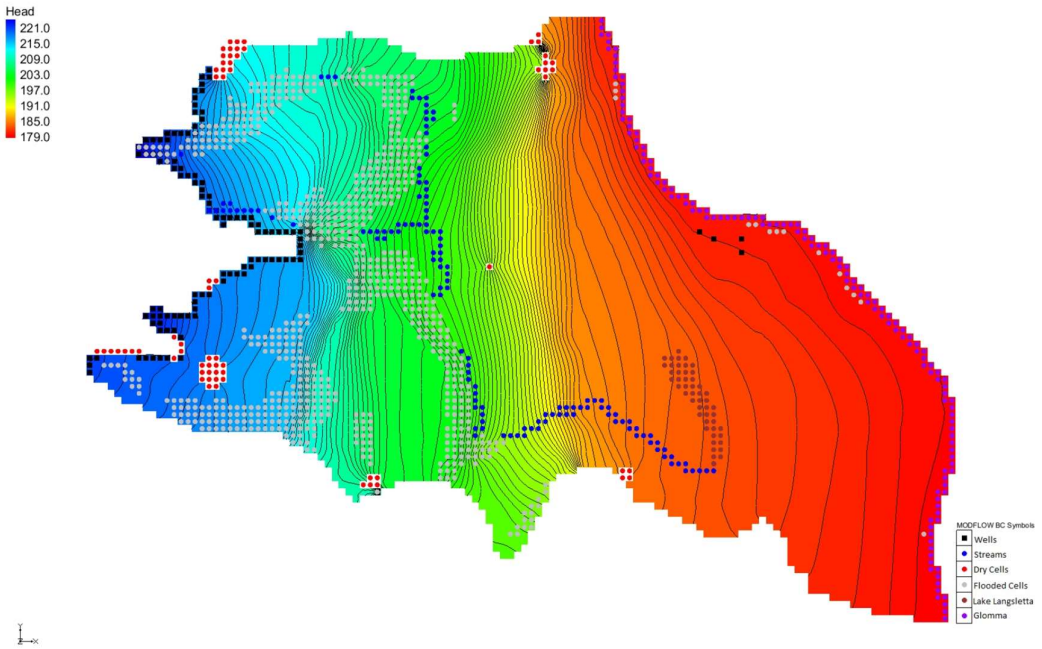

Figure 41 Figure with the simulation of the regional model without the pumping at the Grindalsmoen waterworks.

The simulation produced after the calibration of the model, produced some dry cells, mostly because of the small thickness at the locations. Furthermore, the sediment thickness with lower hydraulic conductivity locally generated some flooded cells. The flooded area located near the southwestern boundary, for instance did not exceed 1 m from the top surface (Figure 42 a). This can be explained and justified, because they are located in two bogs and the sediment thickness is very small. Moreover, at another crossection, (Figure 42 b) that the flooded cells further north of the modeled area, next to the streams where the water exceeds around 1 meter above the top surface, most likely because of lower conductivity locally.

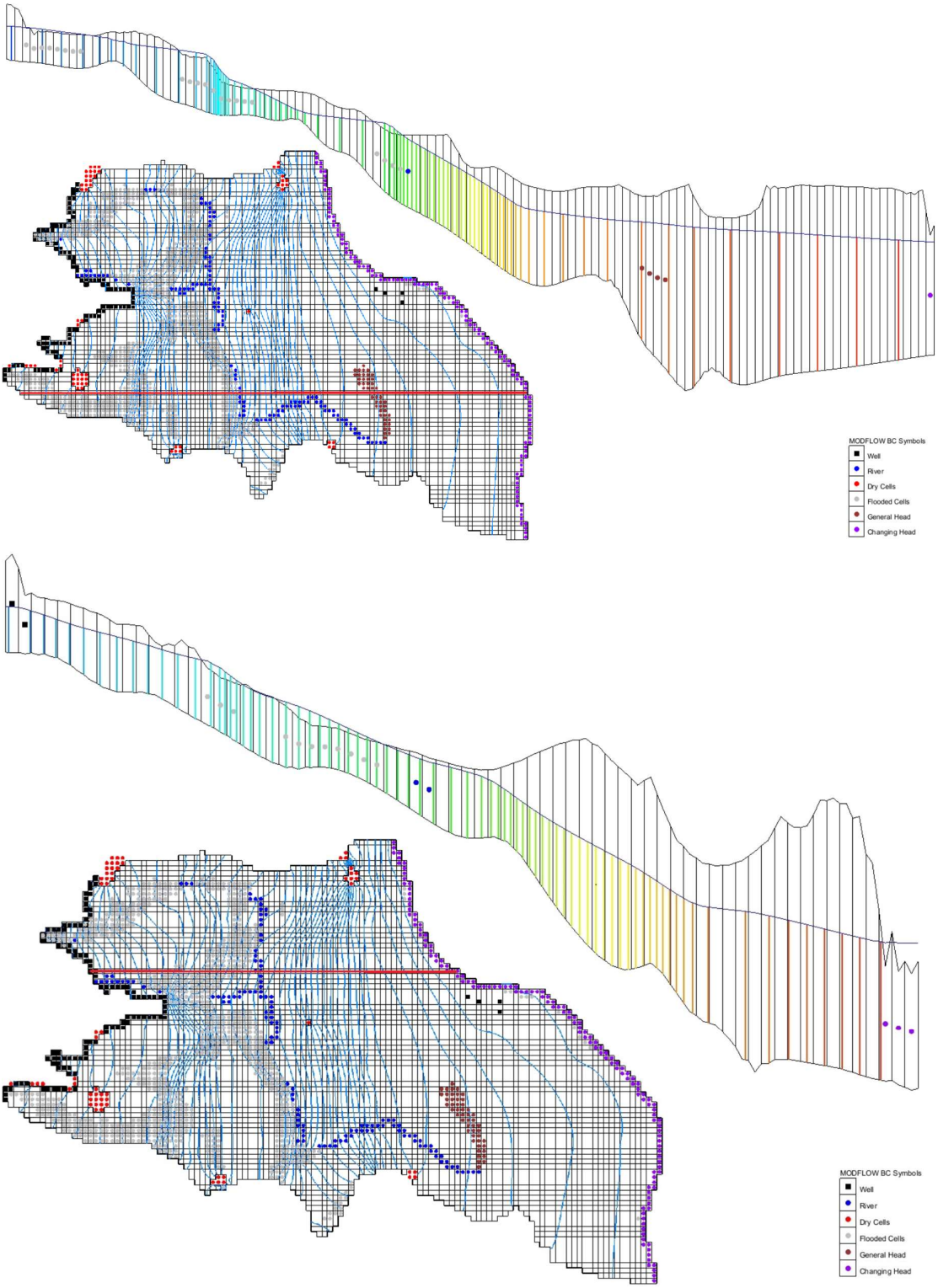

Figure 42 a-b Crossections of the modeled areas without the pumping showing the groundwater table with reference point the top elevation and the bedrock.

Water budget with the waterworks pumping

The pumping rate according to the waterworks in Grindalsmoen is around 5783 m3/d, therefore the total amount of the pumping was distributed to the 4 pumping wells, pumping simultaneously 1445.75 m^3/d each.

The water budget of the groundwater system as it was calculated from GMS is presented in the Table 11.

Table 11 Water budget for the final calibrated model with the pumping with the water flow in and out of the aquifer .

Sources/Sinks	Flow in (m^3/d)	Flow out (m^3/d)
CONSTANT HEAD - River Glomma	3826.11	-1982.91
WELLS – Western Bound / Pumping	1597.59	-5783.00
RIVER LEAKAGE - Streams	0.00	-2541.02
HEAD DEP BOUNDS – Lake Langsletta	844.94	0.00
RECHARGE	4038.32	0.00
Total Source/Sink	10306.96	-10306.93

The water budget of the system changes a lot with the pumping as shown on the table above. The total amount of groundwater entering the aquifer with the waterworks wells pumping is 10306.96 m^3/d with the most of it to come from the recharge both from the modeled area (39.18 %) as well as from the upper cut area with the form of injection wells (15.5 %). Nevertheless, the biggest difference with the pumping at the water budget of the groundwater system is that 3826.11 m^3 water enter every day the aquifer from the river Glomma. The lake Langsletta feeds the system daily with a slightly increased amount of water of 844.94 m^3 (8.2 % of the total).

The amount of water that is taken out of the system is mostly taken out from the pumping (56.1 %). Furthermore, every day almost 20 % of the total discharged water, flows out to river Glomma. Finally, 2541.02 m^3 (24.65 %) is draining from the streams mostly at the same location as without the pumping.

Simulation of the groundwater flow with the waterworks pumping

After the pumping rate was assigned at the wells of the Grindalsmoen water works the simulation of the groundwater flow that was generated (Figure 43).

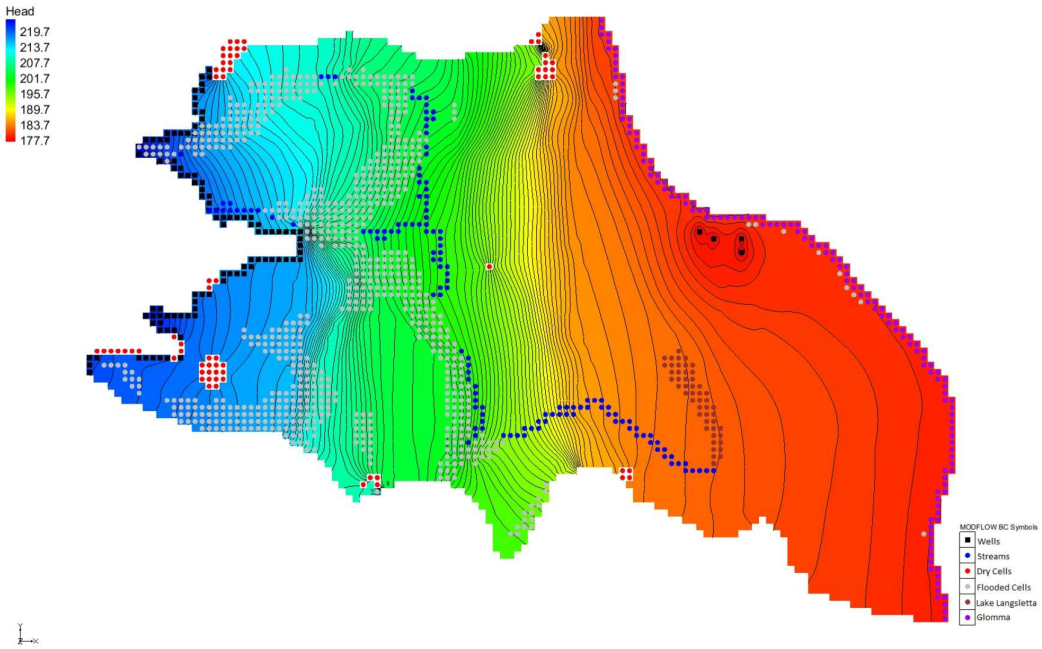

Figure 43. Simulation of the groundwater flow with the pumping of the supplying wells in Grindalsmoen waterworks as it was generated in GMS.

The pumping at the waterworks affects the equipotential lines near the wells but there is not any significant change at the equipotential lines far away as moving towards the western boundary. Furthermore, the flooded remain in spite of the changes indicating that the heads at these locations cells does not affected by the pumping rate.

5.4.6 Testing different scenarios

Scenario 1 – Increase of pumping rate 50 %

The first scenario tested in this thesis, was the calibrated model with increased pumping rate of 50 % to test how the aquifer would react with a possible forthcoming population growth. Therefore, the pumping rate of 8674.5 m^3/d was distributed equally to the four wells. The simulation of the groundwater flow as well as the water budget are presented at the Figure 44 and the Table 12.

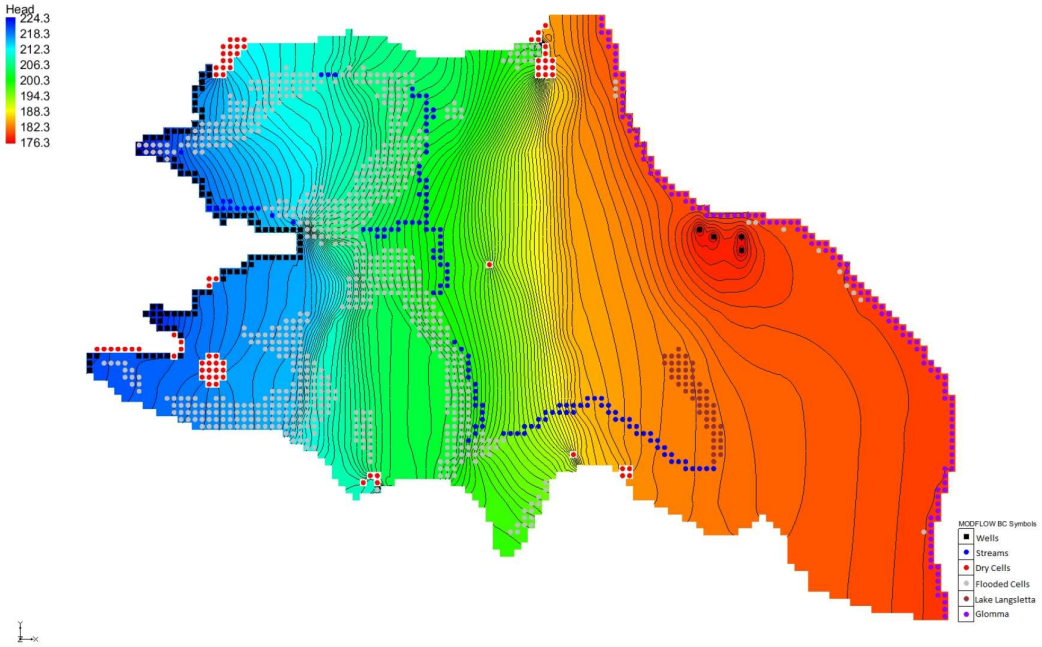

Figure 44 Simulation of the groundwater flow with the 50% increased pumping rate in Grindalsmoen waterworks as it was generated in GMS.

The 50% pumping increase seems to affect a lot the equipotential lines of the hydraulic heads around the waterworks with the flow to be faster, since the equipotential lines are more compressed. Furthermore, there are less flooded cells, while the dry cells on the model increased. Moreover, the model deviated a lot with the computed heads, which makes sense because the model was calibrated without the pumping (C1 in appendices).

Table 12 Computed water budget in GMS with water flowing in and out of the aquifer for scenario 1.

Sources/Sinks	Flow in (m^3/d)	Flow out (m^3/d)
CONSTANT HEAD – River Glomma	6401.01	-1731.96
WELLS – Western Bound / Pumping	1597.59	-8674.50
RIVER LEAKAGE - Streams	0.00	-2540.75
HEAD DEP BOUNDS – Lake Langsletta	913.07	0.00
RECHARGE	4035.52	0.00
Total Source/Sink	12947.20	-12947.22

The water budget for the current model differs a lot in comparison with the initial mode with the actual pumping rate as it can be seen on Table 12. The total amount of water entering the system is 12947.20 m^3/d with the most of it to be from the recharge both of the cut area assigned as flux from injection wells (12.33%) and the surface

recharge of the modeled area (31.16 %). Then almost 50% of the total water enters the system from the river Glomma, while the water fed from the lake to the aquifer is increased (913.07 m3/d)

The water flowing to Glomma river is 1731.96 m3/d while the streams drain 2540.75 m3/d, value is almost the same with the model with the present pumping rate.

Scenario 2 – Flow from the northern boundary

This scenario examined the case that groundwater from the north flows into the aquifer. The report from Gaut et al. (1981) that contained information from wells logs at Grundsetmoen on the north and out of the modeled area indicated only a thin layer above bedrock (1-6m) (Figure A23 at the appendices).

Therefore, it was decided to add a relatively low flux with the form of injection wells on the northern no-flow boundary. The value of the flux tested was 150m^3/d, distributed to the 10 wells equally. The simulation of the groundwater flow and the water budget as they were generated in GMS are presented at Figure 45 and Table 13 respectively.

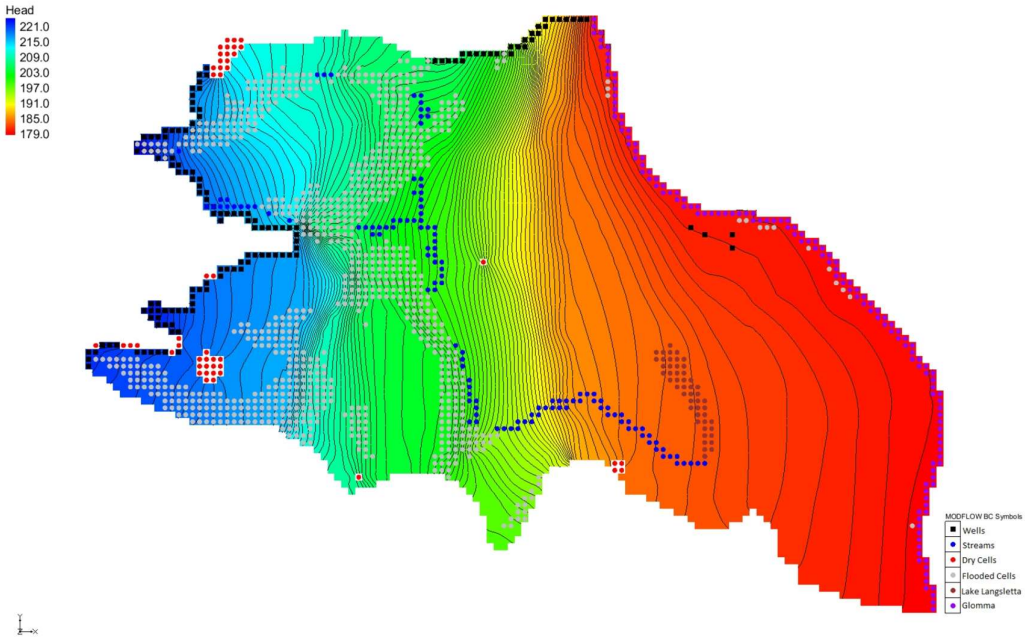

Figure 45 Simulation of the groundwater flow with the flux from the northern boundary.

The groundwater equipotential lines show that there is not any significant difference at the flow with the flux from the north, just some more flooded cells close to the western border and the streams. Other than that, the heads fit very good with the observation points (Figure C2 appendices).

Table 13 Computed water budget in GMS with water flowing in and out of the aquifer for scenario 2.

Sources/Sinks	Flow in (m^3/d)	Flow out (m^3/d)
CONSTANT HEAD – River Glomma	0.00	-3950.38
WELLS – Western Bound / Pumping	1808.50	0.00
RIVER LEAKAGE - Streams	0.00	-2618.64
HEAD DEP BOUNDS – Lake Langsletta	707.54	0.00
RECHARGE	4052.98	0.00
Total Source/Sink	6569.02	-6569.02

Furthermore, by comparing the water budgets of the final calibrated model without the pumping and without any flux from the north (Table 10) and the current model (Table 13) there is a slight increase at the water flowing to river Glomma (plus 153.41 m^3/d), the streams drain 69 m^3/d more while the lake Langsletta feeds the system with 2.51 m^3/d more water than the initial model without the flux from the north. The difference between the two models is very small, so the change is irrelevant.

Scenario 3 – Flow from the northern boundary with current pumping rate

The model of the scenario 2 was tested with the current pumping rate (5783 m^3/d) equally distributed to the 4 pumping wells, to have an indication of how the aquifer would react in case that the scenario 2 was closer to reality. The simulation of the groundwater flow as well as the water budget is presented at the Figure 46 and Table 14 respectively.

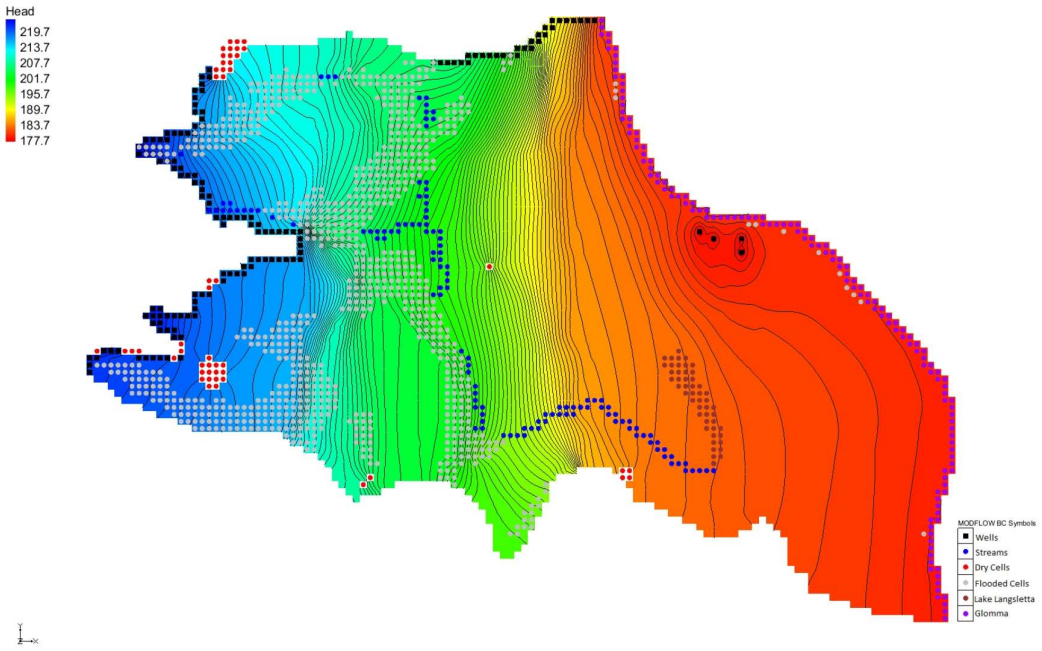

Figure 46 Simulation of the groundwater flow with the flux from the northern boundary and the current pumping rate at the Grindalsmoen waterworks.

The equipotential flow lines of the groundwater of the scenario with the flux from the northern boundary as they were generated in GMS are now changed after the starting of the pumping from the wells in Grindalsmoen waterworks. The flow is faster on the northern part, but other than that the simulation does not differ a lot from the simulation of the initial model with the pumping (Figure 43).

Table 14 Computed water budget in GMS with water flowing in and out of the aquifer for scenario 3.

Sources/Sinks	Flow in (m^3/d)	Flow out (m^3/d)
CONSTANT HEAD – River Glomma	3819.95	-2131.15
WELLS – Western Bound / Pumping	1800.32	-5783.00
RIVER LEAKAGE – Streams	0.00	-2600.23
HEAD DEP BOUNDS - Lake Langsletta	842.53	0.00
RECHARGE	4051.59	0.00
Total Source/Sink	10514.38	-10514.38

The water budget generated from the model as presented in Table 14 shows that for the current scenario 10514.38 m^3/d enter the system from different sources. Most of the water is from the recharge both from the cut area assigned as flux from the injection wells along the western boundary (1650.32 m^3/d) and the surface recharge of the modeled area (38.5 %). Furthermore, 36.3 % of the total water enters the aquifer

from river Glomma while 8 % is fed to the system by the lake Langsletta. Finally, 150 m^3/d comes from the flux assigned at the north boundary with the form of injection wells.

The water taken out from the system every day is 10514.38 m^3, with the most of it to be from the pumping from the Grinsalsmoen waterworks (55 %). Furthermore 24.7 % of water is drained daily from the streams and around 20.3 % flows to river Glomma.

Overall, the current scenario does not differ a lot from the initial model with the pumping, since the water budgets generated from the two models are similar with the main difference the 150 m^3 water coming from the northern boundary that increases the water flowing to river Glomma. Other than that, the computed heads match quite good with the observation points (Figure C3 in appendices)

5.5 Water Chemistry

Groundwater samples and surface water samples were collected during different field campaigns in the area. The different sets of the available water samples were from the field course “Field methods in hydrogeology” in June the years 2017,2018 and 2019 as well as a two days field work campaign during October 2018.

Because of the data sets were incomplete it was decided to use and present the results of the analyses of the samples from the field work in October 2018. The location of water samples analyzed is shown in the map of the Figure 19.

5.5.1 Field measurements

Electrical conductivity

The results of the electrical conductivity (EC) as they were measured in the field, are presented in Figure 47. The values are given in μSiemens/cm (μS/cm).

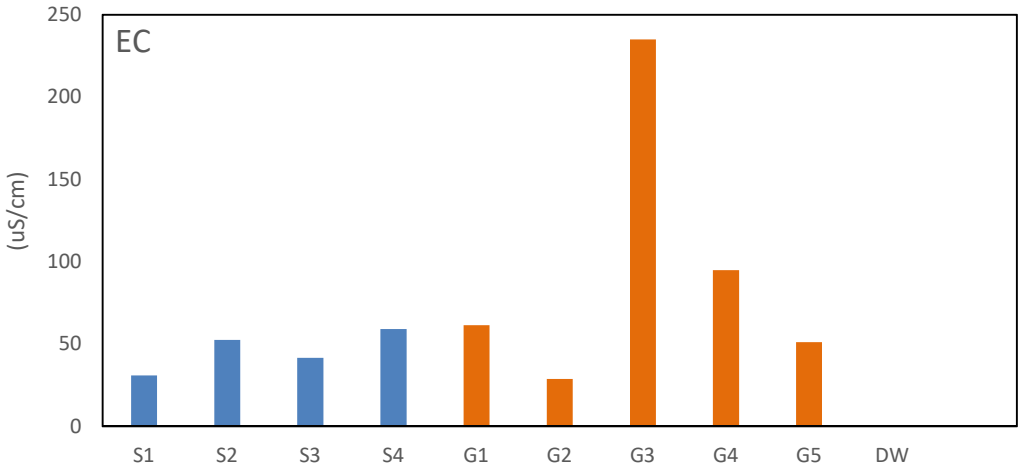

Figure 47. Field measurements of the electrical conductivity analysis for the groundwater (orange) and the surface water (blue) samples.

Groundwater samples range between 51.2 and 235 µS/cm, while the range of the electrical conductivity for the surface water samples is 1.713 -2.29 µS/cm. At the sample from the water supply at the waterworks station the electrical conductivity was not measured.

PH measurements

The results of pH analysis are presented in the Figure 48.

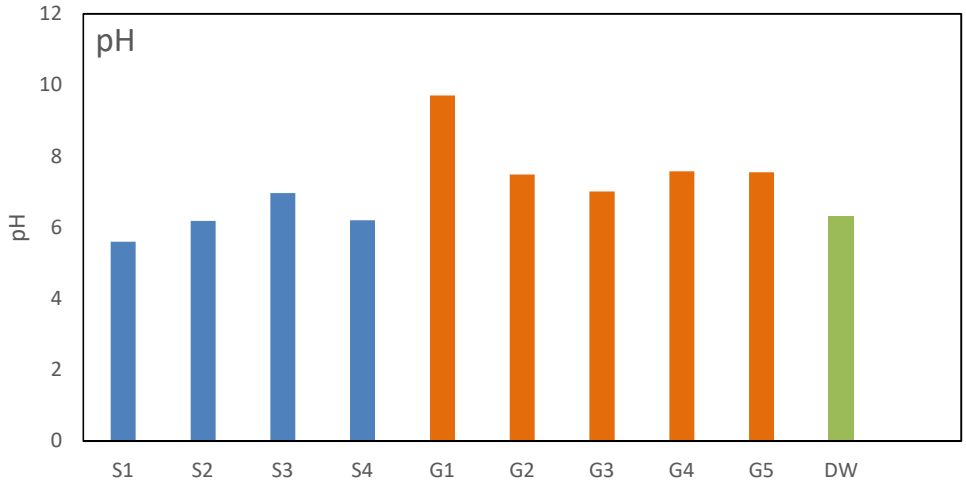

Figure 48. Field measurements of the pH for the groundwater (orange), surface water (blue) samples and the tap water from the waterworks (green).

pH values for the groundwater samples range between 7.01 to 9.71, while the pH range for the surface water is.5.6 -6.97. The pH for the surface water samples is lower than the groundwater samples. At the sample from the water supply at the waterworks station pH value was 6.31.

5.5.2 Laboratory measurements

Alkalinity

The results of the alkalinity analysis on the water samples are presented in Figure 49. The values presented are in mg/L.

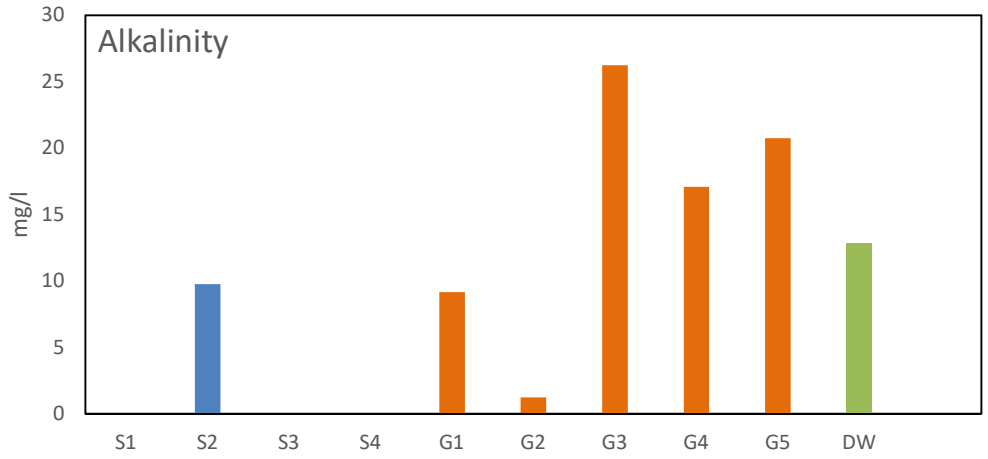

Figure 49. Alkalinity analysis results for the groundwater (orange), surface water (blue) samples and the tap water from the waterworks (green).

The alkalinity analysis for the groundwater samples provided values ranging between 1.22 – 26.23 mg/l, while most of the surface water samples were close to 0 or 0 except sample S2 that was 9.76 mg/l.

The alkalinity the sample from the water supply at the waterworks station was 12.81 mg/l.

Ion chromatography

Cations

The results of the cations from the Ion chromatography analysis on the water samples are presented in Figure 50, Figure 51, Figure 52 and Figure 53 for sodium (Na), potassium (K), calcium (Ca) and magnesium (Mg) respectively. The values presented are in mg/L both for groundwater and surface water samples.

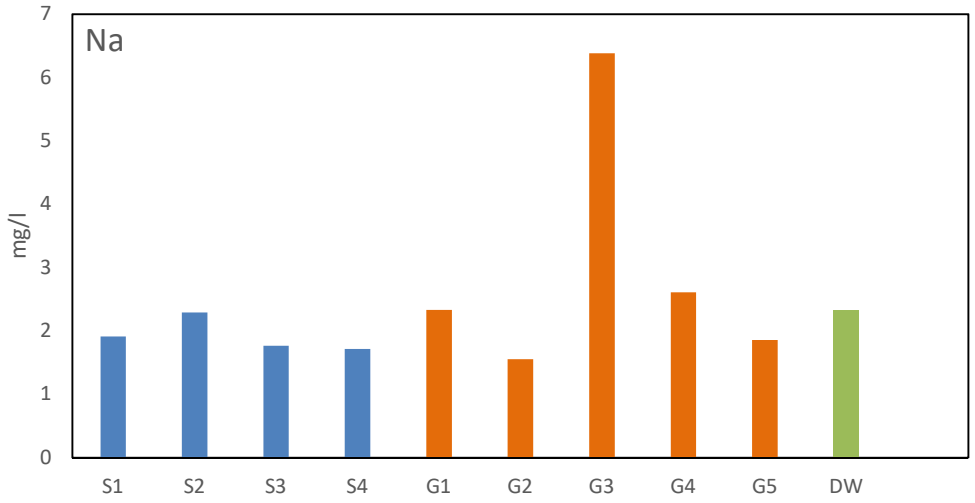

Figure 50 Sodium (Na) concentrations of the groundwater (orange), surface water (blue) samples and the tap water from the waterworks (green).

Sodium concentrations range between 1.55 – 6.38 mg/l. Concentration of sodium in surface water samples range between 1.713 – 2.29 mg/l while the sodium in groundwater samples is 1.555 – 6.38 mg/l. The concentration of sodium in most of the samples does not exceed 2.5 mg/l with exception of the groundwater samples G3 that is 6.38 mg/l.

The concentration at the sample from the water supply at the waterworks station was 2.33 mg/l.

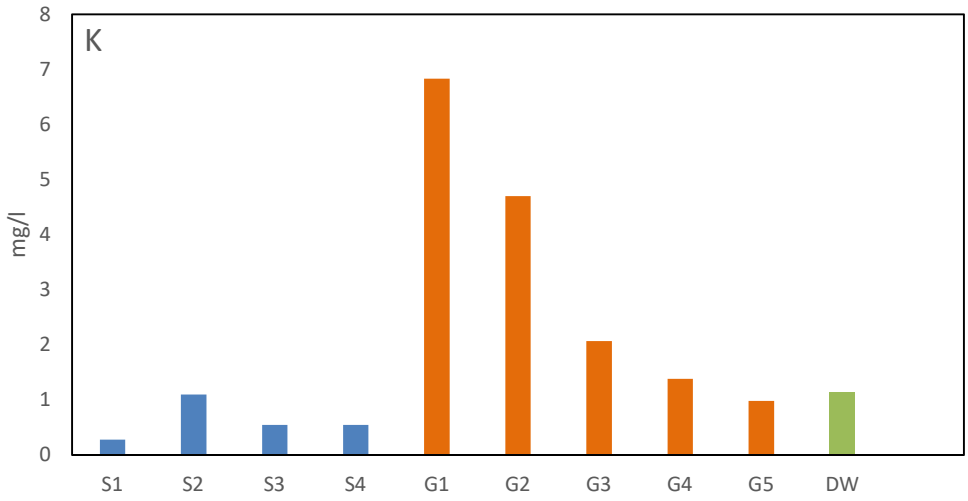

Figure 51. Concentration of Potassium in groundwater (orange), surface water (blue) samples and the tap water from the waterworks (green).

The concentration range of potassium in the water samples is 0.277-6.836 mg/l.. The surface water samples have less potassium (0.277 – 1.099 mg/l), while the groundwater samples range between 0.983 - 6.836 mg/l.. The samples G2 and G1 have the highest concentrations of K with 4.703 mg/l and 6.836 mg/l respectively, distinguishing from all the other samples with much lower concentrations. The reason for this can be that fertilizers are used in the wider area containing potassium. At the sample from the water supply at the waterworks station the concentration in K was 1.127 mg/l.

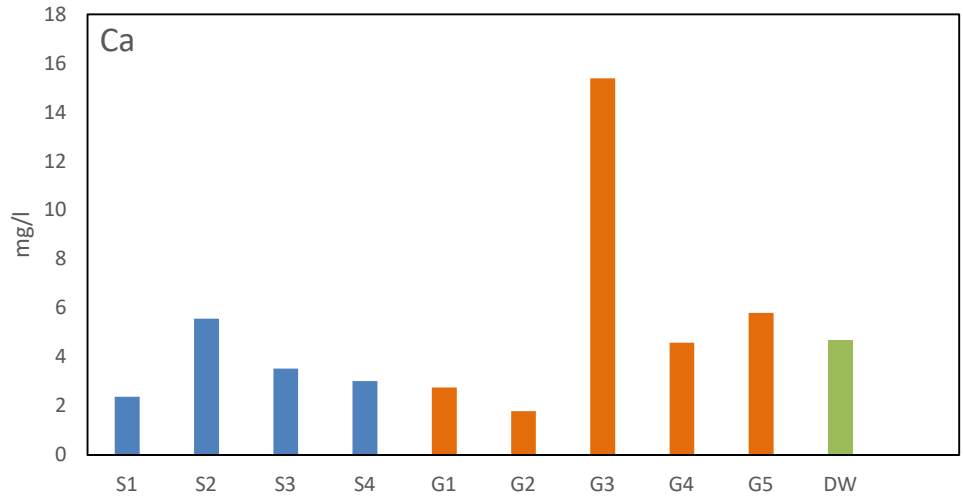

Figure 52. Calcium concentration in groundwater (orange), surface water (blue) samples and the tap water from the waterworks (green).

Calcium concentration for the surface water samples range between 2.37 - 5.56 mg/l, while Ca in the groundwater samples ranges between 1.785 – 15.389 mg/l. The concentration of calcium in all the samples is up to 5.56 mg/l., except the groundwater sample G3 that is 15.389 mg/l. The water sample from the waterworks station contained 4.67 mg/l calcium.

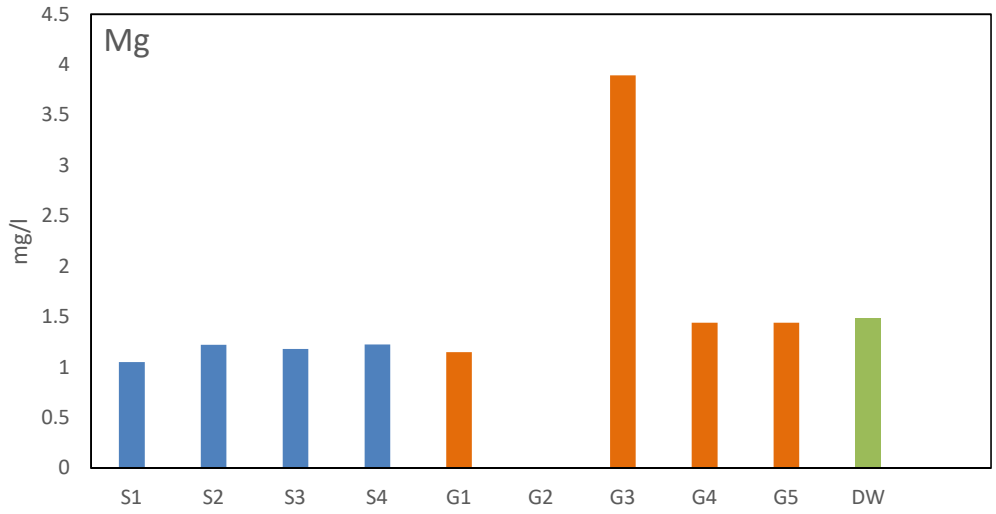

Figure 53 Magnesium concentration in groundwater (orange), surface water (blue) samples and the tap water from the waterworks (green).

Magnesium concentration for all the surface water samples is around 1 mg/l., while in groundwater samples it ranges between 1.148 – 3.894 mg/l. In sample G2 magnesium was lower than the detection limit, therefore it is assumed to be negligible, result that is very strange. Magnesium concentration for the sample from the water supply at the waterworks station was 1.48 mg/l.

Anions

The results of the anions from the Ion chromatography analysis on the water samples are presented in Figure 54, Figure 55, Figure 56, Figure 57 and Figure 58 for fluorine (F), chlorine (Cl), sulfate (SO_4), bromine (Br) and nitrate (NO_3) respectively. The values presented are in mg/L.

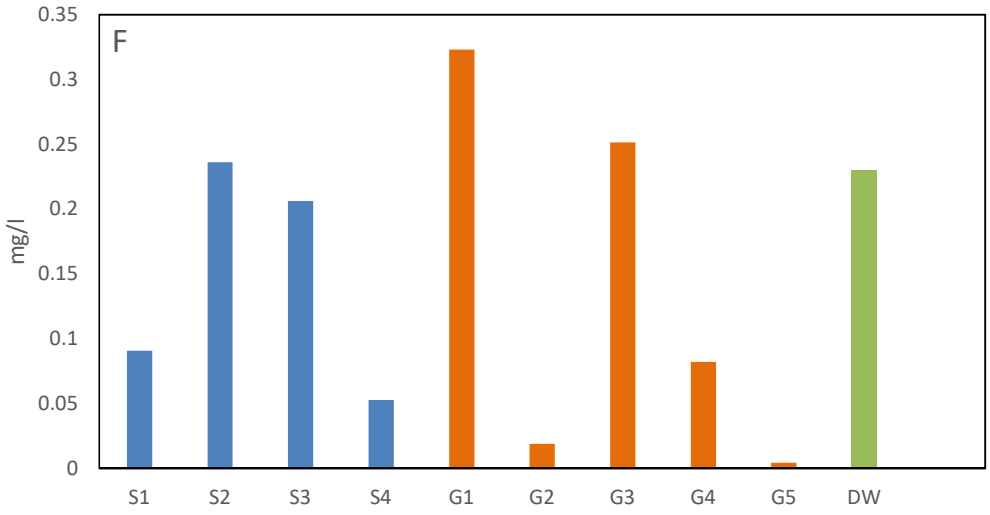

Figure 54. Flurine concentration in groundwater (orange), surface water (blue) samples and the tap water from the waterworks (green).

The concentration of fluorine in the surface water samples ranges between 0.05 – 0.0236 mg/l while at the groundwater samples, fluctuates from 0.004 mg/l to 0.251 mg/l. The groundwater samples G2 and W3ww have the lowest concentrations in fluorine. At the sample from the water supply at the waterworks station the concentration of fluorine was 0.23 mg/l.

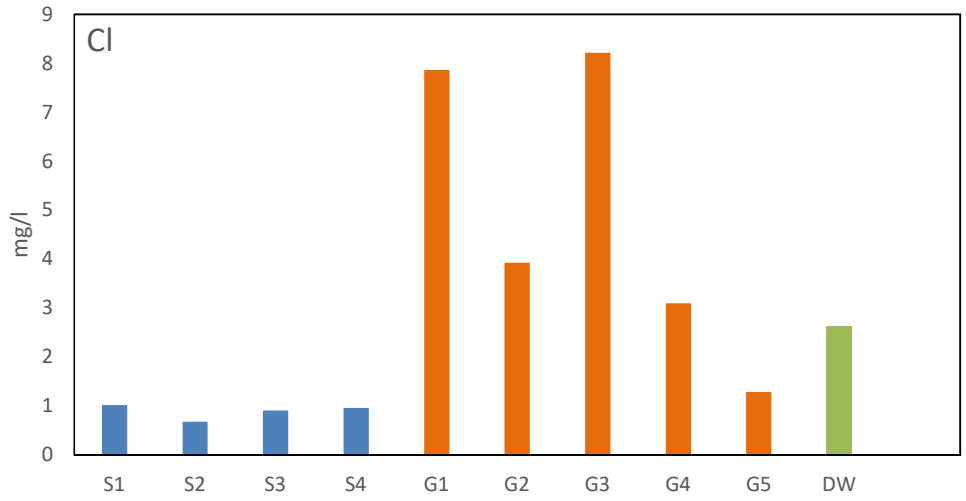

Figure 55. Chlorine concentration in groundwater (orange), surface water (blue) samples and the tap water from the waterworks (green).

Groundwater samples gave values for chlorine ranging 1.28 – 8.21 mg/l. Surface water samples on the other hand show much lower values (0.67 – 1.01 mg/l). Chlorine concentration at the waterworks drinking water was 2.62 mg/l.

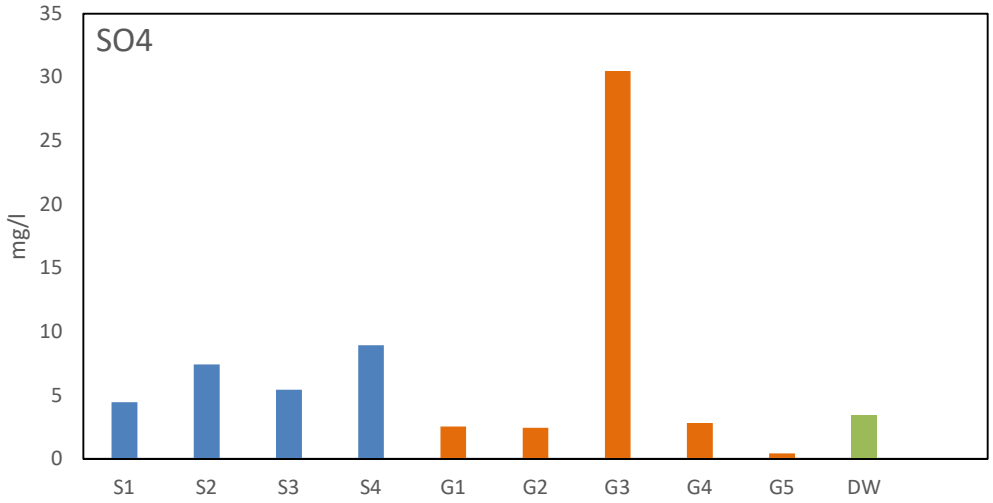

Figure 56. Sulfate concentration in groundwater (orange), surface water (blue) samples and the tap water from the waterworks (green).

Sulfate concentration in surface water samples range between 4.44 – 8.93 mg/l, while in groundwater values were from 0.42 – 30.4901 mg/l. The groundwater sample G3 had the highest concentration in sulfate while W3ww the lowest. The drinking water from the water works contained 3.448 mg/l chlorine.

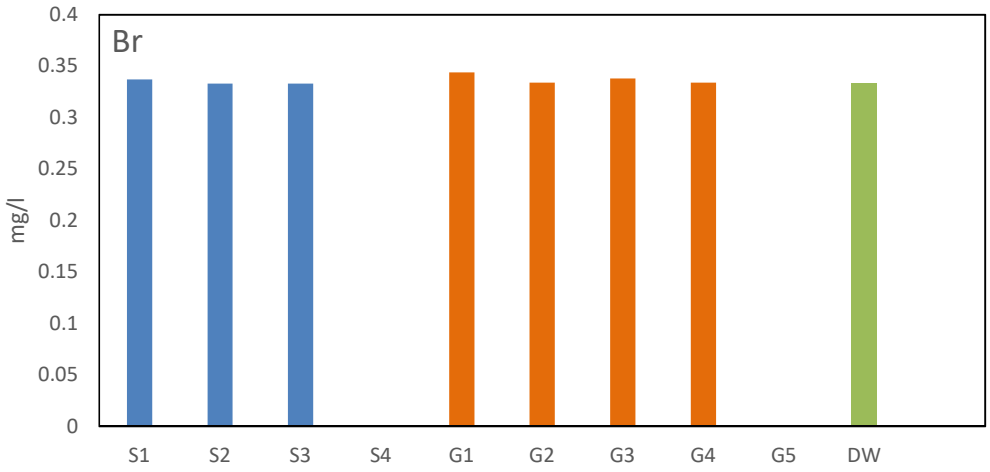

Figure 57. . Bromine concentration in groundwater (orange), surface water (blue) samples and the tap water from the waterworks (green).

Surface and groundwater showed similar concentrations for bromine that are around 0.035 mg/l, except the groundwater sample G5 and surface water sample S4, where the concentrations were below the detection limit, so they were assumed as negligible. The drinking water from the station at the waterworks contained 0.33 mg/l bromine.

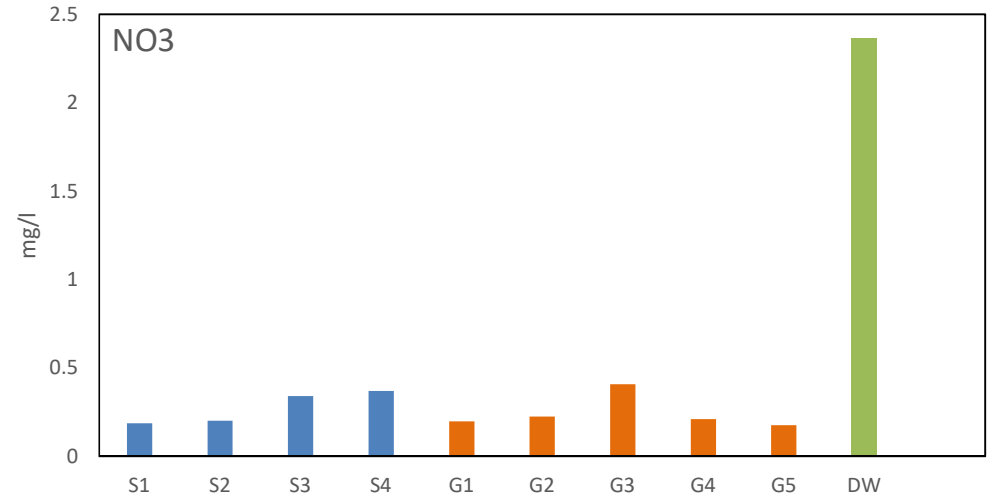

Figure 58. Nitrate concentration in groundwater (orange), surface water (blue) samples and the tap water from the waterworks (green).

Nitrate concentration in surface water ranges between 0.18 – 0.37 mg/l while in groundwater the values of nitrate were from 0.17 – 0.408 mg/l. The nitrate

concentration at the drinking water of the waterworks was higher than all the other samples 2.364 mg/l.

Electrical balance

The results of the samples were imported and interpreted in PHREEQC to investigate the quality of the groundwater samples with the results to be presented at the in the Figure 59.

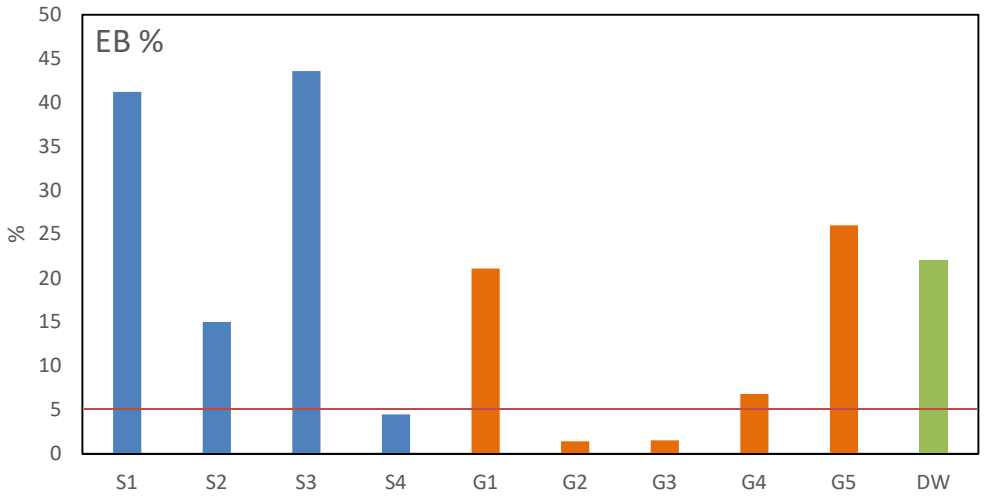

Figure 59. Electrical balance for groundwater (orange), surface water samples and the water sample from the tap of the waterworks, with the red line indicating the error of 5 % that is the limit for an acceptable chemical analysis.

The results of the groundwater and surface water samples are presented in percentage. From the results of the analysis in PHREEQC presented at the Figure 59, above it can be observed that the samples that the all the surface water and the drinking water from the station of waterworks show a high error as well as the groundwater samples G2, G4 indicating an unreliable sampling or analytical process. The rest of groundwater samples show reliable sampling process and chemical analysis.

The results from the ion chromatography for the water samples were plotted a piper diagram (Figure 60), to display the bulk composition of the groundwater samples.

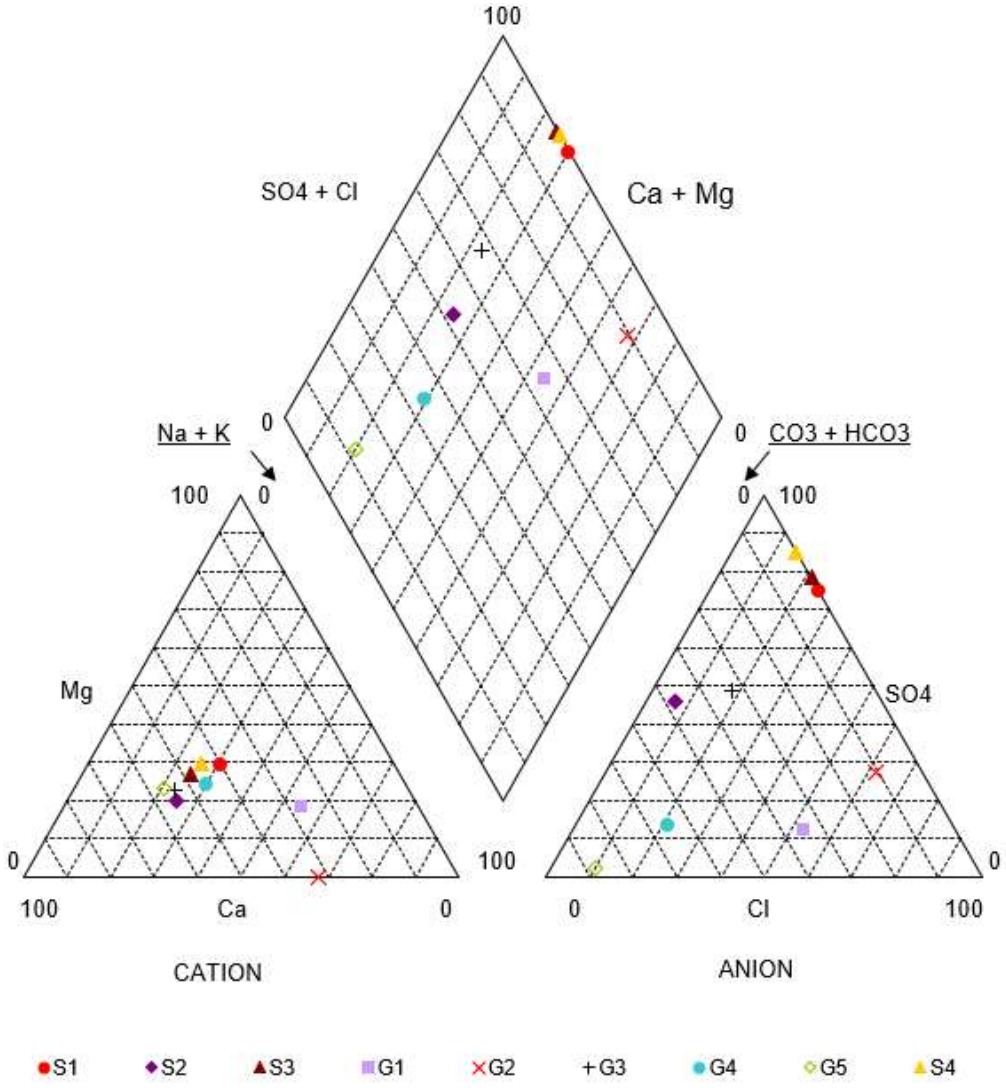

Figure 60 Piper diagram of groundwater and surface water samples.

Inductively coupled plasma mass spectrometry (ICP-MS)

The results from the ICP-MS analysis for the iron (Fe) and manganese (Mn) in the water samples are presented in Figure 61, Figure 62 respectively. The values presented are in mg/l.

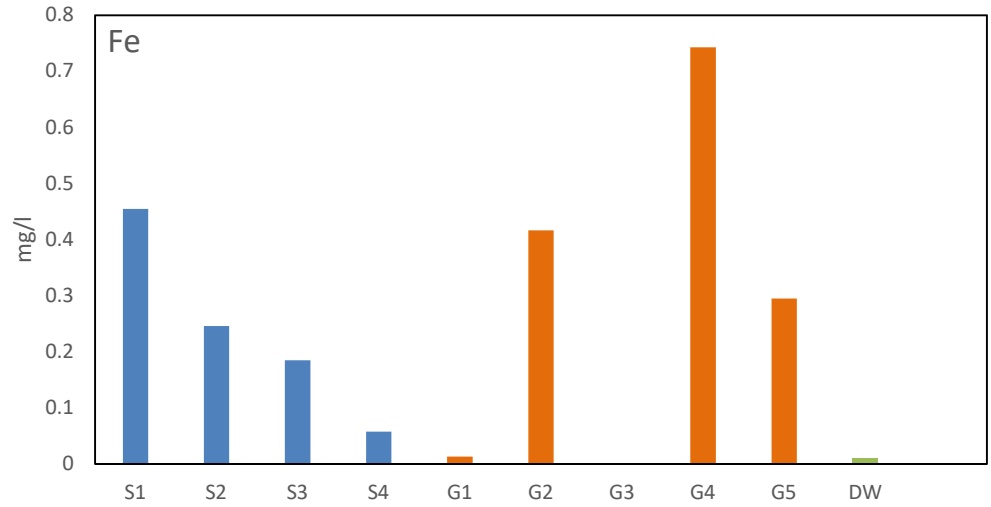

Figure 61. Iron concentration in groundwater (orange), surface water (blue) samples and the tap water from the waterworks (green)..

Iron concentrations range between 0.05 – 0.74 mg/l. Concentration of iron in surface water samples range between 0.05 – 0.45 mg/l while the iron in groundwater samples is from 0.013 – 0.74 mg/l. The concentration of iron in most of the samples does not exceed 0.45 mg/l with exception the groundwater samples G4 that is 0.74 mg/l. The concentration of iron in G3 was below the detection values, therefore, it was assumed as minor. The drinking water sample after the treatment, had very low concentration of iron (0.0098 mg/l)

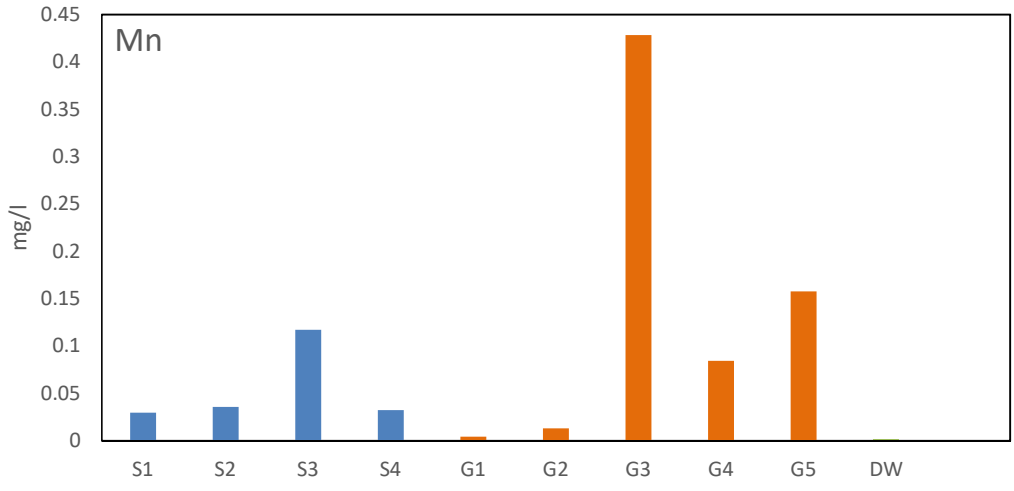

Figure 62. Manganese concentration in groundwater (orange), surface water (blue) samples and the tap water from the waterworks (green).

The concentration of manganese ranges between 0.03 – 0.11 mg/l for the surface water samples. The groundwater samples showed values from 0.01-0.42 mg/l. There amount of manganese in the drinking water from the waterworks station was 0.002 mg/l.

6 Discussion

6.1 Aquifer geometry

The results from the 3 geophysical methods that were used to define the bedrock elevation did not diverge significantly. Therefore, the data from the locations where the geophysical surveys were conducted are trusted. Furthermore, the old GPR data as well as the well logs from the GRANADA gave valuable information about the depth to the bedrock and were used for the interpolation of the bedrock surface elevation in QGIS.

Nevertheless, the number of the points indicating the depth to the bedrock were few in comparison with the study area. The well logs were concentrated mainly near the banks of the river Glomma and extended mostly until the first quarter of the catchment area starting from the river banks. The geophysical surveys were more extended along the whole study area. However, the profiles obtained from all the three of them (GPR, ERT, seismic refraction) were from almost the same locations. As a result, it was easy to compare between the profiles but there was not a wider knowledge about the bedrock elevation for different locations, especially to the half western part of the catchment is more limited. The information for the depth to bedrock that the geotechnical drillings from the new road project by COWI (2016) was very helpful. The road is constructed very close to the location where the model was decided to cut so the data were essential for the bedrock elevation layer.

This deficiency of bedrock elevation points not only led to many problems interpolating the bedrock elevation layer in QGIS but led to many problems to the later developed groundwater flow model in GMS. The method of the interpolation used in GMS as it was described, was a combination of an inverse distance weighing (IDW) and a manual nearest neighbor interpolation. By adding elevation points for the bedrock manually based on the topography, the sediments and field observations helped to have a better result for the layer. Although there were added many bedrock elevation points, manually and the extrapolated layer was functional for GMS, the layer generated, was overlapping in some locations the top elevation of the model.

The measurements for the groundwater table along the study area were also limited. Therefore, it was not possible to create a piezometric map of the hydraulic heads. The values were obtained from geophysical surveys and groundwater measurements with dippers, with most of them taken from the eastern part near the river Glomma, that were used later for calibrating the groundwater flow model.

6.2 Hydrogeological parameters

The porosity value was obtained from Alfnes et al. (2003), for similar sediments in Grindalsmoen, with intention to use it later in the numerical model in case of using transport with MODPATH. Nevertheless, the porosity was not used since MODFLOW does not use porosity in its equation.

The study area is covered by terminal glaciofluvial sediments. Therefore, it was done a correlation with the sediments at Gardermoen's area, about which the literature is very extended. The value estimated for the porosity as it was obtained from Alfnes et al. (2003) is in the range that Hiscock and Bense (2014) gives for typical porosity values for glaciofluvial sediments.

The results from the different methods used to define the hydraulic conductivity of the sediments in the study area if they compared by sediment type, with literature values, they fit quite well. According to Hiscock and Bense (2014) from Table 2 the values obtained from the infiltration tests fit quite good with the values for the glaciofluvial and the fluvial sediments. The hydraulic conductivity values for fluvial sediments from Hiscock and Bense (2014) fit quite good also with the values the both from infiltration tests and the approximation of the pumping test. Till material values from literature are very low in comparison with the values from the methods used, but the till material is probably ablation moraine. Thus, the range for hydraulic conductivity from literature fit with the values obtained from the grain size analysis at the new road area, both for Hazen and Gustafson methods.

6.3 Water balance

The catchment of the surface water for the study area, as it was manually delineated does not match the initial generated catchment area from the NEVINA report (Figure 63).

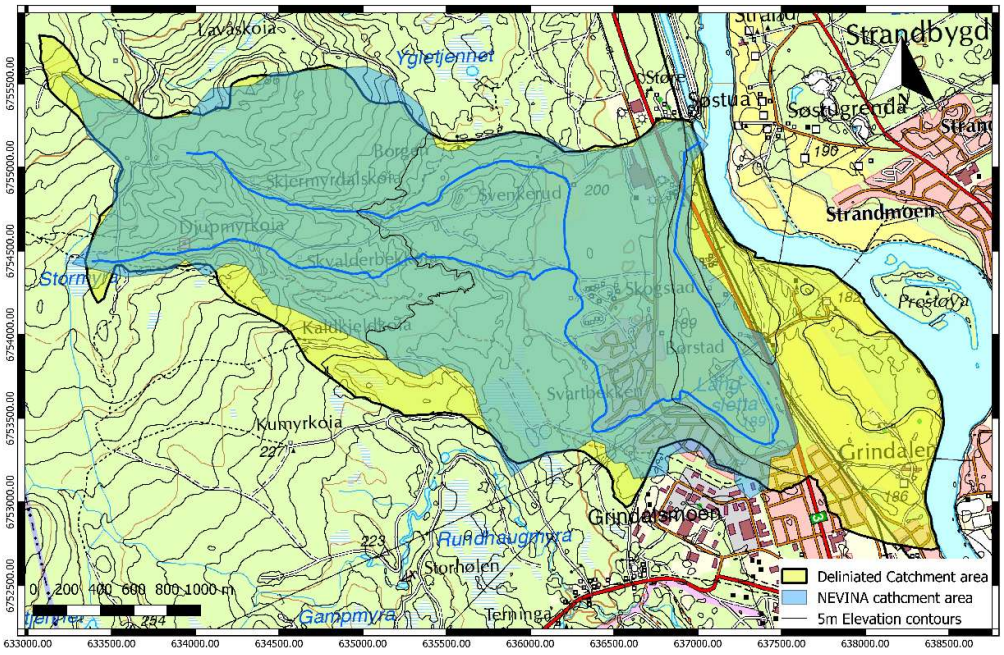

Figure 63 Map showing the delineated and the computed from NEVINA catchment.

The catchment that is generated from NEVINA with code 002.H62 showing the stream flowing to river Glomma is chosen as the discharge point is not wrong, but it is not the whole catchment for the area. The fieldwork during October 2018 was critical as the field observations helped a for the delineation and especially at the southwestern part, that NEVINA was not including. There, it was observed that although the area is mostly flat, there is a slope at the southeastern boundary towards the Grindalsmoen waterworks. Eventually, the catchment was edited in NEVINA by setting the desired boundaries and obtained the parameters that are used.

Furthermore, the catchment as it has mentioned before in this thesis, shows the boundaries for the surface water and not necessarily the groundwater, hence there could be groundwater entering and getting out from the system from the northern and the southern boundary respectively.

A topic that needs to be discussed is the surface runoff from the streams. The edited NEVINA report and the topographic map for the used catchment, implies that the streams transfer water leading it to the river Glomma. Nevertheless, the only water discharge water to Glomma that was observed was from the stormwater drain (Figure 64) and according to Elverum municipality the discharge is very limited.

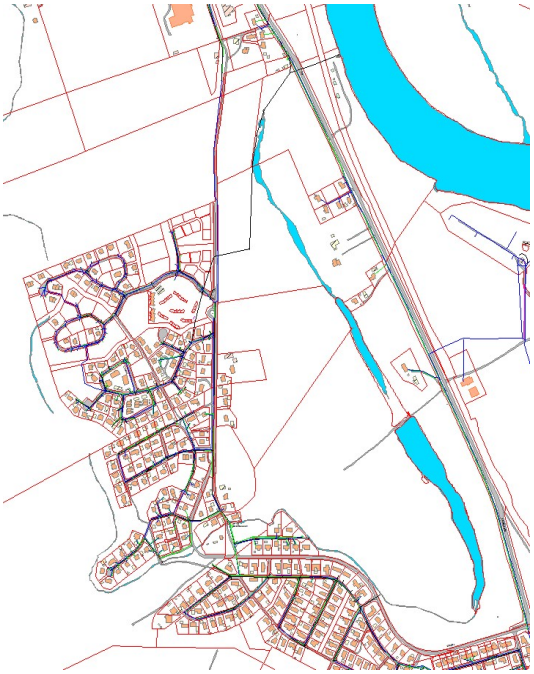

Figure 64 Bird-eye view of the stormwater drain in the area of Grindalsmoen.

6.4 Numerical modelling

The groundwater flow model as it was developed in GMS, used equal cell size dimensions of 30x30m. Even though, this led the simulation to converge faster and save time, locally the model could have been improved by refining the grid.

The top elevation layer of the developed model is quite acceptable, as it was obtained from the digital elevation model for the study area. What can be questioned though is the surface water elevation of the stream that was taken from the DEM file and might not be accurate. Nevertheless, from the annual precipitation values and by comparing the monthly data from 1978-2013 at the Elverum-Fagertun (Table B8 in appendices) whether station, it can be shown that the differences are reduced in the precipitated water to have deviations in the water level elevation of the streams.

The bottom elevation layer used in GMS representing the bedrock, was one of the most challenging parts at constructing the aquifer model. The points indicating the known depth to bedrock were few. Thus, after testing several different interpolation methods, it was concluded that the method used was the best one to obtain the desirable result without huge elevation differences going from cell to cell. There were just a few points where the bedrock layer was overlapping the top layer. However, these locations were "fixed" automatically in GMS by using the "Preserve top fix", that adjusts the bottom elevation by subtracting the minimum thickness from the top layer.

The model developed in GMS is a one-layer model even though the geology of the study area indicates that there are several sediment types in different layers. There are fluvial sediments near the Glomma banks that cover the glaciofluvial sediments and there are tills in other places. Therefore, to model the Grindalsmoen aquifer as close as possible to reality, a two-layer model with different properties should have been developed. The initial thought was to develop such a model by starting with one layer and add the second layer later. Nevertheless, that complicated a lot the modeling process thus it was decided to use a one-layer model. However, because the sediment thickness is quite small to have a better representation of the reality the anisotropy of hydraulic conductivity based on different sediments, was applied as a parameter to the model.

The one-layer model as it was developed, with the very thin sediment thickness especially at the western half of the catchment, created problems with many dry cells. The increased amount of the dry cells led to converging problems of the simulation. In order to solve this problem, it was decided to cut the model along the elevation contour line of 225 masl. This elevation contour of 225 masl. relates to the geology of the study area, as it matches the highest occurrences of the glaciofluvial sediments. The western boundary of the model where the glaciofluvial sediments have been deposited, is where the aquifer thickness starts to increase. This assumption is in line with the near surface investigations, the well logs and the field observations.

Furthermore, when writing about the construction of the groundwater flow model, the boundary conditions as they were modeled can in some cases be discussed.

The decision to model the lake Langsletta with the general head boundary (GHB) was taken after the absence of critical parameters for it to model it with the lake (LAK) package in GMS. In general, the GHB is commonly used to model lakes while the LAK package in GMS is a "more sophisticated alternative to the typical approach of using the GHB to simulate the effect of lakes" (AQUAVEO, 2019). With the LAK package for instance, the stage of the modeled lake is computed automatically depending the water budget of the system, while with the GHB the modeler defines the stage. To model a lake with the LAK package, requires adding parameters that were unknown. Such a parameter was the "lakebed leakance" that is a function of hydraulic conductivity and the thickness of the lake bed. To conclude, the boundary of the lake Langsletta, could have been better modeled with the LAK package but modeling a lake with GHB is the most common option.

For the modeling of the Glomma river it was used a specified head boundary, by assigning the Constant head package (CHD) in MODFLOW. Specified head boundaries are used preferably to model "large bodies of water" such as major rivers, lakes oceans etc. (Anderson et al., 2015). The CHD package is a "time variant specified head". However, in steady state conditions by setting the same "start" and "end" hydraulic heads at every cell when installing the boundary, it is invariant with time. operating as a regular specified head boundary (Anderson et al., 2015).

The possibility of modeling river Glomma with the GHB was also tested but there were huge errors at the water budget. The error at the computed water budget, as Anderson et al. (2015) state, happens when the GHB is used to model perimetric boundaries. This can be solved by expanding the grid and increasing the nodes, resulting the computational burden to increase (Anderson et al., 2015). Finally modeling Glomma river as a specified head, by assigning the CHD package was the option with the less uncertainties.

The streams were modeled as rivers. Initially as mentioned before, it was tested to model the streams of the study area either with the DRN package or STR package. The option to use STR package was declined since this package was complicated to be modeled. Moreover, DRN package was just taking water out from the aquifer and not feeding it at all, and since this possibility was desired to be investigated the RIV package was used to model the streams. Furthermore, the boundary of the streams as

it was modeled (RIV package) was acting almost the same as the DRN package by mainly taking water out of the system, with the main difference that it was feeding it back with very little water.

The last boundary condition modeled, is the western boundary where it was assigned the flux from the cut study area with the form of injection wells along the boundary. The two smaller catchments of the surface water of the cut area ending up to western boundary indicate that the flux as injection rate at the wells should not be distributed equally. It is obvious in the Figure 37, where the two catchments are delineated that the southern catchment is much smaller than the northern one. Therefore, the flux assigned to the corresponding wells should be maybe 5-10 % of the total flux and the rest 95-90 % to be distributed equally to the rest of the wells. However, the simulation was not running with this kind of distribution. The best fit was 25 % of the total flux to be assigned to the corresponding wells and 75 % to the rest of the wells towards the north along the western boundary.

Moreover, the streams flow in the northern catchment, and there could be groundwater drained from the stream from the cut area and transferred through it to the modeled area. The exact amount of groundwater drained by the streams at the western cut part can be questioned but it was decided to subtract just 5 % from the total water ending up to the northern part. Finally, it was assigned 70 % of the total flux to the wells corresponding to the northern part. To summarize from the total recharge of the western cut part it was assigned 70 % to the northern wells and 25% to the southern, with the rest 5 % to be assumed that it was drained and transferred from the streams in the western part.

The zones created for the hydraulic conductivity and anisotropy of the hydraulic conductivity were chosen from the quaternary geology map based on the different sediments. The values for the different zones for hydraulic conductivity after the calibration can match with the values from Hiscock and Bense (2014) and the methods used to obtain them. For instance, the zone 1 (Table 8) with the glaciofluvial sediments near the river banks has a value 6.38 m/d which fits with the approximation from the pumping test conducted in 1981. The zone 2 with the fluvial sediments gave back after the calibration 11.6 m/d, while an infiltration test at this location gave 9.5 m/d. Furthermore, as moving towards the west at the zone 3 with the glaciofluvial

sediments, hydraulic conductivity was calibrated with PEST to be 2.5 – 4 m/d with the values of the grain size analysis with the Hazen method to fit the range of those values. Last the two zones 6 and 7 near the western boundary provided values that were 13.7 m/d and 20 m/d. Nevertheless, there are not any tests conducted at these two locations to compare the hydraulic conductivity but the values can relate with the value that Alfnes et al. (2003) used in the modeling process of project of Gardermoen.

The values for the anisotropy of hydraulic conductivity in the zones 1 and 3 for the calibrated values are close to 1. These two zones are of the same sediments (glaciofluvial). Initially the calibration started by assigning values for anisotropy from 5 – 15. These values were chosen after the similarities at Gardermoen project, where Alfnes et al. (2003) used a range from 5 to 15 for similar sediments. Nevertheless, while the calibration the values for the chosen zones were constantly dropping to result eventually to reach values close 1 for the glaciofluvial sediments and around 3 for the fluvial sediments. The values matching with the values used by Alfnes et al. (2003) were only for the zone with the till material. The anisotropy is less than the values from Alfnes et al. (2003), but there, it was a well-defined delta system so there is no indication that Glaciofluvial sediments in Grindalsmoen were deposited in the same way.

The final model developed fits quite good with the groundwater table observations used to calibrate the model both with and without the pumping. Furthermore, the equipotential lines of the hydraulic heads produced by the simulation without the pumping, are similar to the piezometric map produced for the area by Gaut et al. (1981) (Figure 5).

Furthermore, the computed water budget for the final model without the pumping seems reasonable, with the only question to be the water drained out from the aquifer by the streams. The streams modeled with the RIV package as mentioned before were set to a depth of 30 cm bellow the top elevation. At the location where the streams take out the water, that is near the western boundary, the sediment thickness is small (5-8 meters), and the slope begins to become steeper as moving towards the west. Therefore, the computed water taken out of the system by the stream near the western boundary could happen because of that.

The computed water budget and the hydraulic head equipotential lines for the final model with the assigned pumping of 5783 m^3/d at the Grindalsmoen waterworks, indicate that with the present pumping, there is considerable river water pumped from the wells.

The graph with the combined temperature (Figure 65) by Kalskin et al. (1999) is unclear. It seems that there is no interaction of the river water with the pumped water, (the spring the temperature starts to increase in Glomma before it gets in the groundwater). There is a huge heat resistance because of the sediments, if there is a difference in temperature between the sediments and Glomma river it might take some time for that to be evened out. In general, the figure with the temperatures cannot be perfectly interpreted. Therefore, is questionable if this figure shows no interaction between the groundwater and river water, the current groundwater flow model is more accurate.

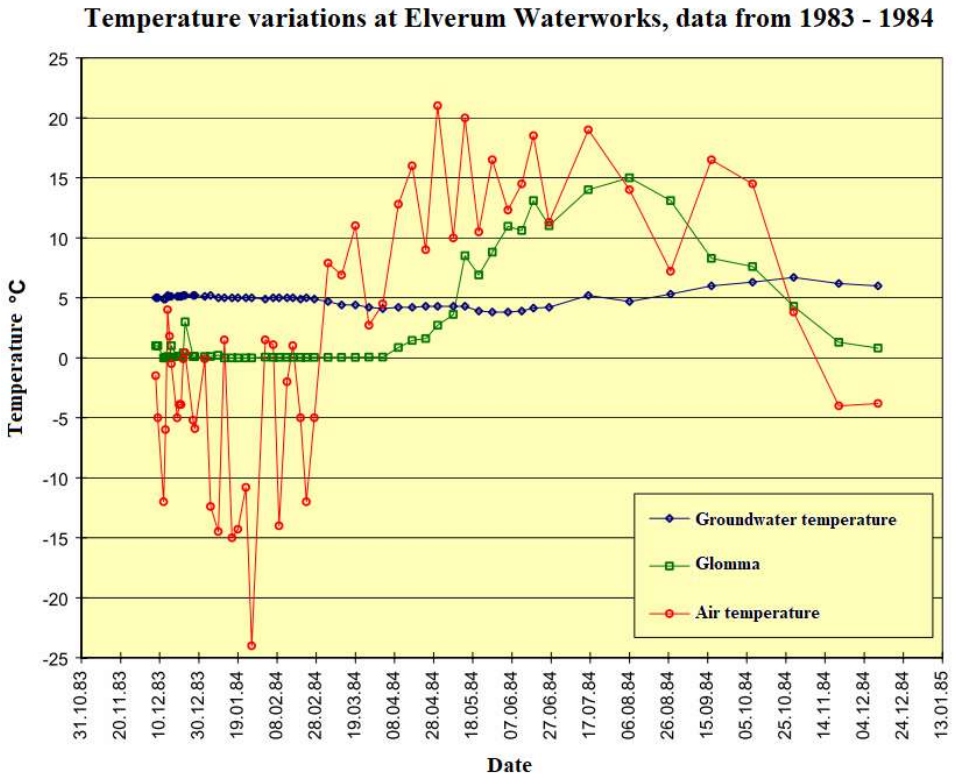

Figure 65 Graph with temperature data from 1983 – 1984 for groundwater temperature, air temperature and the river Glomma water at Elverum water works *(Kalskin and Hilmo, 1999)*

To investigate further this assumption, there was run a simulation with less pumping rate reaching 4752 m3/d, (according to Knudsen (1985) the pumping rate during the long term pumping test was 55 l/s). The results from computed the water budget (Table C1 in appendices) of the system showed that even with less pumping there was water entering the aquifer from the river Glomma.

The water coming from the river can be a modeling error in the water budget generated from the type of boundary (CHD package) used to model the river Glomma in MODFLOW. As Anderson et al. (2015) states that the head at a specified head boundary is fixed in order the flow to depend on the calculated, by the model, head gradient. Therefore, in field conditions the calculated flow may not represent the reality. Furthermore, significant errors can occur in the flow of the water supplied or removed from the model. This can happen when defining the specified heads to mimic the land surface, by extrapolating measurements of the water table from the field. Therefore, a specified head boundary with even small extrapolation errors could compute false flows into and out of the specified boundary heads (Anderson et al., 2015).

If the assumption of the modelling error stands, in the current model the problem with excess river discharge into the system, might be due to the small distance between the wells pumping and the specified head. The pumping affects the head gradient computed by the model and by extend the flow across the boundary.

Scenarios

At the first scenario, the pumping was increased 50% at the wells of the Grindalsmoen waterworks. The computed water budget showed that even more water enters the system than before with the present pumping rate, from river Glomma. Although an increase at the pumping at the Grindalsmoen waterworks would be very interesting to investigate the results in this case are questionable. Because, river Glomma was modeled with the CHD package and the problems that can occur from the type of boundary as discussed earlier. Nevertheless, with an increased pumping rate there is a big possibility to have even more water entering the aquifer from river Glomma.

The second scenario with the flux from the northern boundary tested, fits good with the observed groundwater table values used as well. The groundwater equipotential lines produced, also fit quite well in this case with the piezometric map created by Gaut et al. (1981) (Figure 5). A better fit between the computed equipotential lines of the heads and the piezometric map could be possible if the flux from the north would have assigned since the beginning. Then a calibration would really show how good the model fits with the equipotential lines of the hydraulic heads.

The results from the third tested scenario after assigning the current pumping rate at the wells at the previous scenario, showed similarities with the final calibrated model with the pumping. The similarities were obvious both at the water budgets and the equipotential lines of the hydraulic heads.

6.5 Water chemistry

The results from pH analysis for the water samples from Grindalsmoen showed that the pH is for surface water samples is slightly lower than the groundwater samples as it normally is.

The pH values for both surface and groundwater samples are in the range that Oram (2014) states that can be found in nature. The only dissonance is the groundwater sample G1 that has pH 9.7.

Most of the values from alkalinity analysis for groundwater seem to be normal since pH values lower than 6.3 indicate rather low alkalinity values. What can be questioned is the alkalinity of the groundwater sample G2 that has a low alkalinity value compared to the other groundwater samples. On the other hand, the alkalinity values for the surface water seem quite normal taking under consideration the low pH of the samples.

The ion chromatography analysis results for groundwater samples showed some inaccuracies, especially in the sample G2 where can be found a concentration for all the ions but not for magnesium.

According to Appelo and Postma (2005) and the standards for the composition of drinking water provided, all the concentrations of the ions in all the samples are much lower than the limit of the daily consumption.

Furthermore, PHREEQC simulation for the samples showed from the electrical balance of the samples that most of the samples exceeded 5% error (Figure 59) so the accuracy and the quality of the chemical analysis or the sampling should be questioned. Moreover, the electrical balance was always positive number, indicating that if the analysis is correct there is some wrong analysis with the anions. In Figure 66 it is presented the graph with the sum of the anions and the sum of the cations plotted with the Electrical conductivity of the samples divided by 100. Electrical conductivity divided by 100 give in most cases a good estimate of the sum of the anions and cations (Appelo and Postma, 2005).

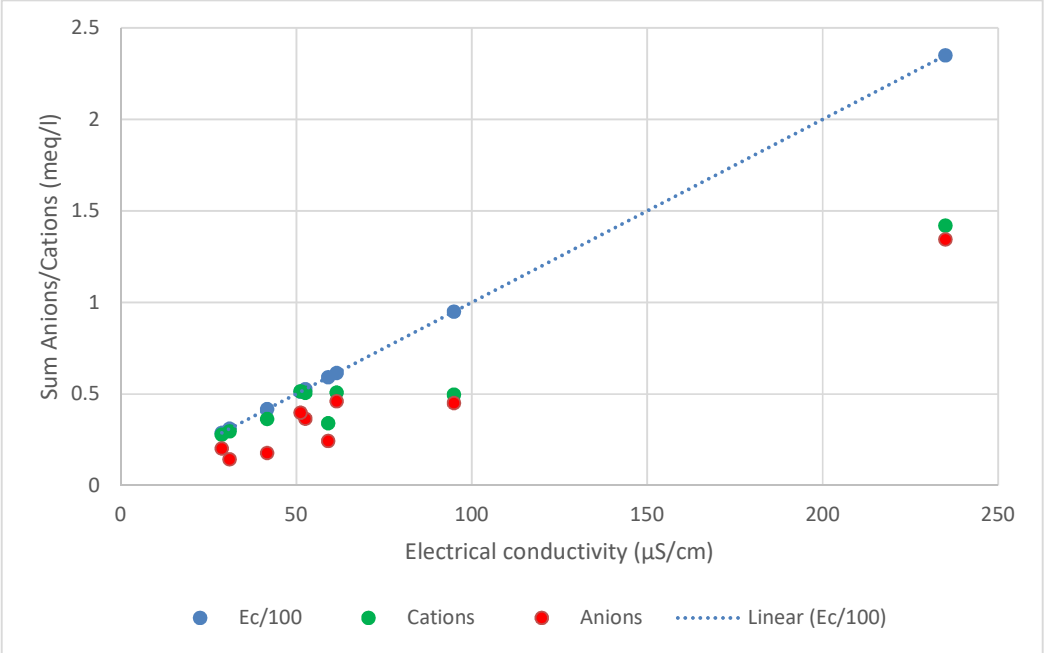

Figure 66 Graph showing the sum of the anions and cations plotted with electrical conductivity.

From the graph above it is indicated that there is a problematic analysis of the anions. Therefore, the results should be questioned.

The ICP-MS analysis showed relatively high concentrations in the samples from Grindalsmoen for the surface water samples. The groundwater samples indicated that at samples where the concentration of manganese was high, the iron concentration

was relatively low and in some occasions 0. This can be explained in the pe-pH diagram showing the stability relation for iron and manganese (Figure 67).

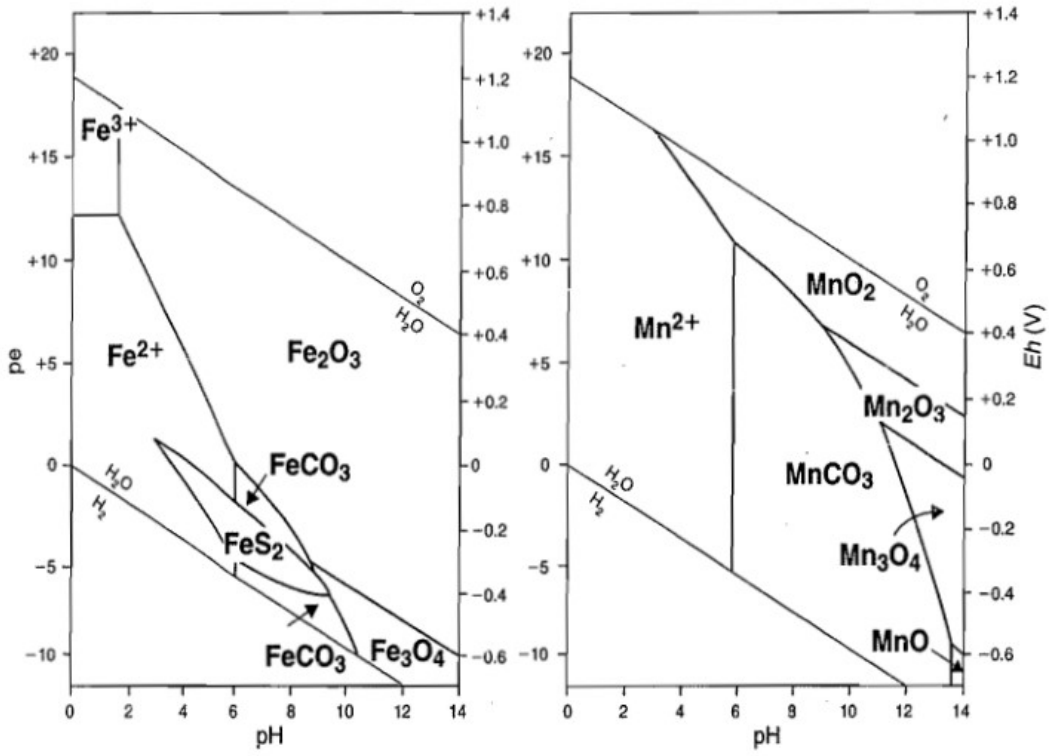

Figure 67 pe-pH stability diagram for iron and manganese at 250 . (Appelo and Postma, 2005)

At the pH range that the groundwater samples are (7.1-9.71), in the graph are maybe areas where iron cannot be found as it is precipitated out, while manganese can still exist. That seems to happen in sample G3, where probably iron precipitates as an oxide (Fe2O3) while manganese is still soluble. In general, dissolved Mn^{2+} has a larger area that can exist than Fe^{2+}. Slight variation in pH and oxidation potential can explain this behavior.

Although there is no proposed health-based guideline value for iron concentration limits for drinking water, for aesthetic reasons concentrations above 0.3 mg/l are noticeable in taste and turbidity as well as color could be developed (World Health Organization, 2006).

For the samples from Grindalsmoen, the surface water samples S1 and the groundwater samples G2, G4 and G5 exceed this value, while surface water S2 is very close (0.29 mg/l.).

Concentrations of manganese exceeding 0.1 mg/l causes the water a bad taste, concentrations below this value are acceptable. The health based guideline for manganese is 0.05 mg/l (World Health Organization, 2006). The samples from Grindalsmoen exceeding the value of 0.05 mg/l are the surface water sample S3 as well as the groundwater samples G3, G4 and G5.

The water sample from the tap of waterworks of Grindalsmoen after the Vyredox process showed significant reduced concentrations in comparison with the samples G4 and G5, from the observation wells at the area of the waterworks.

6.6 Further work

To have a better overview of the aquifer of Grindalsmoen, the interaction of the streams with the groundwater needs to be further investigated. Furthermore, the interaction of the lake with the groundwater needs to be investigated further.

Moreover, more groundwater wells can be drilled, especially inside and outside of the northern and southern borders of the proposed catchment area. This will help to investigate the inflow and out flow from the northern and southern boundary respectively by checking the hydraulic heads and in general the water table. This would provide more information to create an accurate piezometric map.

For a better representation of the reality, a groundwater flow model with multiple layers should be developed. In addition, the cells between river Glomma and the pumping wells should be refined to check again the water budget and the interaction of the river with the groundwater. The streams after having more measurements for their water level in several locations and investigate with geophysical surveys the thickness of the bed, could be modeled with the Stream package (STR) that will give probably a better representation of reality.

The main question that needs to be investigated further is the interaction of the river Glomma with the aquifer when pumping. Therefore, other methods, need to be conducted in the area to answer this question and to quantify the exact possible amount of water coming from the river into the aquifer. Such a method would be to improve the current groundwater flow model by adding a heat transfer part that can

track the Glomma river water into the aquifer. Finally, chemical mixing methods including tracers could take be conducted to investigate the Glomma – aquifer interaction.

The groundwater chemistry needs to be investigated deeper, with more groundwater samples, surface water samples as well as samples from river Glomma, in order to demonstrate the transport of the solutes with a reactive transport model for instance.

7 Conclusion

The Grindalsmoen aquifer, supplying water the waterworks in the area was studied. The geometry of the aquifer was investigated, using data already available from literature, from the participation at the field course in the area as well as field observations. The sediment thickness of the phreatic aquifer of Grindalsmoen is 2-7 meters in the west, until the location where the glaciofluvial sediments are deposited. Here the thickness of the sediments starts to increase as moving towards the Glomma banks ending up to a thickness of approximate 35 meters.

The hydraulic conductivity of the sediments was investigated with different methods and fitted in places with the obtained values after the calibration.

There was an initial challenge in developing the groundwater flow model for the aquifer of Grindalsmoen initially was challenging. Because of the small thickness of the sediments at the western part of the catchment, many dry cells were generated in the model. However, the model was cut at the boundary of the till material with the glaciofluvial sediments, and the recharge of the cut area was distributed at the western boundary as flux from injection wells along the boundary. This flux was assigned with more weight for the wells on the northern part of the western boundary, because of the higher amount of water ending up to there. This decision was taken after delineating the two smaller catchments at the western cut area, and observing that the northern catchment was larger than the southern one.

The computed heads from the simulation of the final model developed, fitted quite good the observed heads used for the calibration of the model. Moreover, the groundwater equipotential lines fitted well the piezometric map produced from Gaut et al. (1981), However, when including water extraction by the waterworks, there was considerably recharge from the river. Temperature observations of the groundwater and river during the test pumping in 1983, indicated that minor water was extracted from Glomma. This apparent contradiction needs further attention. Does the model lead to more recharge from Glomma that actually is the case? Or is another interpretation of the temperature more possible?

This modeling result needs to be questioned, because it could be due to the specified head boundary used to model Glomma river in MODFLOW. Therefore, it is strongly proposed to investigate further the interaction of the river Glomma with the aquifer.

The scenario tested with the flow from the northern boundary didn't show a better fit than the final calibrated model, with the piezometric map by Gaut et al. (1981). Nevertheless, the piezometric map from that year shows that there is some flux from the northern boundary although the well logs presented in Gaut et al. (1981) indicate that the sediment thickness is very small (1-6 m). The amount of water entering the aquifer from the northern boundary as well as the outflow from the southern one need to be investigated further.

The scenario with the increased pumping for the final calibrated model did not give any actual conclusion about the pumping in the waterworks, since there was even more water coming in the aquifer from the river Glomma. Result that is also questionable due to the reasons mentioned above. The same thing stands for the scenario with the flux from the northern boundary with the present pumping rate.

The results from the chemical analysis showed that for all the samples the ion concentration was not exceeding the drinking water limits although the drinking water sample contained relatively high concentration in nitrate. Nevertheless, the electrical balance error exceeded 5 % in all the surface water samples and in the drinking water, thus the results need to be questioned and should be studied further.

The content of iron and manganese in the surface water samples was acceptable for consumption except, S1 and S3 that had concentration in iron and manganese respectively exceeding the proposed health-based guidelines. However, they are surface waters that are not intended for drinking water.

The ICP-MS analysis for the groundwater showed that all the groundwater samples were exceeding the proposed health-based guidelines for either iron or manganese, except groundwater sample G1, that was in the limits.

However, the drinking water from the station in the waterworks had very low content in iron and manganese as the results from ICP-MS analysis showed that the in-situ

treatment method (Vyredox) was effective. The drinking water delivered to the municipality is safe for consumption.

References

Ahmad, M., 2012. Iron and Manganese removal from groundwater Geochemical modeling of the Vyredox method. University of Oslo.

Alfnes, E., Kinzelbach, W., Aagaard, P., 2003. Investigation of hydrogeologic processes in a dipping layer structure: 1. The flow barrier effect. J. Contam. Hydrol. https://doi.org/10.1016/j.jconhyd.2003.08.005

Allaby, M., 2013. A dictionary of Geology and Earth Sciences, 4th ed. Oxford University Press, Oxford, United Kingdom.

Alley, W.M., Reilly, T.E., Franke, O.L., 1999. Sustainability of Ground-Water Resources.

Anderson, M.P., Woessner, W.W., Hunt, R.J., 2015. Applied groundwater modeling; Simulation of Flow and Advective Transport, 2nd ed. Elsevier.

Annan, A.P., 2005. GPR Methods for Hydrogeological Studies, in: Hydrogeophysics. https://doi.org/10.1007/1-4020-3102-5_7

Appelo, C.A.J., Postma, D., 2005. Geochemistry, groundwater and pollution, 2nd ed, Geochemistry, Groundwater and Pollution, Second Edition. CRC Press.

Aqtesolv, 2015. Hvorslev Slug Test Solution for Confined Aquifers [WWW Document]. URL http://www.aqtesolv.com/hvorslev.htm

AQUAVEO, 2019. GMS:LAK Package - XMS Wiki [WWW Document]. URL https://www.xmswiki.com/wiki/GMS:LAK_Package (accessed 7.26.19).

AQUAVEO, 2017. GMS: PEST [WWW Document]. GMS Wiki - online Help GMS. URL https://www.xmswiki.com/wiki/GMS:PEST

Aquaveo LLC, 2017. The groundwater modeling system - GMS.

Barnett, B., Townley, L., Post, V., Evans, R., Hunt, R., Peeters, L., Richardson, S., Werner, A., Knapton, A., Boronkay, A., 2012. Australian groundwater modelling guidelines, Waterlines Report Series. https://doi.org/10.1007/s00767-014-0279-z

Bazilio, A., Weinrich, J., 2012. The Easy Guide to: Inductively Coupled Plasma-Mass Spectrometry (ICP-MS).

Betancur, T., Palacio T., C.A., Escobar M., J.F., 2012. Conceptual Models in Hydrogeology, Methodology and Results, in: Hydrogeology - A Global Perspective. https://doi.org/10.5772/28155

Braester, C., Martinell, R., 1988. The vyredox and nitredox methods of in situ treatment of groundwater. Water Sci. Technol. 20, 149–163.

Brassington, R., 2007. Field Hydrogeology: Third Edition, Field Hydrogeology: Third Edition. https://doi.org/10.1002/9780470057032

Bredehoeft, J., 2005. The conceptualization model problem - Surprise. Hydrogeol. J. 13, 37–46. https://doi.org/10.1007/s10040-004-0430-5

Breivik, A., Bazin, S., Eiken, T., 2018. GEO4120 – "Near-Surface Geophysics." UiO, Oslo.

Buckner, M.Z., 2007. Ion Chromatography [WWW Document]. URL https://serc.carleton.edu/microbelife/research_methods/biogeochemical/ic.html (accessed 5.16.19).

COWI, 2016. Rv. 3 / rv. 25 Løten - Elverum, Geoteknisk datarapport del4, Åkroken - Grundset. Oslo.

Davidson, P., Wilson, S., 2011. Aquifer hydraulic properties, in: Hamill, P. (Ed.), Groundwaters of Marlborough. Marlborough District Council.

Dingman, S.L., 2015. Physical Hydrology, 3rd ed. Waveland Press, Inc, Long Grove, Illinois.

Doherty, J., 2003. Ground water model calibration using pilot points and regularization. Ground Water. https://doi.org/10.1111/j.1745-6584.2003.tb02580.x

Domenico, P.A., Schwartz, F.W., 1997. Physical and chemical hydrogeology. Second edition.

Elverum Kommune, 2018. Vannforsyning [WWW Document]. URL https://www.elverum.kommune.no/plan-bygg-eiendom/vann-og-avlop/vannforsyning (accessed 3.13.19).

Fetter, C.W.C.W., 2001. Applied Hydrogeology, Applied Hydrogeology. https://doi.org/0-13-088239-9

Fitts, C.R., 2013. Groundwater Science, 2nd ed, Groundwater Science. Academic Press.

Gaut, A., Klemetsrud, T., Rohr-Torp, E., 1981. Beskrivelse til vannressurskart "Grunnvann i løsavsetninger." Oslo.

Gaut, S., 2011. Beskyttelse av grunnvannsanlegg – en veileder 45.

Grayline LLC, 2015. Peristaltic Pump Tubing. Waukesha, Winsconsin.

Hallberg, R.O., Martinell, R., 1976. Vyredox — In Situ Purification of Ground Water. Ground Water 14, 88–93. https://doi.org/10.1111/j.1745-6584.1976.tb03638.x

Hansen, L., Rohr-Torp, E., Tønnesen, J.., Rønning, J.S., Mauring, E., 2005. Grunnvann og grunnvarme fra dype dalfyllinger langs Glåma. Rapport nr: 2002.082. Trondheim. https://doi.org/10.1360/zd-2013-43-6-1064

Harbaugh, A.W., 2005. MODFLOW-2005, The U.S. Geological Survey Modular Ground-Water Model-the Ground-Water Flow Process. Reston, Virginia.

Hiscock, K.M., Bense, V.F., 2014. Hydrogeology Principles and Practice, 2nd ed. J. Wiley & Sons.

Høgaas, F., Longva, O., 2016. Mega deposits and erosive features related to the glacial lake Nedre Glomsjø outburst flood, southeastern Norway. Quat. Sci. Rev. 151, 273–291. https://doi.org/10.1016/j.quascirev.2016.09.015

Jaudon, P., Massiani, C., Galea, J., Rey, J., Vacelet, E., 1989. Groundwater pollution by manganese. Manganese speciation: Application to the selection and discussion of an in situ groundwater treatment. Sci. Total Environ. 84, 169–183. https://doi.org/10.1016/0048-9697(89)90381-1

Kalskin, R., Hilmo, B.O., 1999. NGU Rapport 99.008 Kartlegging av potensialet for grunnvarmeuttak fra løsmasser i Elverum.

Kharal, N., 2017. Hydrogeological Conditions at the Water Works of Elverum Kommune. NMBU.

Knudsen, C.-H., 1985. Elverum kommune Grunnvannsforsyning Grindalen langtidsprøvepumping. Drammen.

Knudsen, C.-H., 1983. Elverum kommune Grunnvannsforsyning Beskyttelse av infiltrasjons - omrrådet for nye grunnvannsbrønner. Drammen.

Kresic, N., 2007. Hydrogeology and Groundwater Modeling, Taylor & Francis Group. https://doi.org/10.1017/CBO9781107415324.004

Kresic, N., Mikszewski, A., 2013. Hydrogeological conceptual site models Data Analysis and Visualization. CRC Press.

Landviser LLC, 2002. dipole-dipole | Landviser, LLC [WWW Document]. URL http://www.landviser.net/equipment/accessories/arrays/dipole-dipole (accessed 5.22.19).

Moore, J.E., 2012. Field Hydrogeology: A Guide for Site Investigations and Report Preparation, Second Edition, 2nd ed. CRC Press.

Naoroz, M.S., 2018. Ion Chromatography of (Anions and Cations) with Suppression of Eluent. Oslo.

NGU, 2019. Løsmasser [WWW Document]. URL http://geo.ngu.no/kart/losmasse/ (accessed 5.30.19).

NGU, 2017. Groundwater Use [WWW Document]. URL https://www.ngu.no/en/topic/groundwater-use (accessed 2.10.19).

Oram, B., 2014. Water Research Center - The pH of Water [WWW Document]. URL https://www.water-research.net/index.php/ph (accessed 5.12.19).

Palacky, G.., 1987. Resistivity characteristics of geological targets. In. Electromagnetic Methods in Applied Geophysics, Nabighian, M.N. (ed). Vol. 1 –

Theory, Chapter 3: 53-129. Society of Exploration Geophysicists, Tulsa.

PerkinElmer Inc., 2010. The 30-Minute Guide to ICP-MS. Tech. Note ICP-Mass Spectrom. 1–8.

QGIS Development team, 2016. QGIS Geographic Information System.

Reynolds, J.M., 2011. An introduction to applied and environmental geophysics, 2nd ed. John Wiley & Sons.

Rounds, S.A., 2012. Alkalinity and acid neutralizing capacity (ver. 4.0), in: U.S. Geological Survey Techniques of Water-Resources Investigations, Book 9. pp. 1–45.

Rushton, K.R., 2003. Groundwater Hydrology: Conceptual and Computational Models, 1st ed. Wiley.

Sharma, A.S., Das, D., Koustuvee, K., Dutta, B., Agarwala, R., Sen, S., Thakuria, D., Sarma, A.K., 2016. Impact of Slope and Vegetation on Hydrological Processes, in: Sarma, A.K., Singh, V.P., Kartha, S.A., Bhattacharjya, R.K. (Eds.), Urban Hydrology, Watershed Management and Socio-Economic Aspects. Springer International Publishing, Cham, pp. 3–21. https://doi.org/10.1007/978-3-319-40195-9_1

Singhal, B.B.S., Gupta, R.P., 2010. Applied hydrogeology of fractured rocks: Second edition, Applied Hydrogeology of Fractured Rocks: Second Edition. https://doi.org/10.1007/978-90-481-8799-7

U.S. Environmental Protection Agency, 2016. Resistivity Methods [WWW Document]. URL https://archive.epa.gov/esd/archive-geophysics/web/html/resistivity_methods.html (accessed 3.1.19).

Viessman, W.J., Lewis, G.L., 1996. Introduction to Hydrology, 4th ed. Harpercollins College Div.

Wagener, T., Sivapalan, M., Troch, P., Woods, R., 2007. Catchment Classification and Hydrologic Similarity. Geogr. Compass. https://doi.org/10.1111/j.1749-8198.2007.00039.x

Weibull, J., Sandvik, G., Enander, H., Christensen, J., Joys, C., 2019. Norway | Facts, Points of Interest, Geography, & History [WWW Document]. Encycl. Br. URL https://www.britannica.com/place/Norway

Winston, R.B., 2019. ModelMuse Help - Boundary Conditions [WWW Document]. USGS. URL https://water.usgs.gov/nrp/gwsoftware/ModelMuse/Help/index.html?boundary_conditions5.htm (accessed 5.30.19).

World Health Organization, 2006. Guidelines for Drinking-water Quality FIRST ADDENDUM TO THIRD EDITION Volume 1 Recommendations WHO Library Cataloguing-in-Publication Data.

Appendices

Appendix A: Aquifer geometry and water table

Appendix B: Aquifer properties

Appendix C: Numerical modeling

Appendix D: Water Chemistry

Appendix A

The location of the GPR profiles is shown in Figure 14.

GPRGRA

Line 11

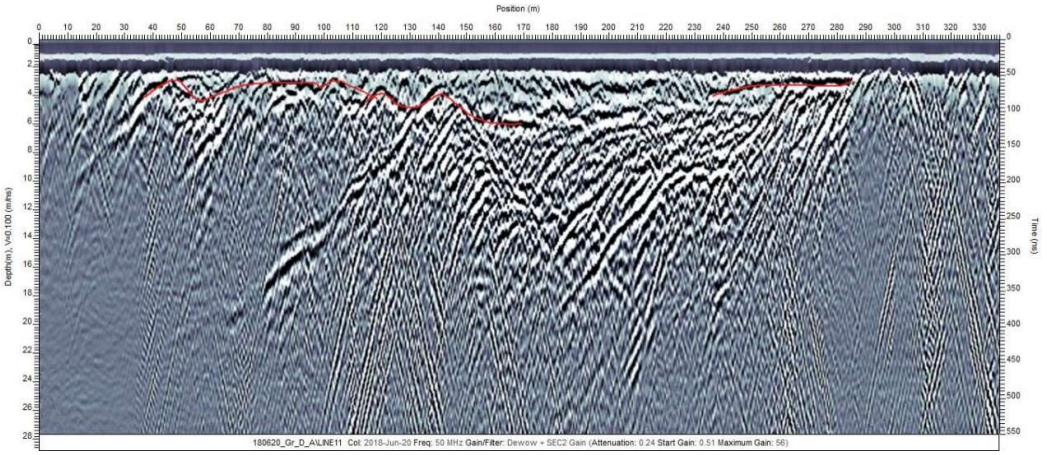

Figure A1 GPR profile from the group GPRA showing with red line the depth to bedrock

Line 12

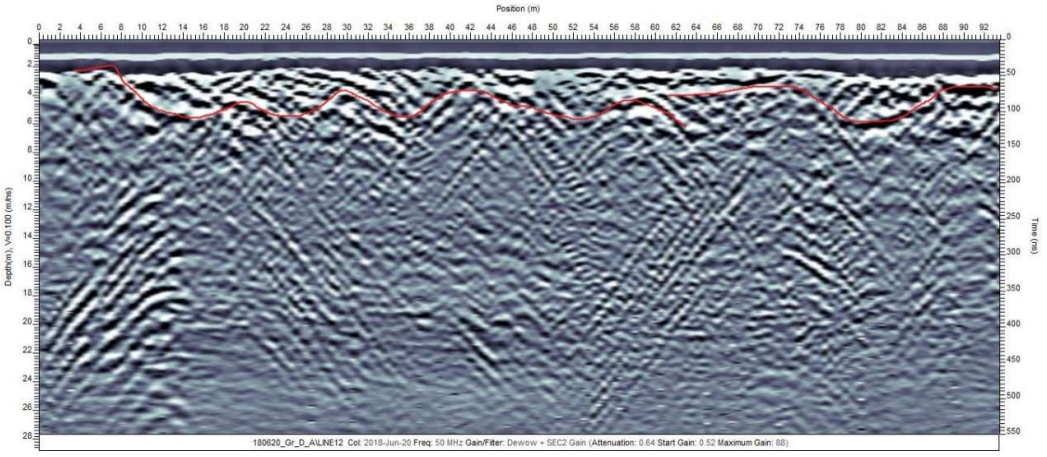

Figure A2 GPR profile from the group GPRA showing with red line the depth to bedrock

Line 13a

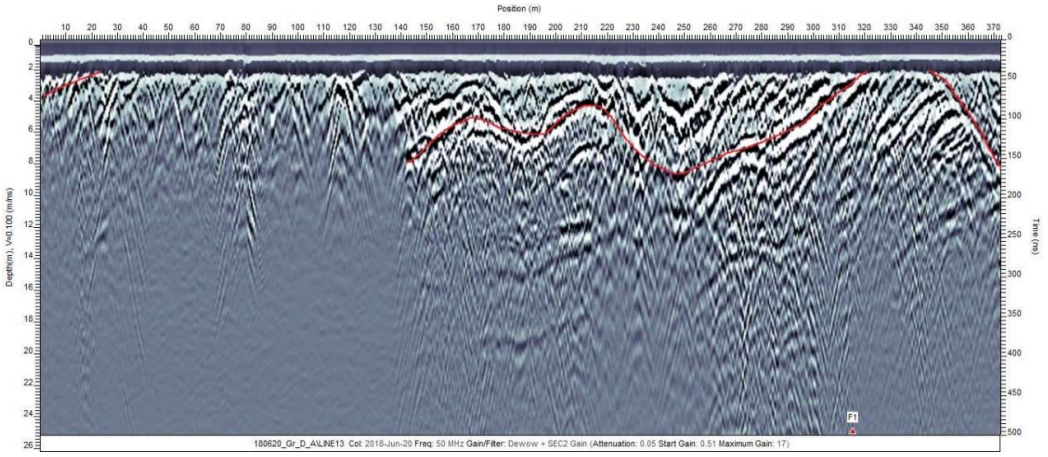

Figure A3 GPR profile from the group GPRA showing with red line the depth to bedrock

Line 13b

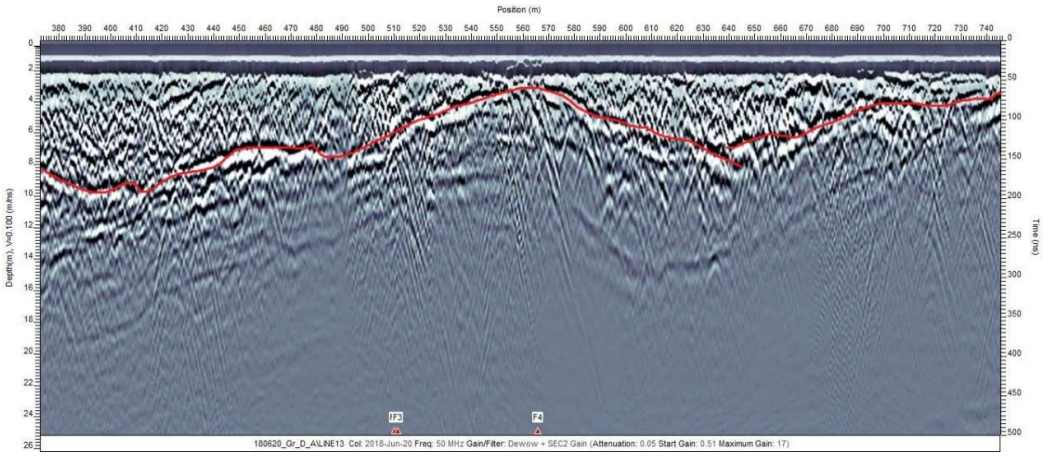

Figure A4 GPR profile from the group GPRA showing with red line the depth to bedrock

Line13c

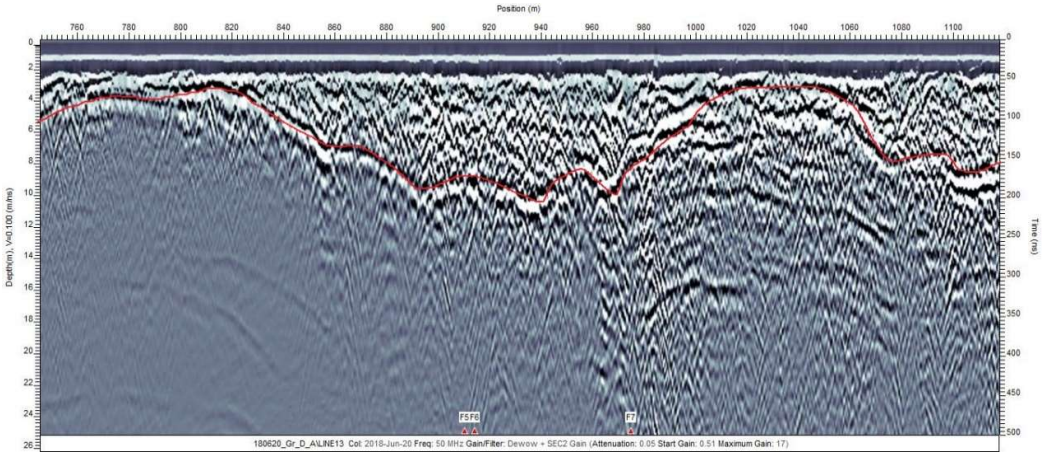

Figure A5 GPR profile from the group GPRA showing with red line the depth to bedrock

Line 13d

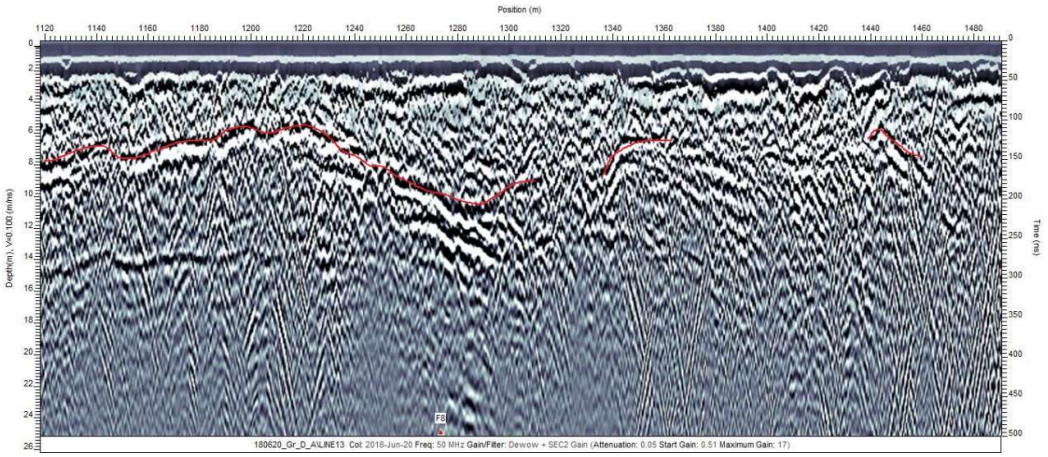

Figure A6 GPR profile from the group GPRA showing with red line the depth to bedrock

GPRB

Line00

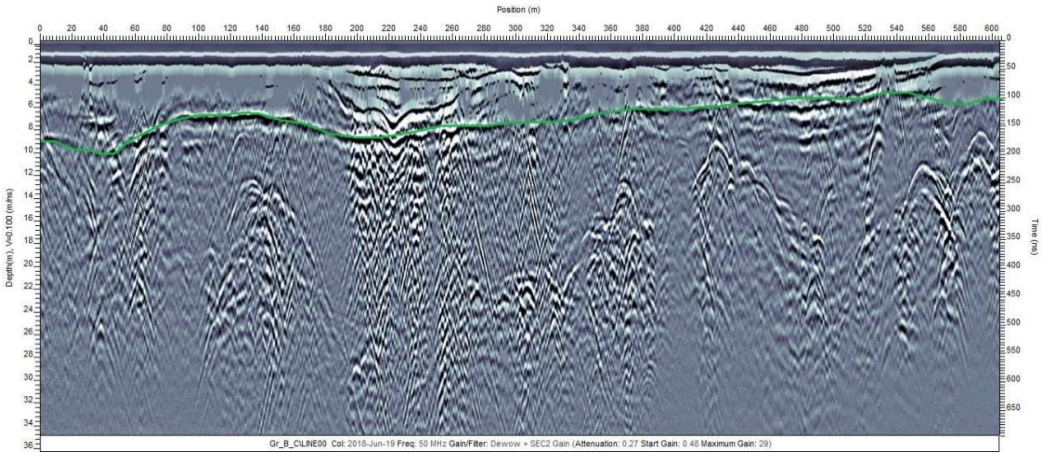

Figure A7 GPR profile from the group GPRB showing with green line the depth to the water table.

Line01

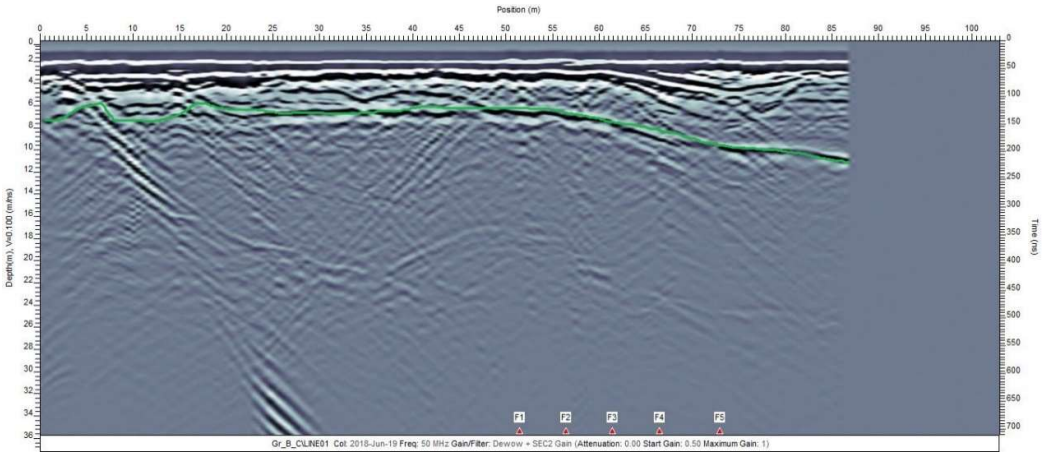

Figure A8 GPR profile from the group GPRB showing with green line the depth to the water table.

Line02

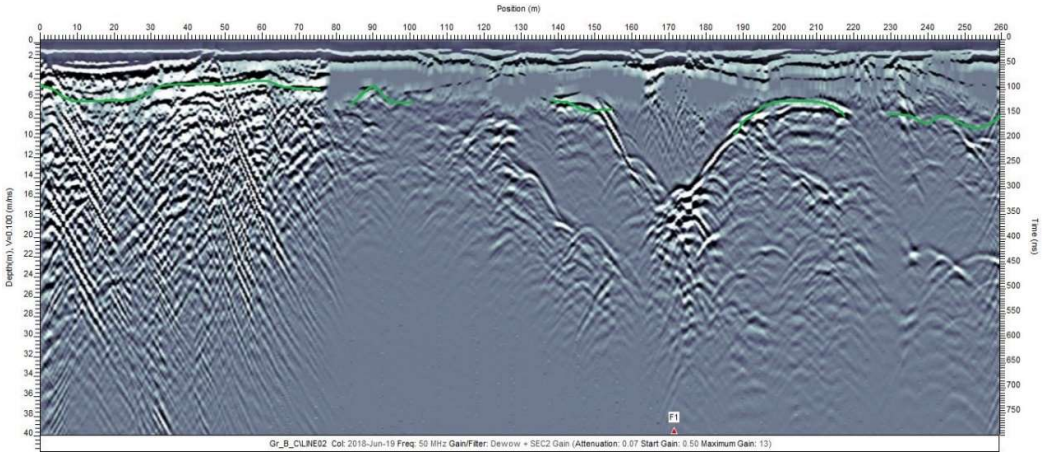

Figure A9 GPR profile from the group GPRB showing with green line the depth to the water table.

Line03

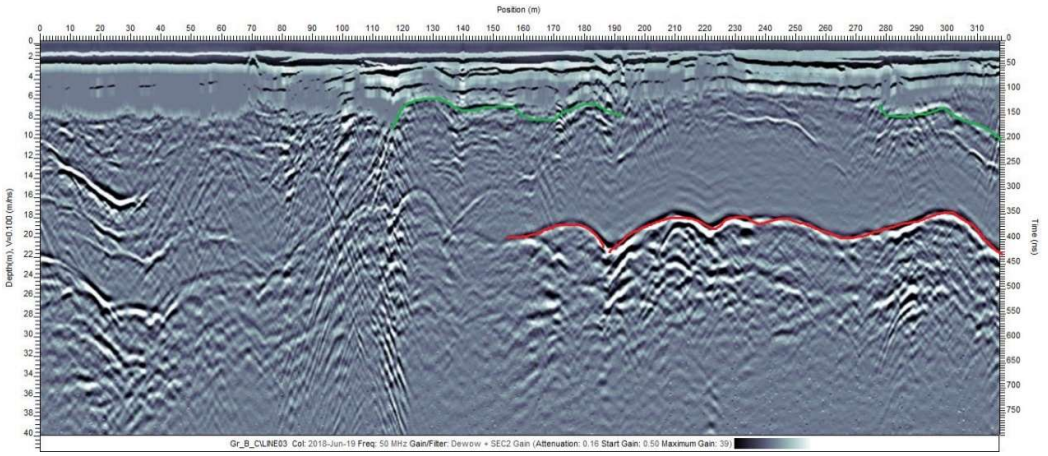

Figure A10 GPR profile from the group GPRB showing with green line the depth to the water table and with red the depth to the bedrock.

Line04

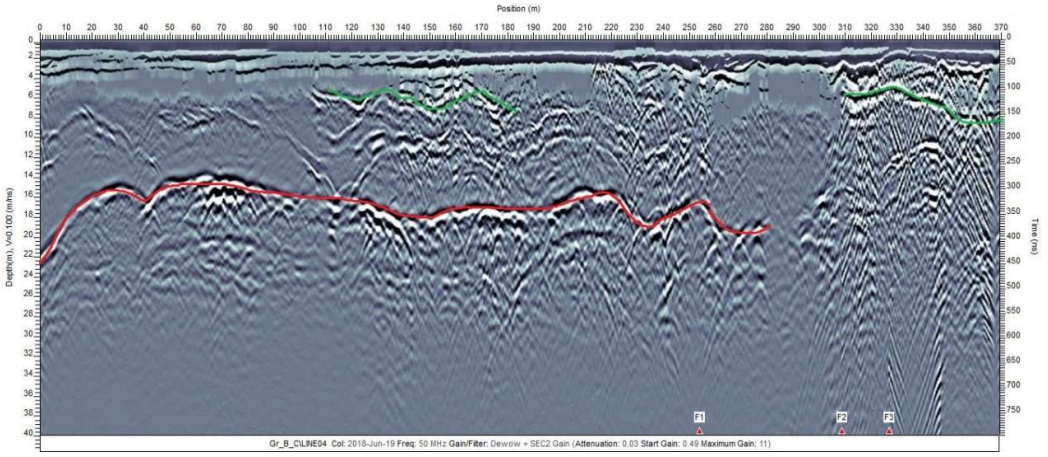

Figure A11 GPR profile from the group GPRB showing with green line the depth to the water table and with red the depth to bedrock.

GPRGRC

Line05

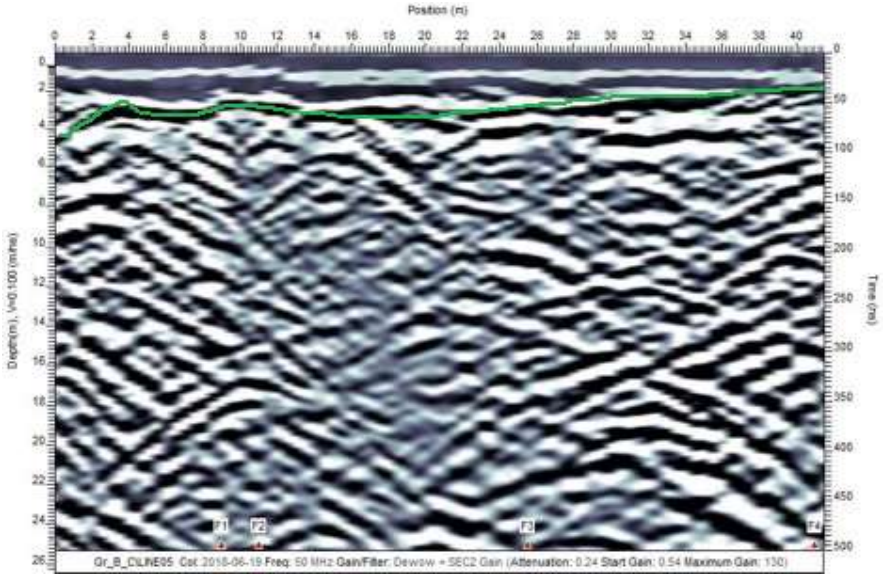

Figure A12 GPR profile from the group GPRC showing with green line the depth to the water table.

Line07

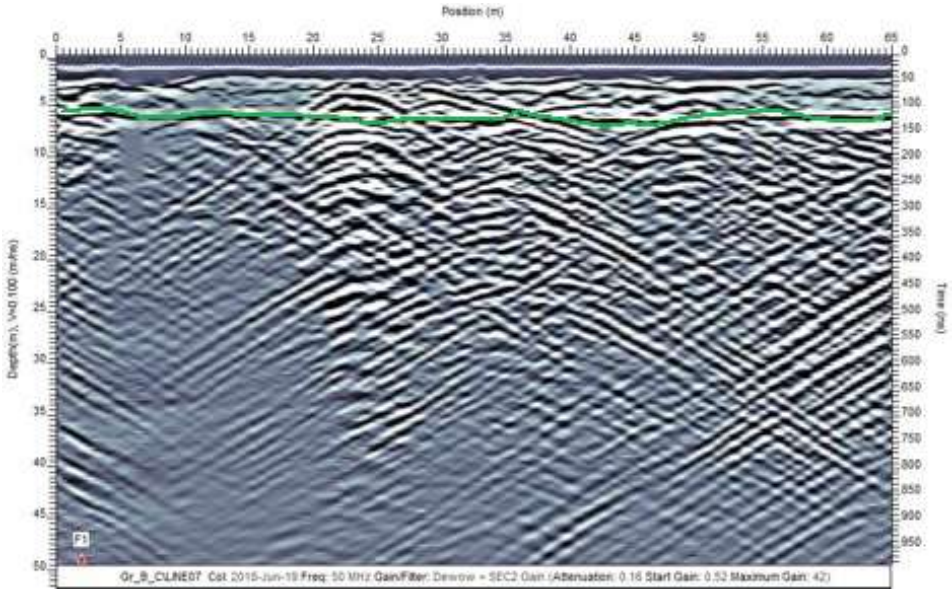

Figure A13 GPR profile from the group GPRC showing with green line the depth to the water table.

Line09

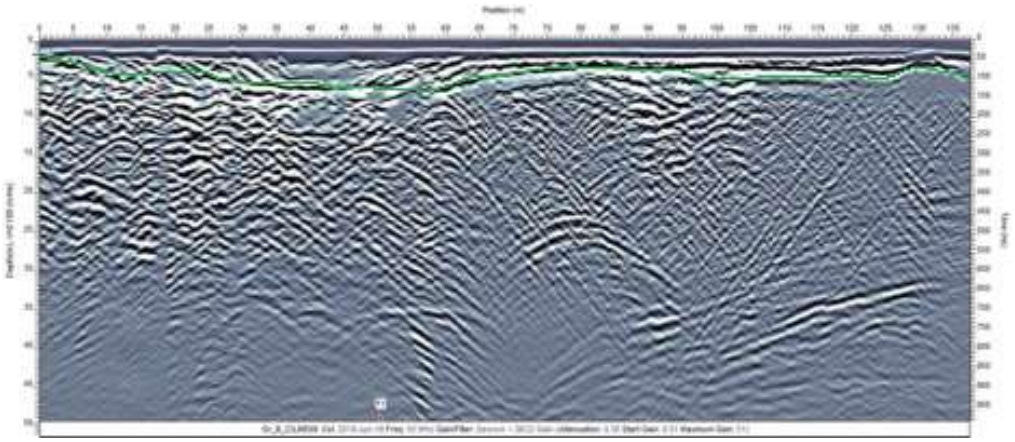

Figure A14 GPR profile from the group GPRC showing with green line the depth to the water table.

GPRGRD

Line10

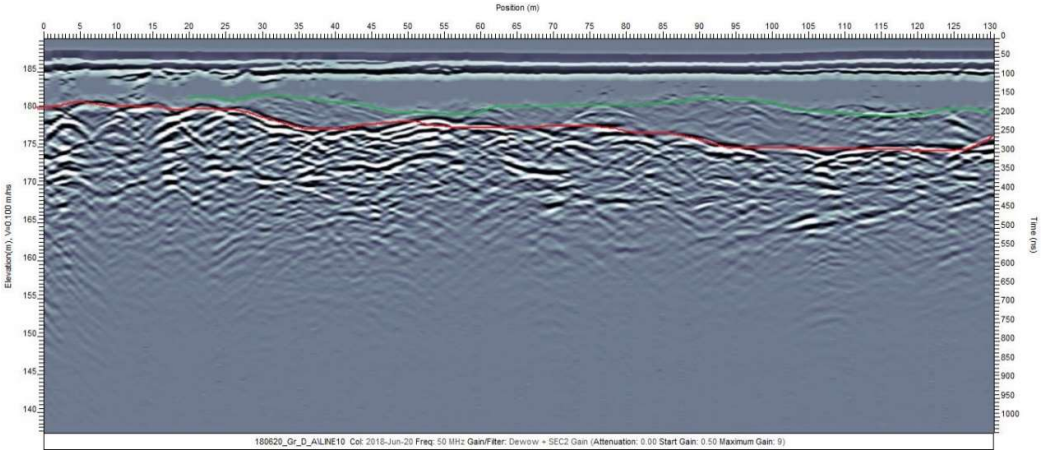

Figure A15 GPR profile from the group GPRD showing with green line the depth to the water table and with red the depth to bedrock.

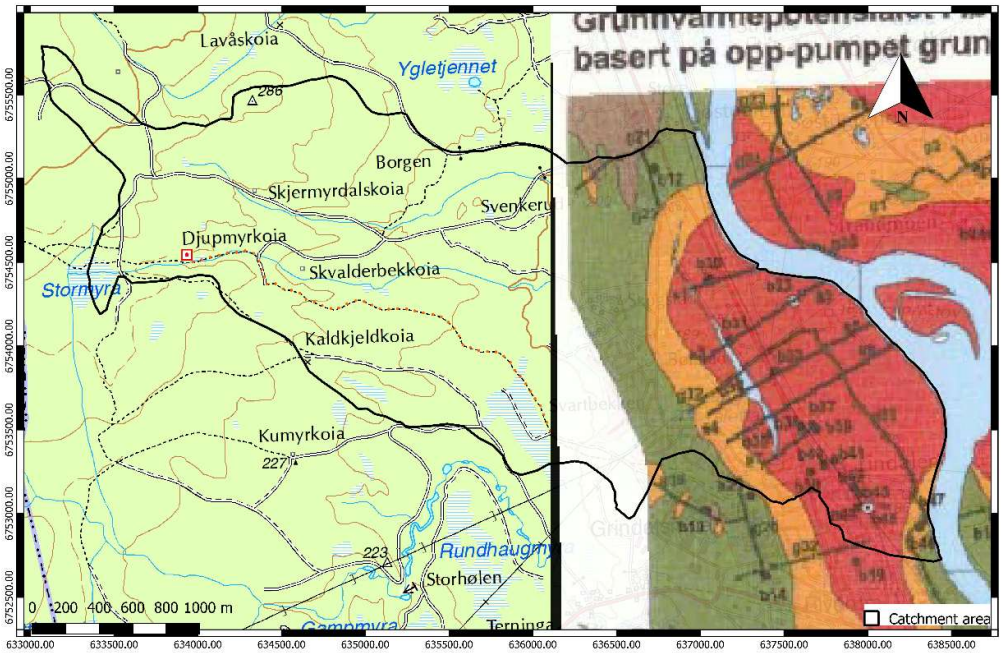

Figure A15 Georeferenced map from Kalskin and Hilmo (1999), showing the location of the GPR profiles.

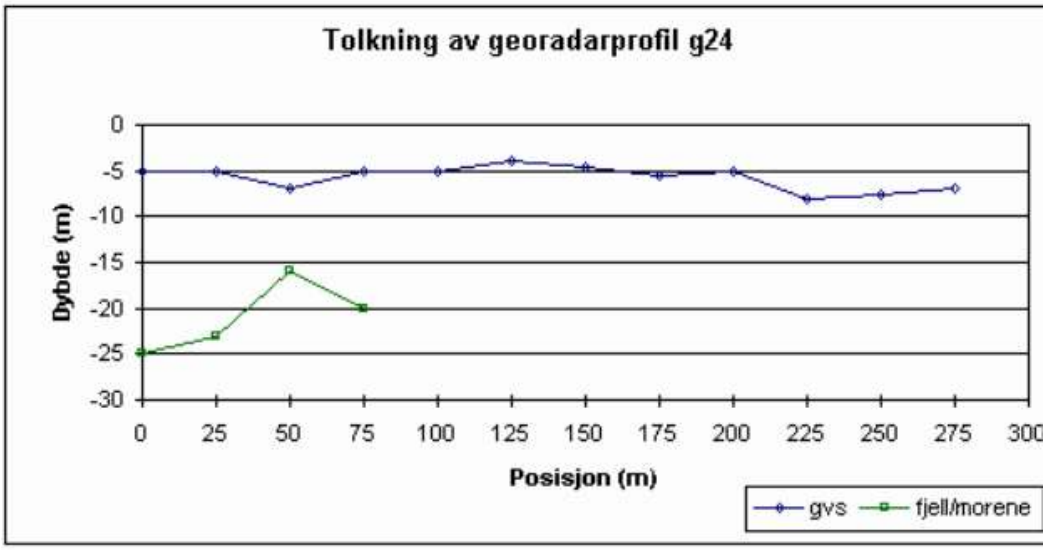

Figure A16 Graph from Kalskin and Hilmo (1999), showing the groundwater table which was not used and the depth to bedrock along the profile.

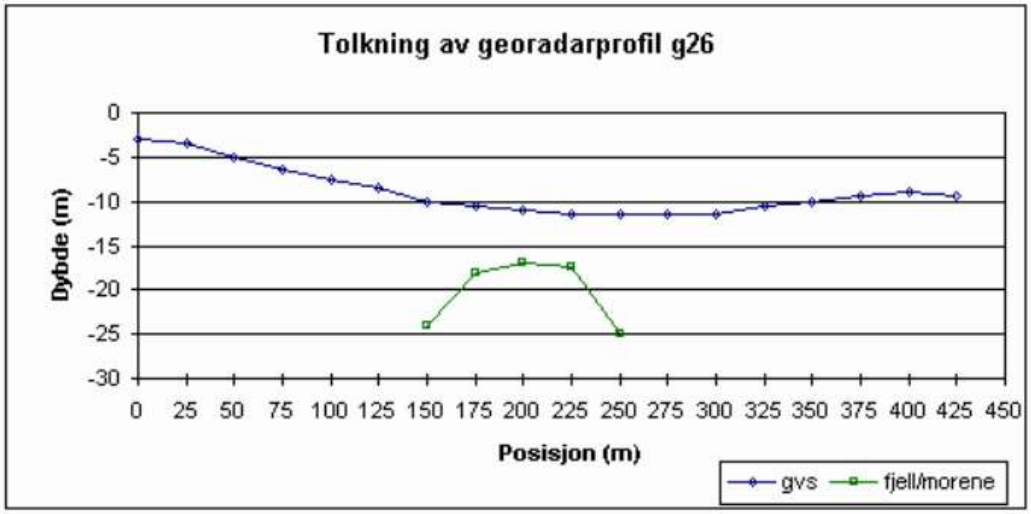

Figure A17 Graph from Kalskin and Hilmo (1999), showing the groundwater table which was not used and the depth to bedrock along the profile.

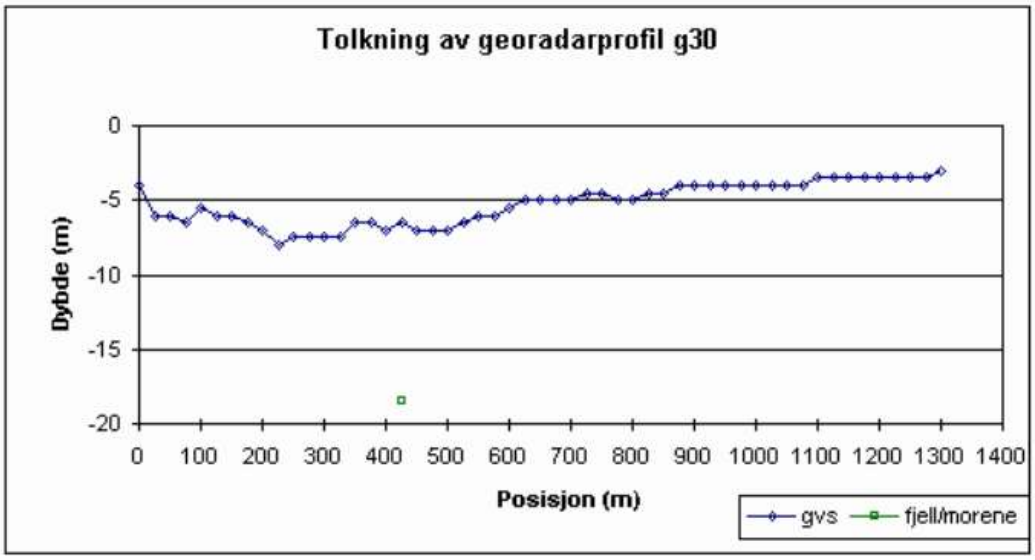

Figure A18 Graph from Kalskin and Hilmo (1999), showing the groundwater table which was not used and the depth to bedrock along the profile.

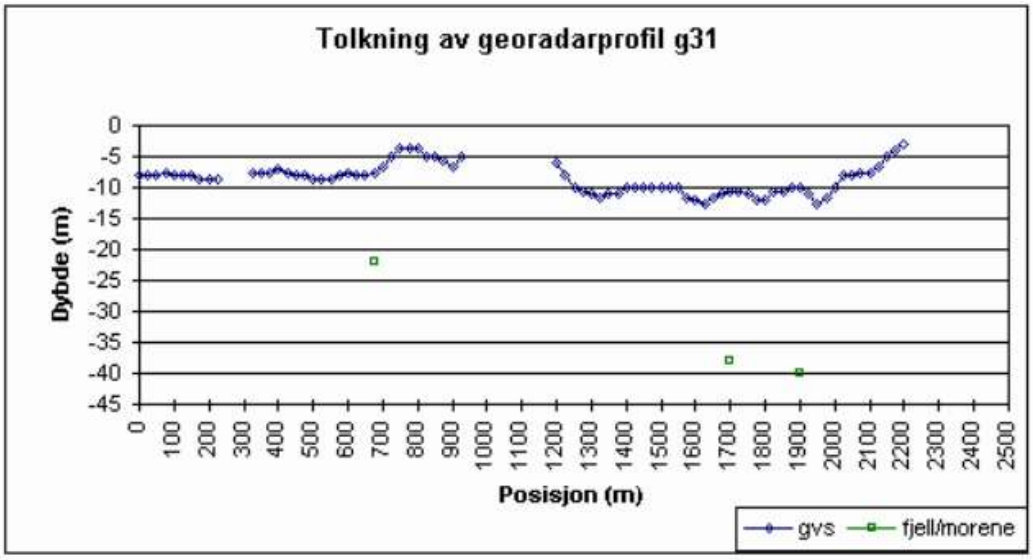

Figure A19 Graph from Kalskin and Hilmo (1999), showing the groundwater table which was not used and the depth to bedrock along the profile.

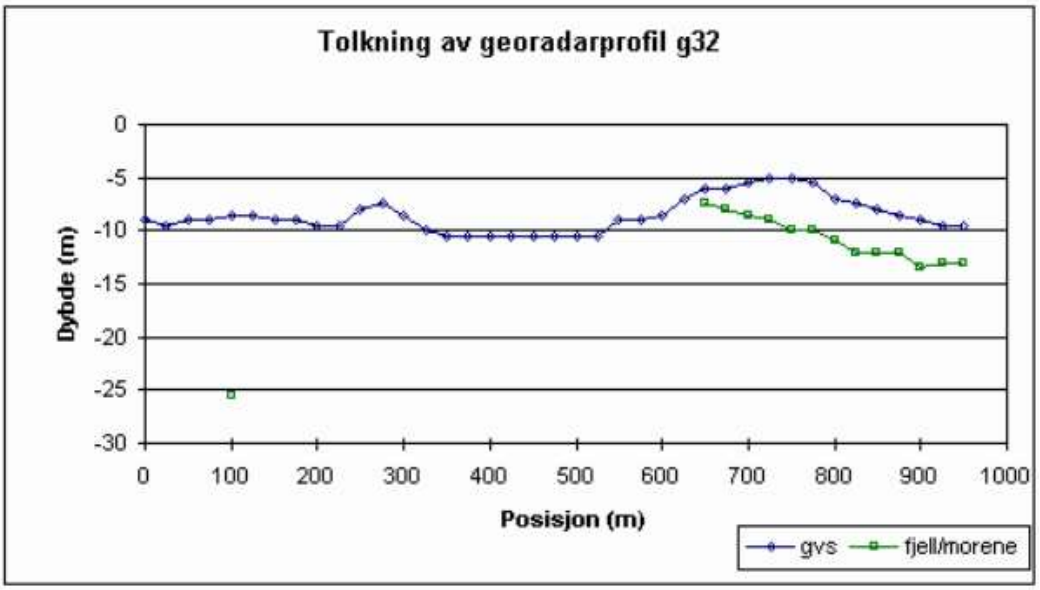

Figure A20 Graph from Kalskin and Hilmo (1999), showing the groundwater table which was not used and the depth to bedrock along the profile.

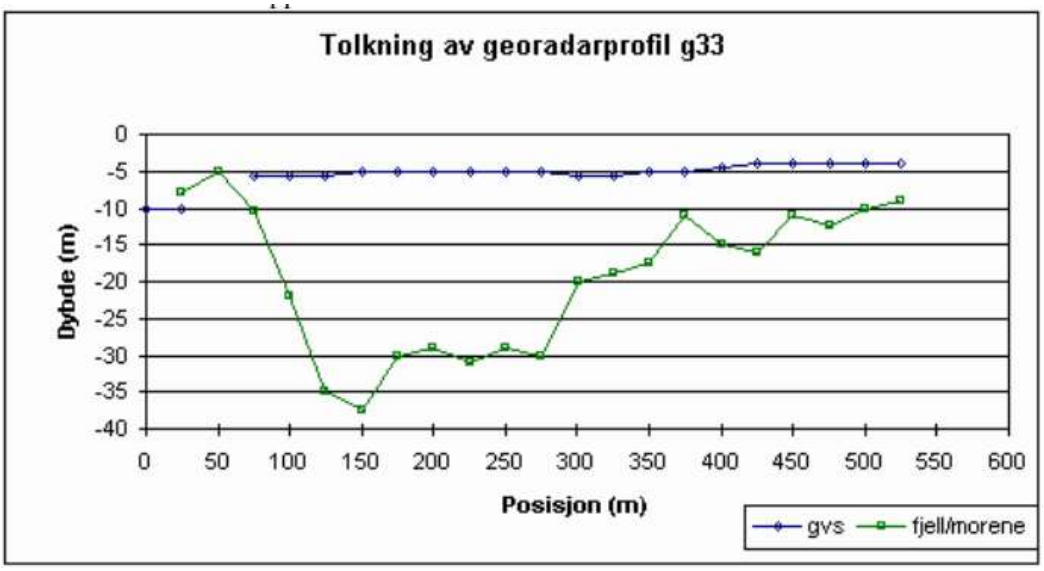

Figure A21 Graph from Kalskin and Hilmo (1999), showing the groundwater table which was not used and the depth to bedrock along the profile.

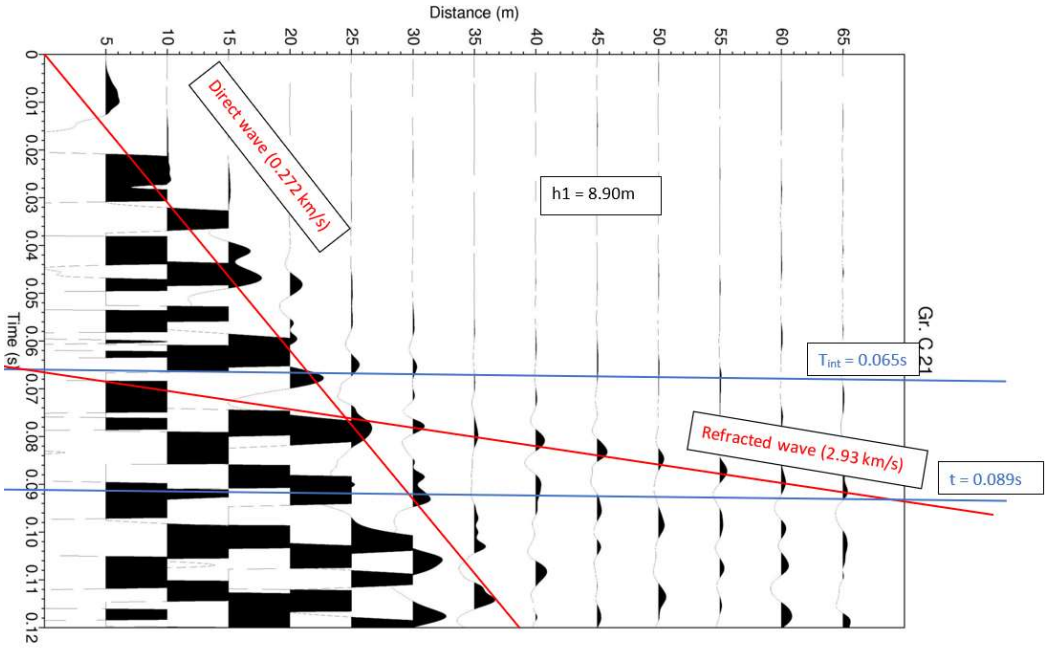

Figure A22 Seismic refraction interpreted data from the students of the field class.

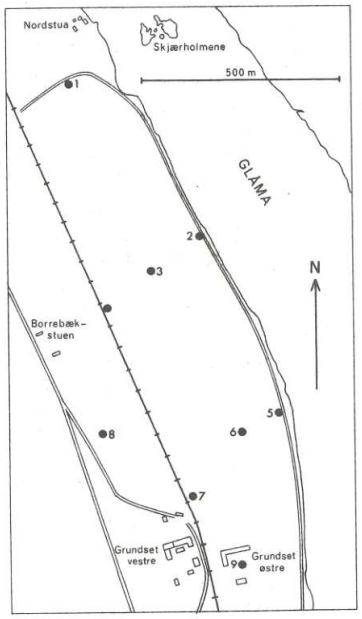

Utsnitt 1, Grundsetmoen 1

Kartblad: 2016 IV ELVERUM

Løpenr.	5	6
Kartsymbol	■1	■1
Lokalitet	361 585	361 585
Utsnitt nr.	1	1
Prøvested	5	6
Prøvetatt av		
Boringens art	S/U	S/U
Dato/år	1978	1978
Merknad:	Vannstandsmåling pr. 24/11-75	Vannstandsmåling pr. 24/11-78

Dyp i meter under mark-overflaten	Lagdeling	Grunnvannsnivå	Masseprøve	Spylt (sl. pumpet (p)	Vannprøve nr.	Vannføring ved kapasitets-pumping (l/min)	Lagdeling	Grunnvannsnivå	Masseprøve	Spylt (sl. pumpet (p)	Vannprøve nr.	Vannføring ved kapasitets-pumping (l/min)
1	Siltig jord						Siltig jord, fast lagret					
2		▽						▽				
3							Stein, grus, sand					
4	Steinig grus						Fjell					
5												
6	Fjell											
7												
8												
9												
10												
11												
12												
13												
14												
15												
16												
17												
18												
19												
20												
21												
22												
23												
24												
25												
26												
27												
28												
29												
30												

Kartblad: 2016 IV ELVERUM

Løpenr.	7	8
Kartsymbol	■1	■1
Lokalitet	361 585	361 585
Utsnitt nr.	1	1
Prøvested	7	8
Prøvetatt av		
Boringens art	S	S
Dato/år	1978	1978
Merknad:		

Dyp i meter under mark-overflaten	Lagdeling	Grunnvannsnivå	Masseprøve	Spylt (sl. pumpet (p)	Vannprøve nr	Vannføring ved kapasitets-pumping (l/min)	Lagdeling	Grunnvannsnivå	Masseprøve	Spylt (sl. pumpet (p)	Vannprøve nr	Vannføring ved kapasitets-pumping (l/min)
1	Silt						Silt/jord					
2	Fjell											
3							Grus/stein					
4												
5							Grus					
6							Fjell					
7												
8												
9												
10												
11												
12												
13												
14												
15												
16												
17												
18												
19												
20												
21												
22												
23												
24												
25												
26												
27												
28												
29												

Figure A23 Map of the location of the wells located in Grudsetmoen (north of Grindalsmoen area) and well log information showing the depth to the bedrock.

Table A1 Measurements and location of the hydraulic heads that were used for calibration as well.

Reference	utmx	utmy	Head (masl)
G1	636384.34	6755113.98	204.6
G2	636820.00	6754530.00	183.93
G4	637593.17	6754264.31	178.43
G7	637658.77	6754313.64	183.45
G5	637363.78	6754411.09	172.44
GPRDstart	636942.05	6753626.34	185
GPRDmid	637161.86	6753796.69	185
GPRDEND	637356.26	6753942.32	182
GPRB1	636773.40	6754823.62	189
GPRB2	636767.26	6754717.62	190
GPRB3	636764.18	6754617.76	185
GPRB4	636751.89	6754516.37	186
GPRB5	636748.82	6754418.04	190
GPRB6	636748.82	6754222.94	189
GPRB7	636678.15	6754353.52	192
GPRB8	636632.07	6754451.84	192
GPRB9	636750.36	6754361.20	189
GPRB10	636983.87	6754453.38	182.5
GPRB11	636925.49	6754657.70	183
GPRB12	636911.67	6754759.10	182
GPRC1	637635.64	6754368.12	177
GPRC2	637584.17	6754259.04	183
GPRC3	637615.67	6754310.51	179

Appendix B

Table B1 Hvorslev analysis for the slug test GRA

mins	seconds	time	pressure	h	h-1	h/h0		K	3.36E-08	m/s
		0	1407.125	385.35		1		K	2.91E-03	m/d
	40	40	1402.51	380.735	-0.63	0.988024		r	0.0175	m
1	47	107	1402.34	380.565	-0.46	0.987583		L	0.85	m
2	51	171	1402.16	380.385	-0.29	0.987116		R	0.0175	m
4	1	241	1402.05	380.275	-0.17	0.98683		T0 (s)	20793.33333	s
5	3	303	1401.88	380.1	0.00	0.986376				
					Relative height equation					
					y = -3E-05x + 0.9938					
					y=	-3.00E-05	0.9938			
					37%	20793.33				

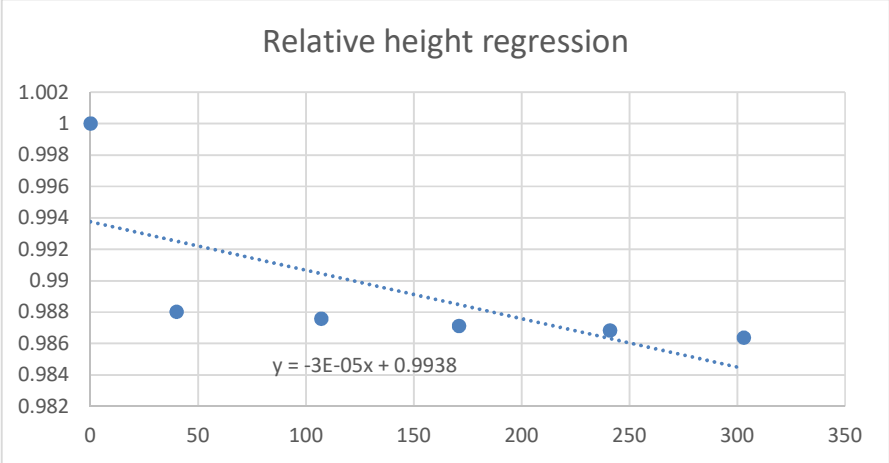

Figure B1 Relative height regression of the pressure and time

Table B2 Hvorslev analysis for the slug test GRB

time		h	h/h0			Km/d	2.52E-04	
12:00:00 AM	1204.475	179.025	1			Km/s	2.91E-09	
12:15:29 PM	1204.3	178.85	0.999022			r	0.0165	m
12:15:30 PM	1204.3	178.85	0.999022			L	0.9	m
12:15:31 PM	1204.3	178.85	0.999022			R	0.0165	m
12:15:32 PM	1204.3	178.85	0.999022			T0(s)	207733.3	s
12:15:33 PM	1204.2417	178.7917	0.998697					
12:15:34 PM	1204.2417	178.7917	0.998697			y	-3.00E-06	0.9932
12:15:35 PM	1204.2417	178.7917	0.998697				37%	207733.3
12:15:36 PM	1204.3	178.85	0.999022					3462.222

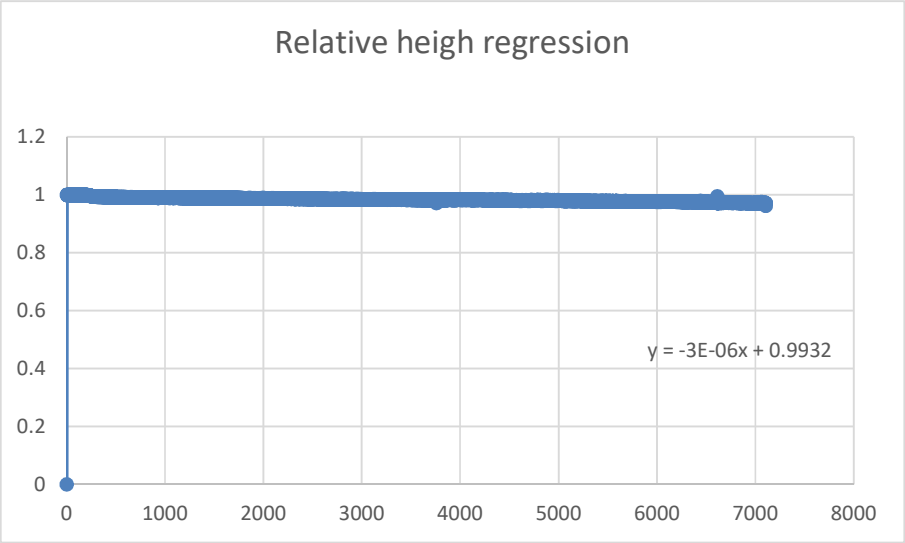

Figure B2 Relative height regression of the pressure and time

Table B3 Interpreted long-term pumping test data, from Kndudsen (1983)

Piezometer	Distance from RB1	Distance Glomma				P5	P9	((h2)^2-(h1)^2)	r2	r1	ln(r2/r1)	K	K
	m	m		masl	mosl	m	m		m	m		m/s	m/d
P2	98	90	February	178.2	179.4	28.2	29.4	69.12	290	5	4.06	5.14E-04	4.45E+01
P4	148	4		178.85	179.4	28.85	29.4	32.04	290	5	4.06	1.11E-03	9.59E+01
P5	5	57		P9/P5	D1								
P9	290	260		179.4	182.5	29.4	32.5	191.89	490	290	0.52	2.39E-05	2.07E+00
C1	517	600		178.2	182.5	28.2	32.5	261.01	490	5	4.58	1.54E-04	1.33E+01
C6	680	700		P5	P2								
D1	490	530		178.2	179.3	28.2	29.3	63.25	98	5	2.98	4.12E-04	3.56E+01
E1	52	320		178.85	179.6	28.85	29.6	43.84	98	5	2.98	5.94E-04	5.14E+01
				P5	P4								
Estimation of K from two observation wells				178.2	179.4	28.2	29.4	69.12	148	5	3.39	4.29E-04	3.71E+01
(Based on steady radial flow in an unconfined aquifer)				178.85	180.2	28.85	30.2	79.72	148	5	3.39	3.72E-04	3.22E+01
	K=Q ln(r2/r1)/2P((h2)^2-(h1)^2)												
	Q=(55 l/s)x(10^-3) m3/l												
	Q	0.055											

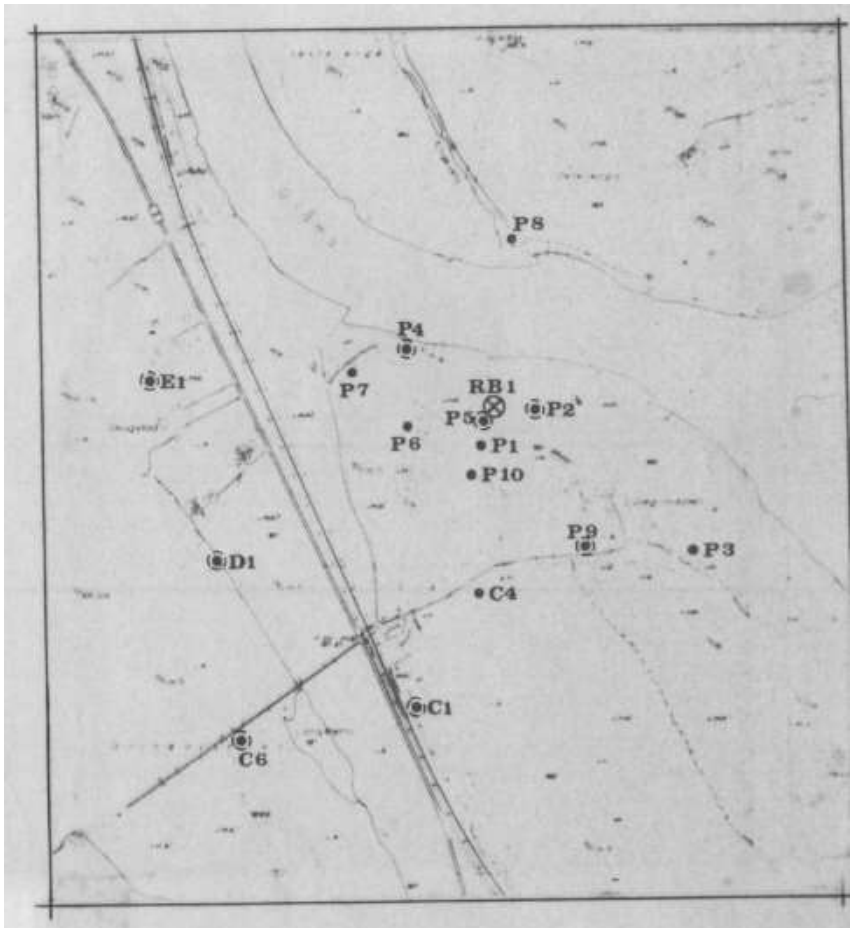

PEILERÖR	AVSTAND RB1	AVSTAND GLOMMA
P2	98	90
P4	148	4
P5	5	57
P9	290	260
C1	517	600
C6	680	700
D1	490	530
E1	52	320

Figure B3 Map of the location the distances of the wells for the data used in Table B3.

Table B4 Grain size analysis data and results

GRA				
Fraction, sieves (mm)	Weight (g)	% of total weight	Cumulative weight (%)	
2	3.046	0.945627945	100	
1	62.386	19.36767728	99.0543721	
0.5	144.895	44.98252172	79.6866948	
0.25	38.452	11.93738863	34.7041731	
0.125	47.202	14.65381821	22.7667844	
0.063	26.133	8.112966217	8.11296622	
Total weight (g)	322.114			
D60	0.4			
D10	0.07			
D60/D10	5.71428571			
K(m/s)	0.000049			
GRD				
Fraction, sieves (mm)	Weight (g)	% of total weight	Cumulative weight (%)	
0.01	0	0	0	
0.063	118.357	15.74333824	15.7433382	
0.125	242.592	32.26854272	48.011881	
0.25	390.322	51.91895088	99.9308318	
0.5	0.52	0.06916816	100	
Total weight:	751.791			
d10	0.058			
d60	0.15			
d60/d10	2.5862069			
K (m/s)	0.00003364	m/s		

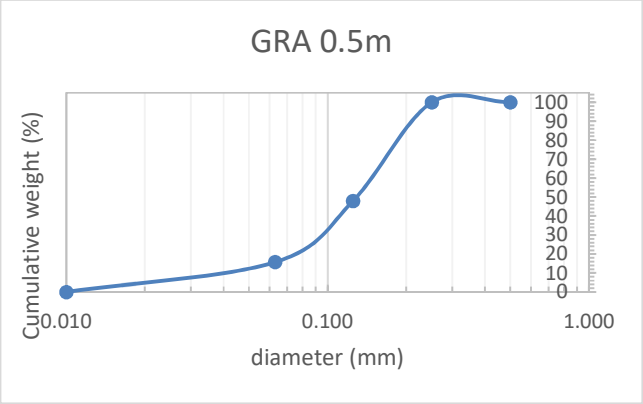

Figure B4 Accumulative curve for GRA sample

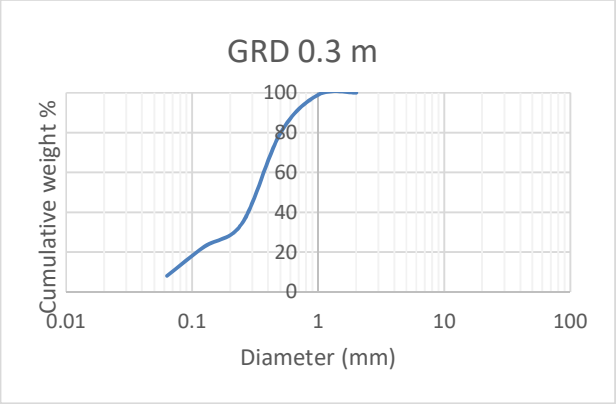

Figure B5 Accumulative curve for GRD sample

Table B5 Grain size analysis from the geotechnical drillings of the new road

Borehole nr	Depth m	D10 med mer	U	e	g(U)	E(U)	K50 m/s	K(Hazen) m/s	LogK50	LogK(Hazen)	K50 m/d	hazen m/d
328	0-1	0.03	3.0	0.339	3.017	3.3E+04	2.94E-05	1.04E-05	-4.53E+00	-4.98E+00	2.54	0.90
335	0-1	0.02	155.4	2.018	1.627	1.0E+07	4.20E-03	4.63E-06	-2.38E+00	-5.33E+00	362.61	0.40
347	0-1	0.012	76.9	1.737	1.643	7.2E+06	1.04E-03	1.67E-06	-2.98E+00	-5.78E+00	90.05	0.14
349	0-1	0.045	2.6	0.243	3.231	1.1E+04	2.29E-05	2.34E-05	-4.64E+00	-4.63E+00	1.98	2.02
376	0-1	0.015	4.8	0.591	2.498	2.1E+05	4.77E-05	2.60E-06	-4.32E+00	-5.58E+00	4.13	0.22
383	0-1	0.018	3.1	0.360	2.972	4.0E+04	1.28E-05	3.75E-06	-4.89E+00	-5.43E+00	1.11	0.32
393	0-1	0.033	2.9	0.318	3.065	2.6E+04	2.88E-05	1.26E-05	-4.54E+00	-4.90E+00	2.49	1.09
396	0-1	0.063	3.0	0.339	3.017	3.3E+04	1.30E-04	4.59E-05	-3.89E+00	-4.34E+00	11.22	3.97
402	0-1	0.063	4.8	0.591	2.498	2.1E+05	8.42E-04	4.59E-05	-3.07E+00	-4.34E+00	72.77	3.97

Norges vassdrags- og energidirektorat

Kartbakgrunn: Statens Kartverk

Kartdatum: EUREF89 WGS84

Projeksjon: UTM 33N

Nedbørfeltgrenser, feltparametere og vannføringsindekser er automatisk generert og kan inneholde feil. Resultatene må kvalitetssikres.

Lavvannskart

Vassdragsnr.: 002.H62
Kommune: Elverum
Fylke: Hedmark
Vassdrag: Glommavassdraget

Vannføringsindeks, se merknader	
Middelvannføring (61-90)	9,2 l/(s*km²)
Alminnelig lavvannføring	l/(s*km²)
5-persentil (hele året)	l/(s*km²)
5-persentil (1/5-30/9)	l/(s*km²)
5-persentil (1/10-30/4)	l/(s*km²)
Base flow	0,0 l/(s*km²)
BFI	

Klima		
Klimaregion		Ost
Årsnedbør	660	mm
Sommernedbør	359	mm
Vinternedbør	302	mm
Årstemperatur	2,6	°C
Sommertemperatur	11,7	°C
Vintertemperatur	-3,9	°C
Temperatur Juli	14,3	°C
Temperatur August	13,5	°C

Feltparametere	
Areal (A)	7,9 km²
Effektiv sjø (S_{eff})	-999,0 %
Elvelengde (E_L)	7,6 km
Elvegradient (E_G)	12,6 m/km
Elvegradient$_{1085}$ (G_{1085})	5,5 m/km
Feltlengde(F_L)	4,0 km
H_{min}	180 moh.
H_{10}	188 moh.
H_{20}	192 moh.
H_{30}	195 moh.
H_{40}	199 moh.
H_{50}	205 moh.
H_{60}	219 moh.
H_{70}	228 moh.
H_{80}	248 moh.
H_{90}	270 moh.
H_{max}	323 moh.
Bre	0,0 %
Dyrket mark	12,1 %
Myr	2,0 %
Sjø	0,3 %
Skog	77,7 %
Snaufjell	0,0 %
Urban	7,1 %

1) Verdien er editert

Det er generelt stor usikkerhet i beregninger av lavvannsindekser. Resultatene bør verifiseres mot egne observasjoner eller sammenlignbare målestasjoner.

I nedbørfelt med høy breprosent eller stor innsjøprosent vil tørrværsavrenning (baseflow) ha store bidrag fra disse lagringsmagasinene.

Figure B6 NEVINA report for the catchment area

Parameternavn	Generert verdi	Editert verdi
ObjectId	71.885	71.885
Vassdragsnummer	002.H62	002.H62
Klimaregion	Ost	Ost
Region	Ost	Ost
Areal (km²)	7,85	7,85
Avrenning (mm/år)	283,71	283,71
Minimum høyde (m)	180	180
Maksimum høyde (m)	323	323
Sjø (%)	0,29	0,29
Bre (%)	0	0
Skog (%)	77,68	77,68
Dyrket mark (%)	12,07	12,07
Myr (%)	1,96	1,96
Snaufjell (%)	0	0
Urban (%)	7,17	7,17

Figure B7 NEVINA report with recharge estimation.

Table B6 Temperature record of Skomuseet

		Skogmuseet Temperature												
month		2008	2009	2010	2011	2012	2013	2014	2015	2016	2017	2018	2019	Average
Jan	1	#DIV/0!	-6.24813	-13.1122	-8.38277	-6.09917	-9.13431	-5.38945	#DIV/0!	-7.41927	-5.56073	-6.49841	-7.1416	-7.4986
Feb	2	#DIV/0!	-9.05338	-10.5958	-8.42332	-4.78212	-14.4518	0.030446	#DIV/0!	-3.28754	-3.74847	-6.90169	-2.5892	-6.38029
Mar	3	#DIV/0!	0.300633	-2.30261	-2.27939	3.345072	-5.2361	3.474034	#DIV/0!	0.002941	0.596438	-5.46888	-0.3825	-0.79504
Apr	4	#DIV/0!	6.397917	4.458089	7.7499	3.596699	3.446306	5.801103	6.240556	3.764163	3.179625	3.796597	5.701306	4.921115
May	5	#DIV/0!	10.44292	7.533327	10.07841	9.985431	11.89062	9.169653	7.217368	10.28551	9.424597	14.0531	8.335081	9.856002
Jun	6	12.46953	13.88522	13.94261	15.11612	12.56169	14.48234	12.50846	12.54769	14.86092	13.27698	15.50271	14.31408	13.7413
Jul	7	17.38729	16.16181	17.07844	16.23209	14.47481	18.09666	18.66301	15.98962	15.93344	14.65301	20.53978	13.73484	16.46702
Aug	8	13.88448	14.28513	14.84579	14.81019	14.18286	14.68062	15.53103	14.06587	13.67559	13.27796	13.99581	#DIV/0!	14.32395
Sep	9	9.173026	10.6136	8.765647	12.41551	8.923715	8.104043	8.465591	10.59177	12.6056	10.09507	9.947375	#DIV/0!	9.975357
Oct	10	4.843001	1.396633	2.833086	3.765889	2.779109	2.779239	6.950874	#DIV/0!	3.680081	3.882839	4.827675	#DIV/0!	3.773842
Nov	11	-1.01657	0.988209	-5.40203	1.865913	1.555291	-1.36663	3.151511	#DIV/0!	-1.83219	-2.59142	0.903569	#DIV/0!	-0.37444
Dec	12	-5.16146	-7.91574	-14.1556	-3.28366	-7.59093	-1.50819	#DIV/0!	-1.5376	-2.75247	-6.87557	-4.20677	#DIV/0!	-5.4988
	AVERAGE	7.368471	4.271235	1.990727	4.972072	4.411037	3.481899	7.123296	9.302182	4.95973	4.134195	5.040905	4.56743	5.186886
														4.375951

Table B7 Temperature record of Stavsberg

		Temperature											
month		2009	2010	2011	2012	2013	2014	2015	2016	2017	2018	2019	Average
Jan	1	-4.53629	-11.7025	-6.61452	-5.47177	-8.76371	-4.77581	-2.83468	-8.34839	-4.34032	-4.5129	-5.50887	-6.12816
Feb	2	-8.65536	-10.7964	-7.48125	-4.8569	-6.65714	0.15	-1.50714	-2.62328	-3.82232	-6.45179	-1.95893	-4.96914
Mar	3	-0.57661	-2.14758	-2.18629	3.36129	-5.39032	2.820161	1.566129	1.584677	0.405645	-5.40081	-0.12258	-0.5533
Apr	4	6.330833	3.745	8.188333	3.1475	2.9125	5.926667	5.503333	4.120833	3.555	3.868333	6.195833	4.863106
May	5	10.89839	9.145968	9.949194	10.35565	11.81048	10.59274	7.641129	11.05484	10.37258	15.34516	8.990323	10.55968
Jun	6	14.23917	13.75093	14.9325	12.5625	13.80333	14.18	12.68083	15.335	13.74917	16.3725	14.55	14.19599
Jul	7	15.80403	16.69839	16.56129	14.99677	17.20645	19.78306	15.08468	16.07581	15.34274	21.51452		16.90677
Aug	8	14.56694	14.78468	14.76613	14.39435	14.92419	14.59919	15.41048	14.46371	13.8879	15.00726		14.68048
Sep	9	11.42167	9.225833	11.28583	9.569167	10.70333	11.20167	11.07417	13.54333	10.60917	11.11583		10.975
Oct	10	2.432258	3.932258	5.756452	3.535484	5.522581	7.190323	5.433065	4.119355	5.422581	5.695161		4.903952
Nov	11	1.643333	-4.5175	2.471667	1.604167	0.4975	2.071429	1.109167	-1.11	-0.61667	1.410833		0.456393
Dec	12	-6.56774	-12.7234	-1.7871	-7.38548	0.062903	-4.64677	-0.30323	-1.26532	-4.85887	-3.90081		-4.33758
	AVERAGE	#DIV/0!	2.449641	5.486854	4.651061	4.719342	6.591055	5.904828	5.579214	4.97555	5.838608	3.690963	#DIV/0!
													5.129434

Table B8 Fagertun precipitation record

month		1978	1979	1980	1981	1982	1983	1984	1985	1986	1987
Jan	1	0	21.5	13.8	17.2	26.9	42	41.8	51.5	45.5	8.1
Feb	2	0	17.7	18.8	24.8	28.4	3.7	20.5	32.2	2.1	23.4
Mar	3	0	51.1	20.3	64.8	52.7	22	21.3	68.7	38.5	49.2
Apr	4	0	64.1	6.8	2.3	41.8	35	14.3	60.5	39.3	15.3
May	5	0	64.8	59.8	41.5	87.8	96.6	70.4	39.4	55.4	89.6
Jun	6	0	64.4	134.9	80.4	13.9	34.5	90.1	76.1	62.3	192.8
Jul	7	0	88.3	77.9	105.9	25.1	44.8	54.7	111.6	47.1	25.8
Aug	8	0	80.3	94.1	21.4	61	30.3	36.2	140.2	107.6	93.2
Sep	9	59.6	65.8	70.6	45.8	123.9	113.9	104.5	133.9	41.8	127
Oct	10	14.3	67.6	125.2	79	35.7	68.9	143.5	39.4	60.4	122.9
Nov	11	25.3	84	51.1	118.3	101.3	12.4	48.5	36.1	61.1	72.9
Dec	12	26.1	45.5	49.5	24.9	45.9	38.4	70.5	54.8	81.6	20.4
Year average		125.3	715.1	722.8	626.3	644.4	542.5	716.3	844.4	642.7	840.6

1988	1989	1990	1991	1992	1993	1994	1995	1996	1997	1998	1999	2000
88.1	20.1	52.5	49.9	12.7	31.4	77.5	61.5	27.2	22	50.6	61.7	20.5
74	48.3	50.6	10.5	27.8	23.2	9.7	44.4	24.8	47.8	22.4	31.4	24.4
61.6	62.8	20.7	56.3	49	4.2	47.2	42.3	3	14.4	42.3	90.6	29
24.6	70.3	99.9	21	66.9	24.7	57.2	33.9	26.6	1.8	96	47.4	86.8
31.3	45.7	32.6	9	35.2	60	23.9	62.8	78.6	153	5.1	39.4	65.2
62	66	66.7	164.3	11.6	34.3	56.5	90.8	71.7	53.4	126.2	134.3	92.8
165.2	79.2	99.8	53.8	105.5	131.6	10.1	75.9	52.4	16.1	70.5	76.9	90
106.7	149.3	29.3	21.7	120.8	124	110.4	22.8	145.7	78.9	91.8	38	105.4
148.9	21.1	69.3	59.3	72.9	32.9	60.5	68	56.9	104.3	93.8	108.4	41.9
62.5	39.7	38.9	66.3	44.4	121.5	37.9	52.6	104.1	55.4	89.2	73.6	146.9
20.6	53.4	42.6	86.5	108.1	59.9	45.7	31.5	78	48.7	25.6	38.7	181.1
32.6	33.6	46.6	32.2	40.3	91.9	44.9	4.2	30.8	65.1	33.3	64.8	88.8
878.1	689.5	649.5	630.8	695.2	739.6	581.5	590.7	699.8	660.9	746.8	805.2	972.8

2001	2002	2003	2004	2005	2006	2007	2008	2009	2010	2011	2012	2013	Monthly a
65.6	63	46.5	59.4	56.3	35.4	76.8	80	33.6	11.9	35.2	49.8	33.6	42.60286
23.1	55.4	34.7	33.6	10.8	44.3	34.5	43.6	41.9	30.1	36.8	25.5	16.4	29.76
42.4	29.5	23.3	24.3	28.2	26.2	20	53	38.9	37.3	8.6	10.7	4.8	35.97714
59.9	31.6	34.1	37.5	28.4	50.7	21.7	31.5	33.2	28.4	44.3	57.5	49.5	41.28
55.3	108.8	76.2	60.9	74.8	110.2	63.7	78.9	45.3	41.2	76.3	52.2	19.8	60.30571
49.8	86	86	65.2	63.6	50.6	79.5	61.8	46.5	107.1	169.1	66.6	0	77.48
107.2	141.8	65.8	63.7	59.3	58.8	109	90.7	189.8	102.4	110.2	235.4	0	84.06571
142	44.7	72.2	83.6	86.8	100.4	37.6	112.7	127.8	160.7	139.2	168.7	0	88.15714
89.7	29.1	104.8	95.6	37.2	78.3	58.5	32.8	43	114.9	138.5	92.4	0	78.28
99	58.2	18.8	68.4	74.7	159.1	30.1	105.8	56.8	48.6	64.2	68	0	72.61714
35	47	59.3	46.9	89.3	94.2	87.5	64.3	113	9.1	26.4	118.8	0	63.49143
49	22	56.1	24.2	28.4	49.5	60.9	30	46.9	22.1	68.1	57.1	0	45.17143
818	717.1	677.8	663.3	637.8	857.7	679.8	785.1	816.7	713.8	916.9	1002.7	124.1	642.04

Table B9 precipitation record from Stavsberg

month		2009	2010	2011	2012	2013	2014	2015	2016	2017	2018	2019	Monthly a
Jan	1	34.6	12.7	45.3	38.3	25.5	31.5	52.4	30.2	11.2	55.4	38.5	34.14545
Feb	2	53.5	24.4	39.2	13	20	47.4	11.3	20.7	26.7	18.5	40.8	28.68182
Mar	3	30.8	13.6	6.6	5.1	3.9	35.8	26.8	23.9	21.2	14	36.6	19.84545
Apr	4	24	24.8	27.1	37.5	18.6	28.3	9.2	37.2	28.3	33.8	1.9	24.60909
May	5	39.3	28.6	54.5	41.6	120.1	49.3	102.8	109.4	54.6	19.8	99.2	65.38182
Jun	6	28.7	85.4	107.5	36.1	98.6	32	54.7	33.2	52.3	48.1	100.8	61.58182
Jul	7	129	98.7	54.9	100.1	7	96.5	103	54.8	62.7	24.2	1.9	66.61818
Aug	8	87.6	123.2	161.9	115.9	54.8	77.4	81.9	57.5	146.2	66	0	88.4
Sep	9	30.2	86.8	116.5	46.2	31.7	38.3	103.9	37.2	73.2	89.2	0	59.38182
Oct	10	29.3	32.2	41.8	46.8	40.7	101.6	4.1	6.8	61.6	25.6	0	35.5
Nov	11	59.5	6.9	12.3	62.9	27.1	58.2	41.7	57.5	55.9	41.4	0	38.49091
Dec	12	31.2	14.5	30.3	43	55	18.6	33.9	12.2	31.3	52.8	0	29.34545
Year average		577.7	551.8	697.9	586.5	503	614.9	625.7	480.6	625.2	488.8	319.7	575.21

Appendix C

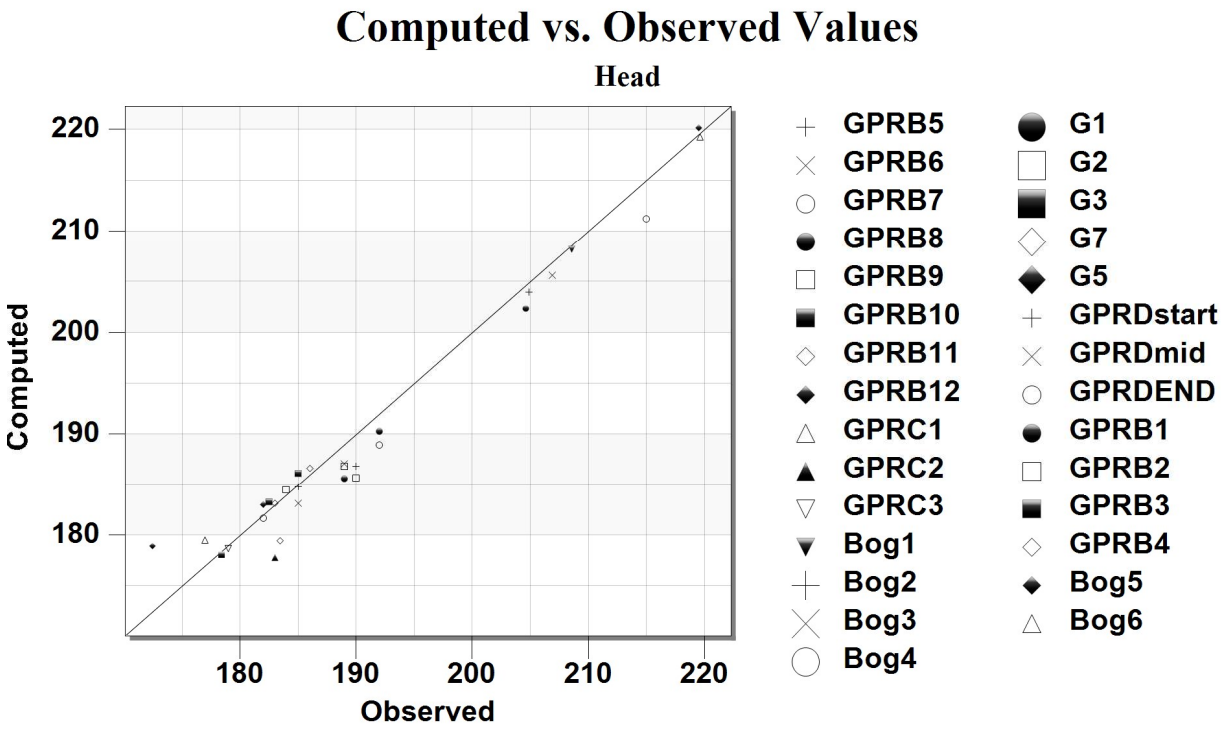

Figure C1 Computed vs Observed heads for scenario 1(increased pumping 50%)

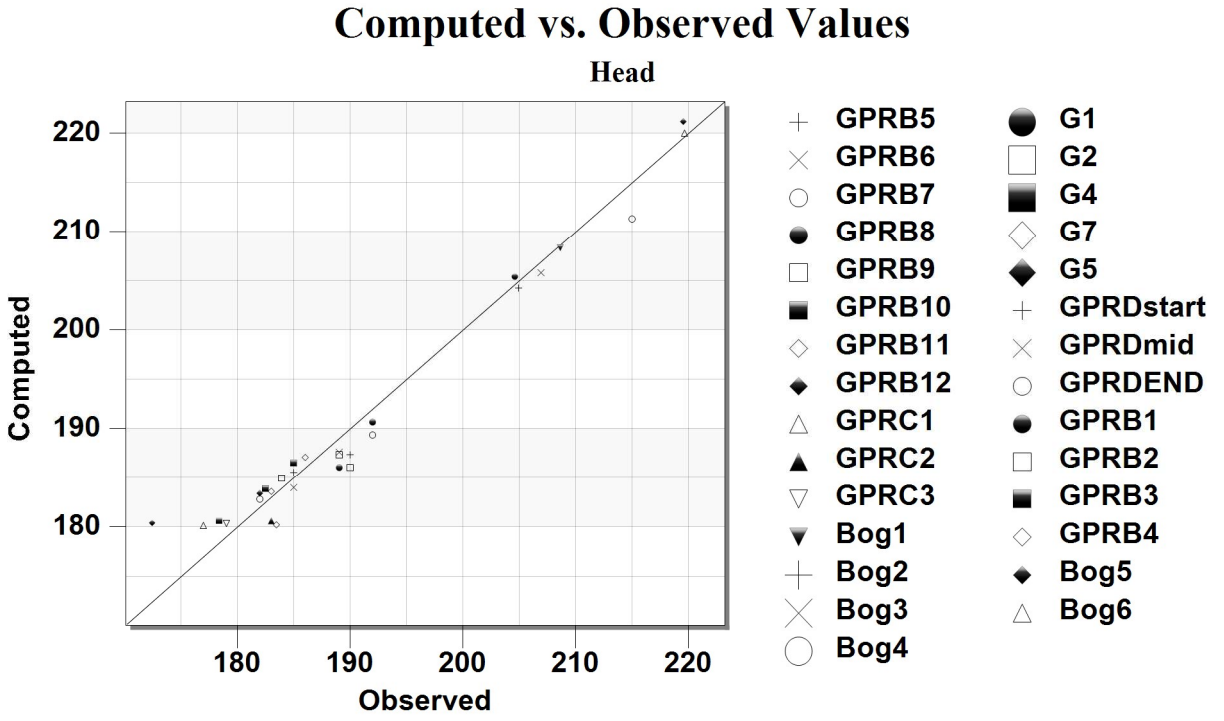

Figure C2 Computed vs Observed heads for scenario 2(Flux from the north)

from the northern boundary

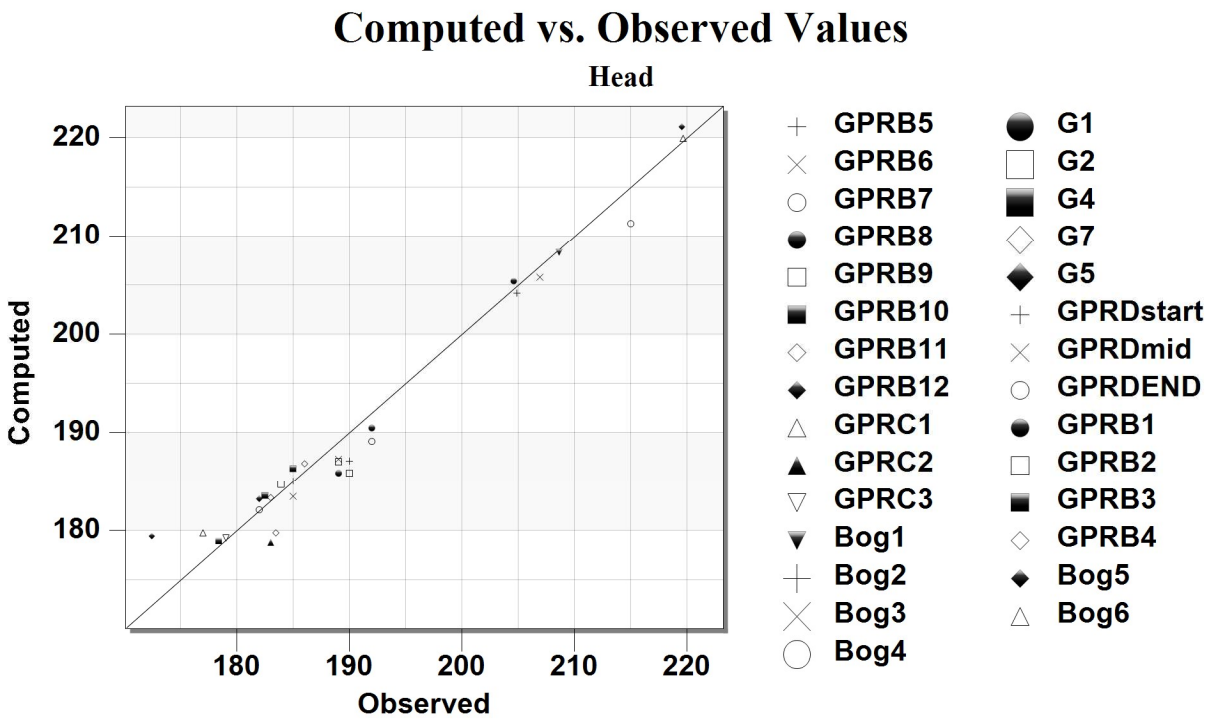

Figure C3 Computed vs Observed heads for scenario 3(Flux from the northern boundary with the current pumping rate)

Table C1 Water budget with the pumping rate (55 l/s = 4.752 m3/d) from the pumping test of 1985.

Sources/Sinks	Flow in (m^3/d)	Flow out (m^3/d)
CONSTANT HEAD – River Glomma	2758.329	-1969.650016
WELLS - Western Bound / Pumping	1597.591	-4752
RIVER LEAKAGE – Streams	0	-2540.773323
HEAD DEP BOUNDS - lake Langsletta	868.2285	0
RECHARGE	4038.315	0
Total Source/Sink	9262.464	-9262.423339

Appendix D

Table D1 Coordinates of the water samples

Sample	utmx	utmy
S1	633142.61	6755543.33
S2	634551.46	6754787.89
S3	635970.95	6755017.62
S4	634372.69	6754556.04
G1	636340.14	6755132.04
G2	636820.00	6754530.00
G3	636825.80	6754533.67
G4	637593.17	6754264.31
G5	637363.78	6754411.09
DW	637576.47	6754278.51

Table D1 Water analysis of the water samples

Sample_ref	T (Celsius)	pH	Eh(SHE) mV	EC (uS/cm)	Na mg/L	K mg/L	Mg mg/L	Ca mg/L	F mg/L	Cl mg/L	SO4 mg/L	Br mg/L	NO3(N) mg/L	PO4 mg/L	Alkalinity mg/L	TDS mg/L
S1	7.8	5.6		31	1.914	0.277	1.052	2.374	0.0908	1.0188	4.4439	0.337	0.1871	n.a.	0	11.6946
S2	8.5	6.18		52.6	2.29	1.099	1.221	5.561	0.2362	0.6766	7.4253	0.333	0.2024	n.a.	9.76	28.8045
S3	7.1	6.97		41.7	1.767	0.542	1.182	3.52	0.2063	0.9057	5.431	0.333	0.3414	n.a.	0	14.2284
G1	14.5	9.71		61.5	2.33	6.836	1.148	2.751	0.3232	7.8659	2.5231	0.344	0.1991	n.a.	9.15	33.4703
G2	7	7.49		28.8	1.555	4.703	n.a.	1.785	0.019	3.9273	2.4347	0.334	0.2252	n.a.	1.22	16.2032
G3	7	7.01		235	6.38	2.069	3.894	15.389	0.2514	8.2174	30.4901	0.338	0.4084	n.a.	26.23	93.6673
G4	7.7	7.58		94.9	2.61	1.379	1.44	4.583	0.0822	3.0975	2.8074	0.334	0.2101	n.a.	17.08	33.6232
G5	12	7.55		51.2	1.857	0.983	1.442	5.806	0.0043	1.2862	0.4256	n.a.	0.1772	n.a.	20.74	32.7213
S4	7.1	6.2		59.1	1.713	0.545	1.225	3.021	0.0529	0.9566	8.9324	n.a.	0.3707	n.a.	0.0122	16.8288
Dw		6.31			2.331	1.127	1.479	4.677	0.2301	2.6252	3.4438	0.333	2.3642	n.a.	12.81	31.4203

Sample_ref		Na mg/L	K mg/L	Mg mg/L	Ca mg/L	F mg/L	Cl mg/L	SO4 mg/L	Br mg/L	NO3(N) mg/L	PO4 mg/L	Alkalinity mg/L (HCO3-)
	Molecular Weig	22.989	39.102	24.305	40.08	18.9984	35.453	96.064	79.904	14.0067		61
S1	mg/mol	0.001914	0.000277	0.001052	0.002374	9.08E-05	0.001019	0.004444	0.000337	0.0001871	n.a.	
S2	mg/mol	0.00229	0.001099	0.001221	0.005561	0.000236	0.000677	0.007425	0.000333	0.0002024	n.a.	
S3	mg/mol	0.001767	0.000542	0.001182	0.00352	0.000206	0.000906	0.005431	0.000333	0.0003414	n.a.	
G1	mg/mol	0.00233	0.006836	0.001148	0.002751	0.000323	0.007866	0.002523	0.000344	0.0001991	n.a.	
G2	mg/mol	0.001555	0.004703	#VALUE!	0.001785	0.000019	0.003927	0.002435	0.000334	0.0002252	n.a.	
G3	mg/mol	0.00638	0.002069	0.003894	0.015389	0.000251	0.008217	0.03049	0.000338	0.0004084	n.a.	
G4	mg/mol	0.00261	0.001379	0.00144	0.004583	8.22E-05	0.003098	0.002807	0.000334	0.0002101	n.a.	
G5	mg/mol	0.001857	0.000983	0.001442	0.005806	4.3E-06	0.001286	0.000426	#VALUE!	0.0001772	n.a.	
S4	mg/mol	0.001713	0.000545	0.001225	0.003021	5.29E-05	0.000957	0.008932	#VALUE!	0.0003707	n.a.	
Dw	mg/mol	0.002331	0.001127	0.001479	0.004677	0.00023	0.002625	0.003444	0.000333	0.0023642	n.a.	
S1	mmol/L	0.083257	0.007084	0.043283	0.059232	0.004779	0.028737	0.04626	0.004218	0.013357893	n.a.	
S2	mmol/L	0.099613	0.028106	0.050237	0.138748	0.012433	0.019084	0.077295	0.004168	0.014450227	n.a.	
S3	mmol/L	0.076863	0.013861	0.048632	0.087824	0.010859	0.025546	0.056535	0.004168	0.02437405	n.a.	
G1	mmol/L	0.101353	0.174825	0.047233	0.068638	0.017012	0.221868	0.026265	0.004305	0.014214626	n.a.	
G2	mmol/L	0.067641	0.120275	#VALUE!	0.044536	0.001	0.110775	0.025345	0.00418	0.01607802	n.a.	
G3	mmol/L	0.277524	0.052913	0.160214	0.383957	0.013233	0.231783	0.317394	0.00423	0.029157475	n.a.	
G4	mmol/L	0.113533	0.035267	0.059247	0.114346	0.004327	0.087369	0.029224	0.00418	0.014999964	n.a.	
G5	mmol/L	0.080778	0.025139	0.059329	0.14486	0.000226	0.036279	0.00443	#VALUE!	0.012651088	n.a.	
S4	mmol/L	0.074514	0.013938	0.050401	0.075374	0.002784	0.026982	0.092984	#VALUE!	0.026465906	n.a.	
Dw	mmol/L	0.101396	0.028822	0.060852	0.116692	0.012112	0.074047	0.035849	0.004168	0.16879065	n.a.	

	Charge	1	1	2	2	-1	-1	-2	-1	-1		-1		SUM+	SUM-	EB(%)
S1	meq/L	0.083257	0.007084	0.086567	0.118463	-0.00478	-0.02874	-0.09252	-0.00422	-0.013357893	n.a.	0	0	0.295371	-0.14361	34.57087
S2	meq/L	0.099613	0.028106	0.100473	0.277495	-0.01243	-0.01908	-0.15459	-0.00417	-0.014450227	n.a.	0.16	-0.16	0.505687	-0.36473	16.1948
S3	meq/L	0.076863	0.013861	0.097264	0.175649	-0.01086	-0.02555	-0.11307	-0.00417	-0.02437405	n.a.	0	0	0.363637	-0.17802	34.26899
G1	meq/L	0.101353	0.174825	0.094466	0.137275	-0.01701	-0.22187	-0.05253	-0.00431	-0.014214626	n.a.	0.15	-0.15	0.507919	-0.45993	4.958371
G2	meq/L	0.067641	0.120275	#VALUE!	0.089072	-0.001	-0.11077	-0.05069	-0.00418	-0.01607802	n.a.	0.02	-0.02	0.276988	-0.20272	15.48143
G3	meq/L	0.277524	0.052913	0.320428	0.767914	-0.01323	-0.23178	-0.63479	-0.00423	-0.029157475	n.a.	0.43	-0.43	1.418779	-1.34319	2.736765
G4	meq/L	0.113533	0.035267	0.118494	0.228693	-0.00433	-0.08737	-0.05845	-0.00418	-0.014999964	n.a.	0.28	-0.28	0.495986	-0.44932	4.93612
G5	meq/L	0.080778	0.025139	0.118659	0.289721	-0.00023	-0.03628	-0.00886	#VALUE!	-0.012651088	n.a.	0.34	-0.34	0.514296	-0.39802	12.74553
S4	meq/L	0.074514	0.013938	0.100802	0.150749	-0.00278	-0.02698	-0.18597	#VALUE!	-0.026465906	n.a.	0.0002	-0.0002	0.340003	-0.2424	16.75857
Dw	meq/L	0.101396	0.028822	0.121703	0.233383	-0.01211	-0.07405	-0.0717	-0.00417	-0.16879065	n.a.	0.21	-0.21	0.485305	-0.54082	-5.40971

PHREEQC results fot the water samples

```
Initial solution 1.      S1

-----------------------------Solution composition----------

      Elements           Molality       Moles

      Br                 4.218e-06   4.218e-06
      Ca                 5.923e-05   5.923e-05
      Cl                 2.874e-05   2.874e-05
      F                  4.779e-06   4.779e-06
      K                  7.084e-06   7.084e-06
      Mg                 4.327e-05   4.327e-05
      N(-3)              1.336e-05   1.336e-05
      Na                 8.326e-05   8.326e-05
      S(6)               4.626e-05   4.626e-05

----------------------------Description of solution--------

                                     pH  =   5.600
                                     pe  =   4.000
      Specific Conductance (µS/cm,   8°C)  = 17
                           Density (g/cm³)  =   0.99987
                                Volume (L)  =   1.00014
                        Activity of water   =   1.000
                  Ionic strength (mol/kgw)  =   3.671e-04
                        Mass of water (kg)  =   1.000e+00
                  Total alkalinity (eq/kg)  =  -2.583e-06
                     Total carbon (mol/kg)  =   0.000e+00
                         Total CO2 (mol/kg)  =   0.000e+00
                           Temperature (°C)  =   7.80
                   Electrical balance (eq)   =   1.810e-04
 Percent error, 100*(Cat-|An|)/(Cat+|An|)   =  41.23
                                Iterations   =   3
                                   Total H   = 1.110125e+02
                                   Total O   = 5.550640e+01


Initial solution 2.      S2

-----------------------------Solution composition----------

      Elements           Molality       Moles

      Alkalinity         1.950e-04   1.950e-04
      Br                 4.168e-06   4.168e-06
      Ca                 1.388e-04   1.388e-04
      Cl                 1.908e-05   1.908e-05
      F                  1.243e-05   1.243e-05
      K                  2.811e-05   2.811e-05
      Mg                 5.022e-05   5.022e-05
      N(-3)              1.445e-05   1.445e-05
      Na                 9.961e-05   9.961e-05
      S(6)               7.730e-05   7.730e-05

----------------------------Description of solution--------

                                     pH  =   6.180
                                     pe  =   4.000
      Specific Conductance (µS/cm,   9°C)  = 33
                           Density (g/cm³)  =   0.99985
                                Volume (L)  =   1.00020
                        Activity of water   =   1.000
                  Ionic strength (mol/kgw)  =   7.120e-04
                        Mass of water (kg)  =   1.000e+00
                     Total carbon (mol/kg)  =   5.728e-04
                         Total CO2 (mol/kg)  =   5.728e-04
                           Temperature (°C)  =   8.50
                   Electrical balance (eq)   =   1.348e-04
 Percent error, 100*(Cat-|An|)/(Cat+|An|)   =  14.99
                                Iterations   =   7
                                   Total H   = 1.110127e+02
                                   Total O   = 5.550787e+01
```

Initial solution 3. S3

-----------------------------Solution composition----------

Elements	Molality	Moles
Br	4.168e-06	4.168e-06
Ca	8.783e-05	8.783e-05
Cl	2.555e-05	2.555e-05
F	1.086e-05	1.086e-05
K	1.386e-05	1.386e-05
Mg	4.862e-05	4.862e-05
N(-3)	2.437e-05	2.437e-05
Na	7.686e-05	7.686e-05
S(6)	5.654e-05	5.654e-05

-----------------------------Description of solution--------

pH	=	6.970
pe	=	4.000
Specific Conductance (µS/cm, 7°C)	=	20
Density (g/cm³)	=	0.99991
Volume (L)	=	1.00010
Activity of water	=	1.000
Ionic strength (mol/kgw)	=	4.600e-04
Mass of water (kg)	=	1.000e+00
Total alkalinity (eq/kg)	=	-5.644e-08
Total carbon (mol/kg)	=	0.000e+00
Total CO2 (mol/kg)	=	0.000e+00
Temperature (°C)	=	7.10
Electrical balance (eq)	=	2.344e-04
Percent error, 100*(Cat-|An|)/(Cat+|An|)	=	43.58
Iterations	=	3
Total H	=	1.110125e+02
Total O	=	5.550644e+01

Initial solution 9. S4

-----------------------------Solution composition---------

Elements	Molality	Moles
Alkalinity	2.438e-07	2.438e-07
Ca	7.538e-05	7.538e-05
Cl	2.698e-05	2.698e-05
F	2.784e-06	2.784e-06
K	1.394e-05	1.394e-05
Mg	5.039e-05	5.039e-05
N(-3)	2.647e-05	2.647e-05
Na	7.451e-05	7.451e-05
S(6)	9.299e-05	9.299e-05

-----------------------------Description of solution-------

pH	=	6.200
pe	=	4.000
Specific Conductance (µS/cm, 7°C)	=	23
Density (g/cm³)	=	0.99991
Volume (L)	=	1.00010
Activity of water	=	1.000
Ionic strength (mol/kgw)	=	5.049e-04
Mass of water (kg)	=	1.000e+00
Total carbon (mol/kg)	=	2.580e-06
Total CO2 (mol/kg)	=	2.580e-06
Temperature (°C)	=	7.10
Electrical balance (eq)	=	1.505e-04
Percent error, 100*(Cat-|An|)/(Cat+|An|)	=	26.03
Iterations	=	7
Total H	=	1.110125e+02
Total O	=	5.550659e+01

Initial solution 4. G1

-----------------------------Solution composition----------

Elements	Molality	Moles
Alkalinity	1.828e-04	1.828e-04
Br	4.305e-06	4.305e-06
Ca	6.864e-05	6.864e-05
Cl	2.219e-04	2.219e-04
F	1.701e-05	1.701e-05
K	1.748e-04	1.748e-04
Mg	4.722e-05	4.722e-05
N(-3)	1.422e-05	1.422e-05
Na	1.014e-04	1.014e-04
S(6)	2.627e-05	2.627e-05

----------------------------Description of solution--------

pH	=	9.710
pe	=	4.000
Specific Conductance (µS/cm, 15°C)	=	49
Density (g/cm³)	=	0.99920
Volume (L)	=	1.00083
Activity of water	=	1.000
Ionic strength (mol/kgw)	=	6.463e-04
Mass of water (kg)	=	1.000e+00
Total carbon (mol/kg)	=	1.279e-04
Total CO2 (mol/kg)	=	1.279e-04
Temperature (°C)	=	14.50
Electrical balance (eq)	=	4.356e-05
Percent error, 100*(Cat-|An|)/(Cat+|An|)	=	4.48
Iterations	=	4
Total H	=	1.110126e+02
Total O	=	5.550673e+01

Initial solution 5. G2

-----------------------------Solution composition---------

Elements	Molality	Moles
Alkalinity	2.438e-05	2.438e-05
Br	4.180e-06	4.180e-06
Ca	4.454e-05	4.454e-05
Cl	1.108e-04	1.108e-04
F	1.000e-06	1.000e-06
K	1.203e-04	1.203e-04
N(-3)	1.608e-05	1.608e-05
Na	6.764e-05	6.764e-05
S(6)	2.534e-05	2.534e-05

----------------------------Description of solution-------

pH	=	7.490
pe	=	4.000
Specific Conductance (µS/cm, 7°C)	=	20
Density (g/cm³)	=	0.99991
Volume (L)	=	1.00010
Activity of water	=	1.000
Ionic strength (mol/kgw)	=	3.113e-04
Mass of water (kg)	=	1.000e+00
Total carbon (mol/kg)	=	2.664e-05
Total CO2 (mol/kg)	=	2.664e-05
Temperature (°C)	=	7.00
Electrical balance (eq)	=	1.020e-04
Percent error, 100*(Cat-|An|)/(Cat+|An|)	=	21.11
Iterations	=	3
Total H	=	1.110125e+02
Total O	=	5.550640e+01

Initial solution 6. G3

-----------------------------Solution composition----------

Elements	Molality	Moles
Alkalinity	5.242e-04	5.242e-04
Br	4.230e-06	4.230e-06
Ca	3.840e-04	3.840e-04
Cl	2.318e-04	2.318e-04
F	1.323e-05	1.323e-05
K	5.292e-05	5.292e-05
Mg	1.602e-04	1.602e-04
N(-3)	2.916e-05	2.916e-05
Na	2.775e-04	2.775e-04
S(6)	3.174e-04	3.174e-04

----------------------------Description of solution--------

pH	=	7.010
pe	=	4.000
Specific Conductance (µS/cm, 7°C)	=	100
Density (g/cm³)	=	0.99999
Volume (L)	=	1.00011
Activity of water	=	1.000
Ionic strength (mol/kgw)	=	2.220e-03
Mass of water (kg)	=	1.000e+00
Total carbon (mol/kg)	=	6.751e-04
Total CO2 (mol/kg)	=	6.751e-04
Temperature (°C)	=	7.00
Electrical balance (eq)	=	3.968e-05
Percent error, 100*(Cat-|An|)/(Cat+|An|)	=	1.42
Iterations	=	7
Total H	=	1.110131e+02
Total O	=	5.550936e+01

Initial solution 7. G4

-----------------------------Solution composition----------

Elements	Molality	Moles
Alkalinity	3.413e-04	3.413e-04
Br	4.180e-06	4.180e-06
Ca	1.144e-04	1.144e-04
Cl	8.737e-05	8.737e-05
F	4.327e-06	4.327e-06
K	3.527e-05	3.527e-05
Mg	5.923e-05	5.923e-05
N(-3)	1.500e-05	1.500e-05
Na	1.135e-04	1.135e-04
S(6)	2.923e-05	2.923e-05

----------------------------Description of solution--------

pH	=	7.580
pe	=	4.000
Specific Conductance (µS/cm, 8°C)	=	34
Density (g/cm³)	=	0.99990
Volume (L)	=	1.00014
Activity of water	=	1.000
Ionic strength (mol/kgw)	=	7.028e-04
Mass of water (kg)	=	1.000e+00
Total carbon (mol/kg)	=	3.673e-04
Total CO2 (mol/kg)	=	3.673e-04
Temperature (°C)	=	7.70
Electrical balance (eq)	=	1.533e-05
Percent error, 100*(Cat-|An|)/(Cat+|An|)	=	1.53
Iterations	=	7
Total H	=	1.110128e+02
Total O	=	5.550741e+01

Initial solution 8. G5

-----------------------------Solution composition----------

Elements	Molality	Moles
Alkalinity	4.144e-04	4.144e-04
Ca	1.449e-04	1.449e-04
Cl	3.628e-05	3.628e-05
F	2.263e-07	2.263e-07
K	2.514e-05	2.514e-05
Mg	5.931e-05	5.931e-05
N(-3)	1.265e-05	1.265e-05
Na	8.078e-05	8.078e-05
S(6)	4.431e-06	4.431e-06

-----------------------------Description of solution--------

pH	=	7.550
pe	=	4.000
Specific Conductance (µS/cm, 12°C)	=	36
Density (g/cm³)	=	0.99953
Volume (L)	=	1.00051
Activity of water	=	1.000
Ionic strength (mol/kgw)	=	7.001e-04
Mass of water (kg)	=	1.000e+00
Total carbon (mol/kg)	=	4.450e-04
Total CO2 (mol/kg)	=	4.450e-04
Temperature (°C)	=	12.00
Electrical balance (eq)	=	6.712e-05
Percent error, 100*(Cat-|An|)/(Cat+|An|)	=	6.82
Iterations	=	7
Total H	=	1.110129e+02
Total O	=	5.550754e+01

Initial solution 10. DW

-----------------------------Solution composition----------

Elements	Molality	Moles
Alkalinity	2.560e-04	2.560e-04
Br	4.168e-06	4.168e-06
Ca	1.167e-04	1.167e-04
Cl	7.405e-05	7.405e-05
F	1.211e-05	1.211e-05
K	2.882e-05	2.882e-05
Mg	6.084e-05	6.084e-05
N(-3)	1.688e-04	1.688e-04
Na	1.014e-04	1.014e-04
S(6)	3.585e-05	3.585e-05

-----------------------------Description of solution--------

pH	=	6.310
pe	=	4.000
Specific Conductance (µS/cm, 7°C)	=	38
Density (g/cm³)	=	0.99993
Volume (L)	=	1.00012
Activity of water	=	1.000
Ionic strength (mol/kgw)	=	7.460e-04
Mass of water (kg)	=	1.000e+00
Total carbon (mol/kg)	=	6.360e-04
Total CO2 (mol/kg)	=	6.360e-04
Temperature (°C)	=	7.00
Electrical balance (eq)	=	2.361e-04
Percent error, 100*(Cat-|An|)/(Cat+|An|)	=	22.08
Iterations	=	7
Total H	=	1.110134e+02
Total O	=	5.550789e+01